UNIVERSIDAD POLITÉCNICA DE MADRID

ESCUELA TÉCNICA SUPERIOR DE INGENIEROS DE TELECOMUNICACIÓN

MÁSTER UNIVERSITARIO EN INGENIERÍA DE TELECOMUNICACIÓN

TRABAJO FIN DE MÁSTER

SPHERICAL DIELECTRIC RESONATOR BANDPASS FILTER

JULIO ALBERTO GONZÁLEZ MARÍN

SEPTIEMBRE 2016

TÍTULO:

SPHERICAL DIELECTRIC RESONATOR BANDPASS FILTER

AUTOR:

JULIO ALBERTO GONZÁLEZ MARÍN

TUTOR:

MS.c DANIEL LÓPEZ CUENCA

INSTITUCIÓN:

UNIVERSITÄT STUTTGART

FECHA Y LUGAR DE LECTURA Y DEFENSA:

Stuttgart, 08 de Septiembre de 2016 (Alemania)

UNIVERSIDAD POLITÉCNICA DE MADRID

ESCUELA TÉCNICA SUPERIOR DE INGENIEROS DE TELECOMUNICACIÓN

MÁSTER UNIVERSITARIO EN INGENIERÍA DE TELECOMUNICACIÓN

TRABAJO FIN DE MÁSTER

SPHERICAL DIELECTRIC RESONATOR BANDPASS FILTER

JULIO ALBERTO GONZÁLEZ MARÍN

SEPTIEMBRE 2016

Resumen

Esta master tésis, de título Filtros Basados en Resonadores Esféricos Dieléctricos (Spherical dielectric resonator bandpass filter), ha sido realizada por Julio Alberto González Marín bajo la supervisión de MSc. Daniel López Cuenca en la Universität Stuttgart, en el departamento IHF. La defensa de la misma ha sido realizada el 08 de Septiembre de 2016 en Stuttgart, Alemania.

El espectro de frecuencias es un recurso limitado y debe ser compartido entre señales procedentes de distintas fuentes. Los filtros de microondas son esenciales para separarlos. En los últimos años, están apareciendo nuevas tecnologías a altas frecuencias.

Algunas de estas aplicaciones no tienen acceso a grandes cantidades de energía, por lo tanto, sus elementos deben tratar de minimizar la atenuación que producen. Es por eso que utilizan filtros en guía de onda u otras tecnologías que no producen muchas pérdidas. Hay otros usos que requieren filtros on-chip, tales como osciladores, que tienen normalmente muchas pérdidas (lo que significa un bajo factor Q).

Esta master tésis introduce la síntesis de filtros y se centra en filtros con resonadores dieléctricos on-chip, que son una alternativa que introduce muchas menos pérdidas que los filtros planares. Se aborda el proceso de diseño y se extraen ecuaciones y gráficos mediante simulaciones para sintetizar filtros del rizado y ancho de banda requeridos usando resonadores de esferas de alumina. Después, se estudian alternativas para reducir las pérdidas del filtro, ya que este es uno de los objetivos de usar este tipo de resonadores. Finalmente, se construyen algunos prototipos para comprobar la precisión de las simulaciones.

Las mediciones finales cuadran muy bien con las simulaciones. Esto significa que el modelo de simulación es suficientemente preciso. Además, las simulaciones cuadran con el filtro ideal previsto, lo que significa que el calculo de las ecuaciones y los gráficos es preciso.

En un esfuerzo por reducir aún más la pérdida de potencia, este documento presenta un método para obtener filtros con sobreacoplo, que alcanzan mejores pérdidas de inserción que los filtros normales, usando los gráficos y las ecuaciones ya obtenidos. Además, los métodos desarrollados pueden ser extendidos a otro tipo de filtros u otras bandas de frecuencia.

Palabras clave: filtro, resonador, dieléctrico, alumina, esfera, sobreacoplo, Chebyshev, paso banda, pérdidas, synthesis, factor Q, CST, simulación, inversores, acoplo, medida, frecuencia de resonancia, inserción, equivalente, anisotropía, prototipo.

Keywords: filter, resonator, fielectric, alumina, sphere, overcoupling, Chebyshev, passband, loss, Q factor, CST, simulation, inverters, coupling, measurement, resonance frequency, insertion, equivalent, anisotropy, prototype, external quality factor, unloaded quality factor, loaded quality factor.

Universität Stuttgart
Institut für Hochfrequenztechnik
Prof. Dr. Jan Hesselbarth

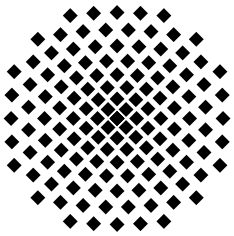

Master Thesis

Spherical dielectric resonator bandpass filter

Julio Alberto González Marín

Start date	: 01.04.2016
Submission date	: 06.09.2016
Professor	: Prof. Dr. Jan Hesselbarth
Supervisor	: MSc. Daniel López Cuenca

Erklärung

Hiermit versichere ich, dass

- Ich die Arbeit selbständig verfasst habe,

- Ich keine anderen als die angegebenen Quellen benutzt habe und alle wörtlich oder sinngemäß aus anderen Werken übernommenen Aussagen als solche gekennzeichnet habe,

- Die eingereichte Arbeit weder vollständig noch in wesentlichen Teilen Gegenstand eines anderen Prüfungsverfahrens gewesen ist,

- Ich die Arbeit noch nicht veröffentlich habe und

- Das elektronische Exemplar mit den anderen Exemplaren übereinstimmt

Stuttgart, am 06. September 2016

Julio Alberto González Marín

Abstract

The frequency spectrum is a limited resource and it must be shared among signals from a lot of different sources. Microwave filters are essential to separate them. In the last years, new technologies at high frequencies are appearing.

Some of these applications only have access to a very restricted quantity of energy, so their elements should try to minimize attenuation. Therefore, they use waveguide filters or other technologies that have low loss. There are other uses that require on-chip filters, such as oscillators, which are usually very lossy (that is, low Q factor).

This report takes an insight into filter synthesis and focuses in on-chip dielectric resonator filters, which are a much less lossy alternative to equivalent planar filters. The design process is addressed, and equations and graphs are extracted by simulation to synthesize filters of the required ripple and bandwidth using alumina spherical resonators. Then, some efforts are made to decrease as much as possible the loss of the filter, since that is one of the goals of using these kind of resonators. Lastly some prototypes are built to test the accuracy of the simulations.

The final measurements fit accurately with the simulations. This means that the simulation model is sufficiently precise. Also the simulations fit with the ideal expected filter, meaning that the calculated equations and graphs are correct.

In an effort to further decrease the power loss, this document presents a method to obtain overcoupled filters, which achieve less insertion loss than normal filters, using the calculated graphs and equations. In addition, the developed methods can be extended to other types of filters or other frequency bands.

List of abreviations

- DRA: Dielectric resonator antenna
- RF: Radiofrequency
- Q: Quality factor
- Q_0: Unloaded quality factor
- Q_e: External quality factor
- Q_l: Loaded quality factor
- TE mode: Transverse electric mode
- TM mode: Transverse magnetic mode
- TEM mode: Transverse electromagnetic mode
- FDS: Frequency domain solver
- FEM: Finite element method
- CST: Computer simulation technology

Contents

Chapter 1

Introduction

1.1 Objectives

In the last decades, new technologies like remote sensing radar, millimetre wave scanner, wifi or satellite communication are appearing or being developed. The high frequency spectrum is getting crowded, so microwave filters play an essential role in these systems.

Current technologies at these frequencies are usually quite lossy, and not advisable for using them in systems with limited access to energy, like satellites. These applications usually take advantage of waveguide filters which have low loss at high frequencies compared with other alternatives. Nevertheless, some of them need on-chip filters to have a more compact and cheaper system.

The absence of conductor in dielectric resonators makes them a suitable on-chip option to obtain low loss filters at high frequencies. Also their reduced size provides additional advantages over other kinds of resonators.

The main goal of this report is to create methods to synthesize filters using alumina spherical resonators of 9 mm radius and a relative permittivity of 9.5 at 5.8 GHz. This methods should provide graphs and equations to build fast a remarkably good first approximation of a filter without using any kind of optimization. These methods should also be scalable to other frequencies and technologies.

The coupling to the resonators is also addressed, and a method to decrease the filter loss by overcoupling some of the resonators is conceived.

Lastly, several prototypes are built in order to test the accuracy of the methods described above and to investigate the low loss overcoupled filters.

1.2 Structure of the report

The report is organised in the following way:

- Chapter 2 gives an insight into the dielectric resonators: history, advantages and recent publications.

- Chapter 3 describes circuital models and equations of microwave filters and clarifies how to measure important parameters of the filters in order to create them as specified.
- Chapter 4 deepens into the spherical dielectric resonator filters. The important parameters are measured, simulating also some filters. After that, losses are introduced into the model. Finally a method to minimize filter loss is presented.
- Chapter 5 presents some filter prototypes, measuring some important parameters like the sphere permittivity, the loss of the lines and the loss of the filter. It also checks the accuracy of the simulations comparing them with the measurements.
- Chapter 6 states the conclusions of the report.
- In the appendices, additional information is provided, like examples of filter responses with and without losses, the important parameters of the model, and a flowchart of the main program.

Chapter 2

State of the Art

There is an increasing number of wireless applications that require more and more the use of the electromagnetic spectrum. This is a limited resource, so challenges and stringent requirements arise in the design of RF/microwave filters, for higher performance, smaller size, lighter weight, lower cost and higher frequencies.

Filters can be implemented using a wide variety of technologies: lumped LC elements, planar (microstrip, stripline), coaxial, waveguide cavities, electroacustic, or dielectric resonators. The last ones require a special attention for their advantages. In the next paragraphs, a brief introduction to their history, applications and advantages is presented.

2.1 Dielectric resonators

In the late 19th century, Lord Rayleigh demonstrated that dielectric materials could be used to fabricate waveguides [1]. Later, in 1939, Robert D. Richtmyer published a study showing that dielectric structures can be used to develop resonators [2]. He also demonstrated that this kind of resonators radiate if they are exposed to free space because of the dielectric-to-air interface. These results were used to develop Dielectric Resonator Antennas (DRA). After Richtmyer's study was published, dielectric resonators were not treated for two decades because of the World War II and the lack of appropriate techniques and advanced materials. Nevertheless, in the 1960's, dielectric resonators started gaining significance again due to the interest of the industry.

In the 1980's, Long carried out studies on the properties of different resonators topologies for the design of DRAs [3], [4], [5].

It can be seen, as specified in [6], that the number of publications regarding DRA has been increasing during the last years, receiving more attention.

On the other hand, dielectric resonator filters are not widely used yet. The existence of other technologies, easier to implement at low frequencies, has not encouraged their development. Some publications exist from the 1980's trying to introduce this topic [7], [8].

During the last decade, a series of dielectric bandpass filter designs have been published. These filters are usually intended to operate in the X-band [9], [10], but there are also designs for higher and lower frequency bands [11], [12]. Some other publications

show methods to synthesize filters with these type of resonators [13], [14] while others focus on the problems that arise when dealing with them, like the appearance of spurious modes [15].

The main advantages of dielectric resonators are their reduced size (the higher the permittivity, the lower the size), much lower loss than other on-chip technologies and therefore higher unloaded Q (in the order of 10000), also much less weight since they are more compact. There is also a reduction of the overall cost with comparable performances due to their simplicity. They can can also handle more power than other alternatives using conductors.

Figure 2.1 shows a comparison of different resonator technologies, ordering them from higher to lower insertion loss, size, and Q.

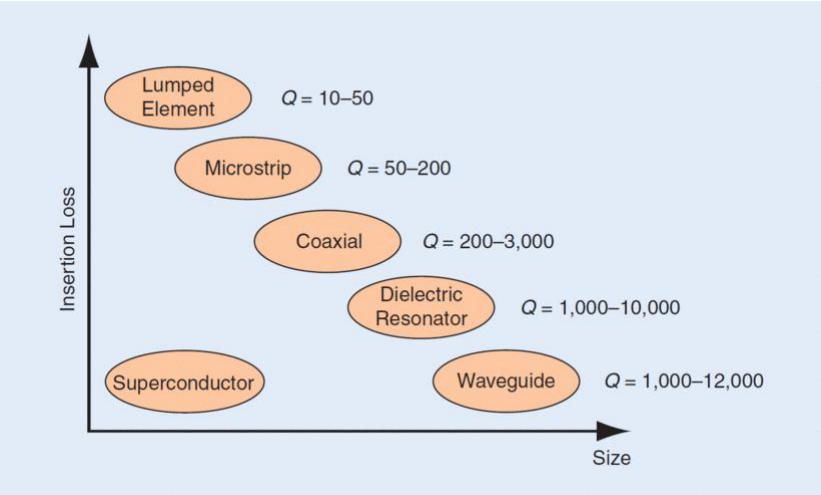

Figure 2.1: *Resonator technologies comparing size and insertion loss [16]*

Most common applications for dielectric resonators include filters (band-pass or band-stop), oscillators and DRA.

Many designs can be used as dielectric resonators. A lot of morphologies with different degrees of freedom and different achievable possibilities. Figure 2.2 presents some of the possible shapes used in the literature.

Different geometries have different advantages, like for example, selection of the resonance frequency, better positioning, better feeding possibilities or better cancellation of the spurious modes.

2.2 Microwave filters theory history

The history of microwave filters starts in 1937 with the publication of W.P.Mason and R.A. Sykes of a paper using ABCD parameters to derive filters. Major advances were made during World War II from 1941 to 1945 at the MIT radiation laboratory, the Harvard Radio Research laboratory and the Bell Laboratories. One of the major advances was the introduction of the network theory by S. Darlington. The later appearance of equations to synthesize low pass prototypes made it easy for any engineer to design a wide range of filters with several different responses.

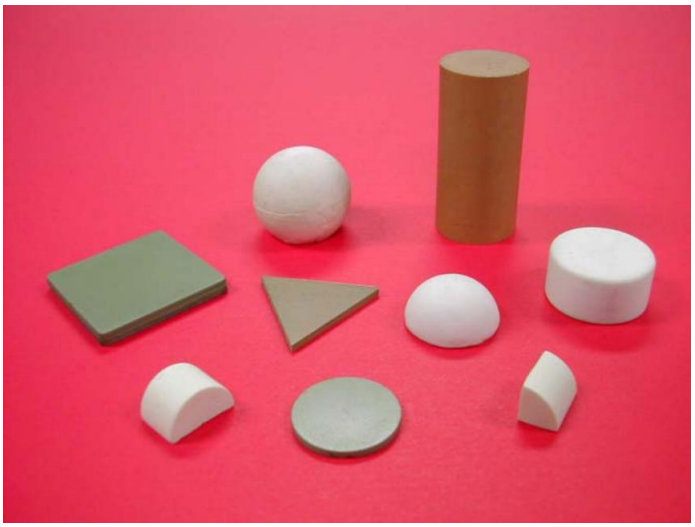

Figure 2.2: *Dielectric resonator geometrical shapes [17]*

In 1948, Paul I. Richards published a series of transformations which allow to obtain an equivalence between lumped and distributed elements, making it easier to do filters with these technologies [18]. The work made by Kuroda introducing his self-named equivalences [19], allowed the separation of the stubs in distributed line filters. This was made by introducing the figure of the impedance and admittance inverters.

Almost all the filter theory was reunited in 1955 in a book by Matthaei et al. [20], which continues to be a reference in filter design and theory for engineers.

A more detailed vision of the history of the microwave filters is found in [19].

Chapter 3

Microwave filters

3.1 Filter design

Filters are usually specified in terms of their out of band attenuation and their maximum ripple in their pass band and stop band. These specifications define the transmission mask of the filter.

There are two methods to synthesize filters: the image method and the network method.

The image method functions are defined in terms of an infinite chain of identical filter sections connected together. Nevertheless, using a finite network with resistive terminations causes the image impedances to be matched only at discrete frequencies. Although this method is conceptually simple, it requires a good deal of trial and error.

Network methods are on the other hand more precise. They start out by specifying a transfer function as a function of the complex frequency. From the transfer function, the input impedance can be found. Then, by various expansion procedures, the input impedance is expanded to give the element values of the circuit.

Three of the most usual classes of filters derived from network methods are: Butterworth, Chebyshev and Cauer as seen in figure 3.1. The class of a filter refers to the class of polynomials from which the filter is mathematically derived. The order of a filter is the number of filter elements present in the filter's ladder implementation.

- Butterworth filters are referred to as maximally flat. Their response in the frequency domain is the smoothest one compared to other filters with the same order. They do not have ripple and are monotone.
- Chebyshev type I filters have faster cut-off transition than a Butterworth, but they present ripples within the passband. Chebyshev type II filters present these ripples in the stop band.
- Elliptic filters (also called Cauer) have equal maximum ripple in the passband and stopband. They have the fastest possible transition between pass and stop bands than any other filter of the same order and therefore, need the lowest order to fulfill a given mask. This filter is a generalization of the other filters, in asymptotic situations it is equivalent to them.

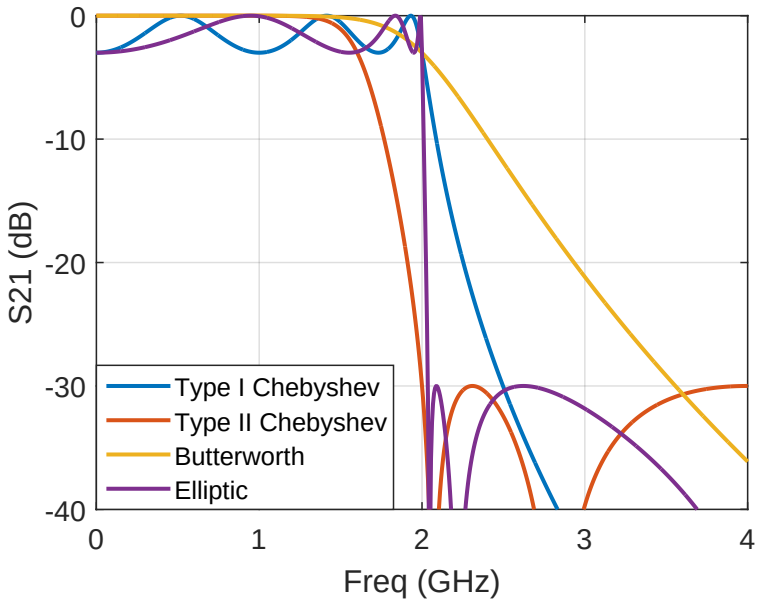

Figure 3.1: *Graph comparing different types of low pass filters with similar characteristics: 3 dB ripple in the passband, 30 dB ripple in the stop band, order 6 and cut-off frequency 2 GHz*

3.1.1 Low pass prototype

In this report the Chebyshev filters are described in detail to obtain passband filters as explained in Matthaei [20].

To design a filter, it is desirable to start from the low pass lumped elements prototype. Later, this prototype can be transformed to other types of filters (bandpass, stop band...), including definitions more useful to synthesize them with distributed elements.

Equations 3.1 determine the out of band attenuation for different filter orders as a function of the ripple.

$$\begin{aligned} La(w') &= 10\log_{10}\left(1+\epsilon\cos^2\left[n\cos^{-1}\left(\frac{w'}{w'_1}\right)\right]\right)_{w'\leq w'_1} \\ La(w') &= 10\log_{10}\left(1+\epsilon\cosh^2\left[n\cosh^{-1}\left(\frac{w'}{w'_1}\right)\right]\right)_{w'\geq w'_1} \\ \epsilon &= 10^{\frac{La_{\mathrm{dB}}}{10}}-1 \end{aligned} \tag{3.1}$$

Figure 3.2 represents equations 3.1 and can be used to determine the needed filter order for a specific out of band attenuation.

Once the necessary order n of the filter is determined, the equivalent ladder circuit can be built. Figure 3.3 presents two possibilities leading to the same circuit response.

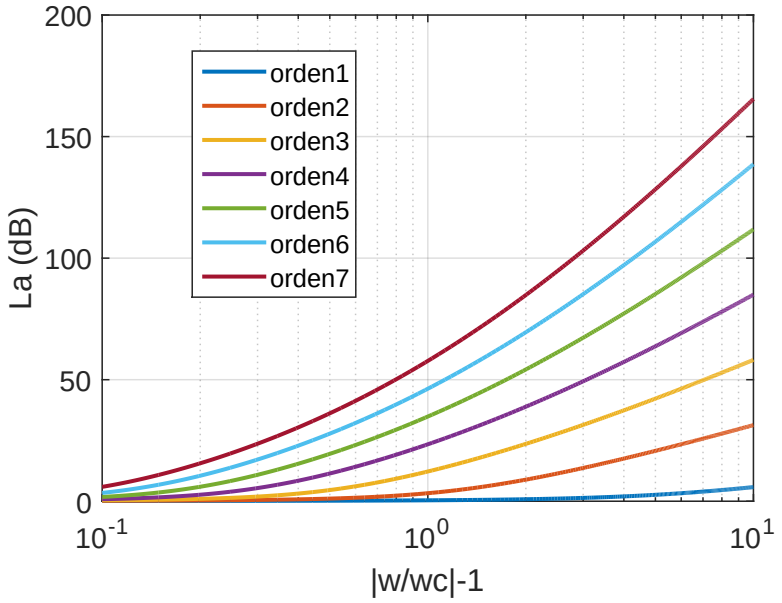

Figure 3.2: *Attenuation characteristic of 0.1 dB ripple Chebyshev filters for different orders*

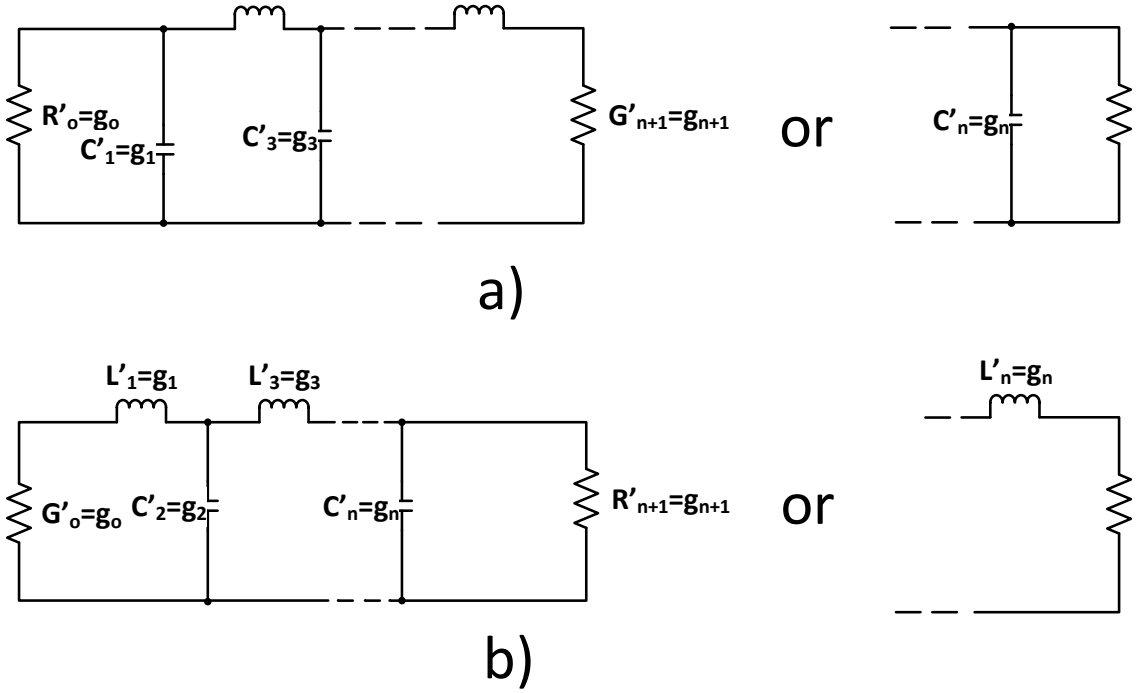

Figure 3.3: *Possible ladder models for a low pass equivalent circuit [20]. (a) starting in shunt capacitance. (b) starting in series inductance.*

The elements g_0 and g_{n+1} correspond to the termination resistance or admittance (depending on the chosen topology). The elements g_k correspond to series inductances or shunt capacitors. An additional parameter w_1' is also defined. This parameter is the radian frequency at the band pass edge. These w_1' and g_0 values are normalized and are always equal to 1 in this report.

The g_k values are calculated using equations 3.2.

$$\begin{aligned}
\beta &= \ln\left(\coth\frac{L_{ar}\text{dB}}{17.37}\right) \\
\gamma &= \sinh\left(\frac{\beta}{2n}\right) \\
a_k &= \sin\left(\frac{(2k-1)\,\pi}{2n}\right), k = 1, 2, ..., n \\
b_k &= \gamma^2 + \sin^2\left(\frac{k\pi}{n}\right), k = 1, 2, ..., n \\
g_1 &= \frac{2a_1}{\gamma} \\
g_k &= \frac{4a_{k-1}a_k}{b_{k-1}g_{k-1}}, k = 1, 2, ..., n \\
g_{n+1} &= 1 \text{ for n odd} \\
&= \coth^2\left(\frac{\beta}{4}\right) \text{ for n even}
\end{aligned} \tag{3.2}$$

For example, if a filter with 0.1 dB ripple and an out of band attenuation at w=3 equal to 39 dB or better would have to be designed, an order 4 filter is necessary with the parameters of table 3.1.

Table 3.1: Chebyshev coefficients of a 0.1 dB ripple 4 order filter

g_0	g_1	g_2	g_3	g_4	g_5
1	1.1088	1.3062	1.7704	0.8181	1.3554

The filter is represented in figure 3.4. The impedances of the terminations have been fixed to the values of g_0 and g_5 respectively. When one of the terminations is near an inductor, its value defines its conductance, but when it is near a capacitor it defines its resistance. The values are stated in Ohms, Henries and Farads. Figure 3.5 shows the response of this filter.

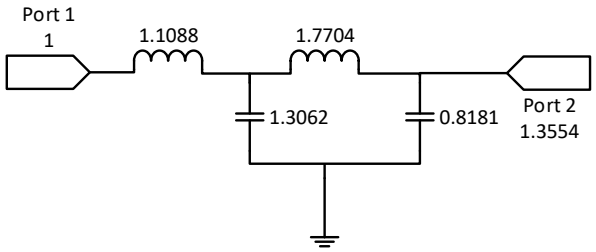

Figure 3.4: *Low pass 4^{th} order filter prototype circuit with 0.1 dB ripple, $w_1' = 1$ and $w_0 = 1$*

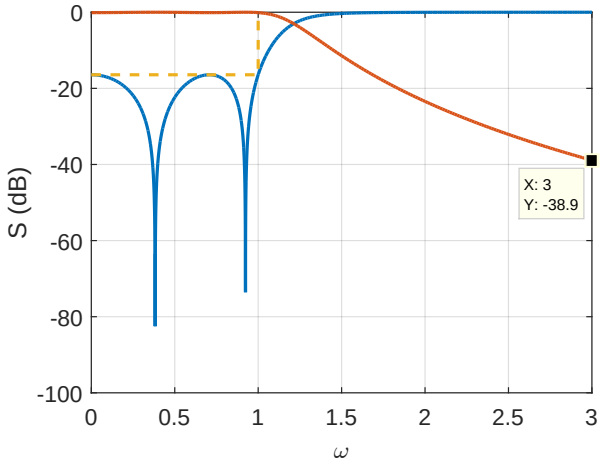

Figure 3.5: *Low pass 4^{th} order filter prototype response with 0.1 dB ripple, $w_1' = 1$ and $w_0 = 1$*

As it is a lossless filter, the S_{11} parameter can be calculated using equation 3.3.

$$S_{11} = 10\log_{10}(1 - 10^{\frac{-0.1}{10}}) = -16.43\,\text{dB} \tag{3.3}$$

At $w = 3$ the attenuation is almost 39 dB as expected.

3.1.2 Bandpass transformation

From the low pass equivalent circuit, it is simple to obtain a transformation to a band pass filter. A band pass filter of equivalent ripple and out of band attenuation can be created substituting the elements of the low pass prototype by resonators.

A resonator is an element that exhibits resonance at a certain frequency. A resonator is defined by its resonance frequency and its slope parameter.

Figure 3.6 shows the two basic types of lumped element resonators: series and shunt.

(a) (b)

Figure 3.6: *Lossy resonators equivalent circuits [20]. (a) Series circuit. (b) Shunt circuit.*

The resonance frequency of a resonator is the one at which the reactances (capacitance and inductance) cancel each other.

$$w_0 = \frac{1}{\sqrt{LC}} \tag{3.4}$$

On the other hand, the slope parameter depends on the type of resonator. For series resonators, the reactance slope parameter α is defined as:

$$\alpha = \frac{w_0}{2}\frac{\mathrm{d}X}{\mathrm{d}x}\,|_{w_0} \qquad \alpha = w_0 L \tag{3.5}$$

For shunt resonators the susceptance slope parameter b is defined as:

$$b = \frac{w_0}{2}\frac{\mathrm{d}B}{\mathrm{d}x}\,|_{w_0} \qquad b = w_0 C \tag{3.6}$$

The importance of the slope parameter is that it states an equivalence between different resonators. In a filter, the resonators can be substituted by other resonators with the same resonance frequency and slope parameter with no change in the final response. This is of crucial importance at high frequencies, where distributed resonators are necesary because large parasitic effects appear in lumped elements. The slope parameter of the distributed resonators can be measured, so these resonators can be used in filters.

It is also convenient for the band pass transformation to define the fractional bandwidth:

$$w = \frac{w_2 - w_1}{w_0} \tag{3.7}$$

The transformations are the following ones:

- A shunt capacitor is transformed into a shunt resonator with:

$$C_j = \frac{g_j}{w w_0} \tag{3.8}$$

$$L_j = \frac{w}{g_j w_0} \tag{3.9}$$

- A series inductance is transformed into a series resonator with:

$$C_j = \frac{w}{g_j w_0} \tag{3.10}$$

$$L_j = \frac{g_j}{w w_0} \tag{3.11}$$

For example to synthesize a filter similar to the previous one: order 4, ripple 0.1 dB, central frequency of 5.8 GHz and fractional bandwidth of 6 %, the values are calculated in table 3.2.

Table 3.2: Values of the bandpass filter elements

j	g_j	C_j	L_j
0	1	-	-
1	1.1088	1.485 pF	0.507 nH
2	1.3062	0.597 nF	1.26 pH
3	1.7704	0.93 pF	0.81 nH
4	0.8181	0.3741 nF	2.01 pH
5	1.3554	-	-

Figure 3.7 shows the circuit and figure 3.8 the S parameters.

The ripple has been maintained. The start and stop frequencies are 5.629 GHz and 5.977 GHz. The central frequency is

$$f_0 = \sqrt{f_1 f_2} = 5.8\,\text{GHz} \tag{3.12}$$

and the fractional bandwidth is

$$w = \frac{f_2 - f_1}{f_0} = 0.06 \tag{3.13}$$

as specified.

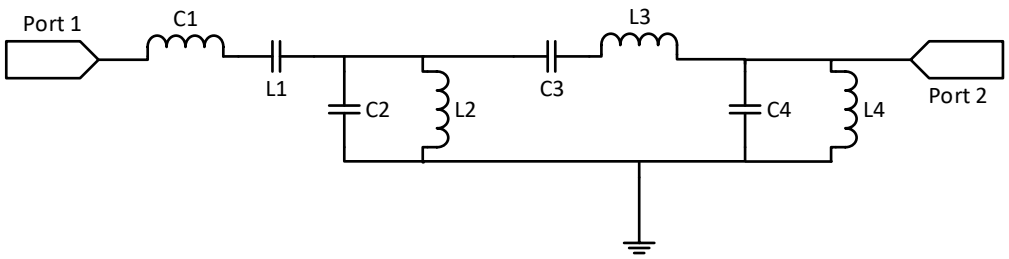

Figure 3.7: *Bandpass order 4 filter prototype with 0.1 dB ripple and central frequency 5.8 GHz circuit*

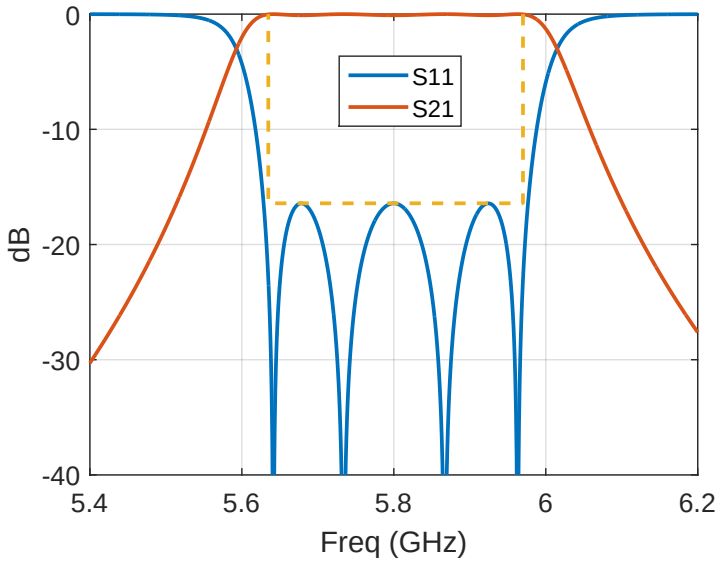

Figure 3.8: *S parameters of the bandpass 4 order filter prototype with 0.1 dB ripple and central frequency 5.8 GHz*

A convenient visual way of checking if a filter fulfills the specifications is by means of a mask. In figure 3.8 the mask is represented by the yellow dashed lines. Masks for out of band attenuation can also be included.

3.1.3 Inverters

Sometimes, it is convenient to have only series resonators or only parallel resonators. This is done with the aid of impedance and admittance inverters. An idealized impedance inverter operates like a quarter-wavelength line of characteristic impedance K at all frequencies. An admittance inverter operates similarly but like a quarter-wavelength line of characteristic admittance J.

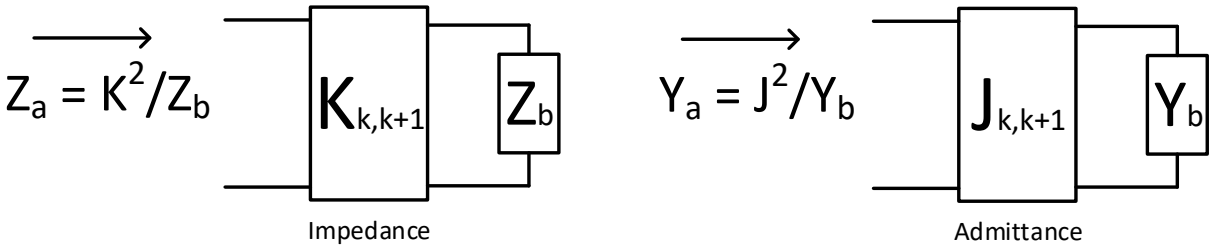

(a) (b)

Figure 3.9: *Types of inverters [20]. (a) Impedance-inverter/K-inverter. (b) Admittance-inverter/J-inverter*

A series inductance with an inverter at both sides, operates like a shunt capacitance. In the same way, a series resonator operates like a shunt resonator. Only admittance inverters are explained in this section as they are suitable for the resonators used in this report.

A model of an admittance inverter can be made out of capacitances as in figure 3.10. This J inverter presents a J = wC. Taking into consideration the existence of inverters and the definition of a resonator made by its slope parameter, a model of a filter can be made using these elements.

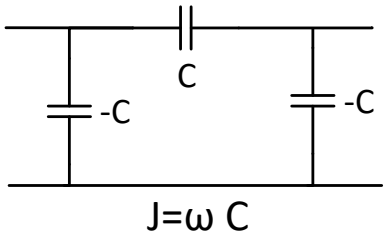

Figure 3.10: *Lumped elements model of an admittance inverter [20]*

It must be noticed that, since inverters change the level of impedance of a resonator or a circuit element, it does not matter the value of the slope parameter of the resonator or the impedance of the terminated lines, since these can be corrected changing the value of the inverters. Therefore, resonators of arbitrary slope parameter can be used.

The values of the inverters depend on the slope parameter of the employed resonators, on the impedance of the terminations, on the bandwidth and on the g parameters of the

low pass prototype. Equations 3.14 are used to calculate the value of the inverters.

$$\begin{aligned} J_{01} &= \sqrt{\frac{G_a b_1 w}{g_0 g_1 w_1'}} \\ J_{n,n+1} &= \sqrt{\frac{G_a b_n w}{g_n g_{n+1} w_1'}} \\ J_{j,j+1}\,|_{j=1 \text{ to } n-1} &= \frac{w}{w_1'}\sqrt{\frac{b_j b_{j+1}}{g_j g_{j+1}}} \\ w = \text{fractional bandwidth} &= \frac{w_2 - w_1}{w_0} \end{aligned} \tag{3.14}$$

An example is made using the previous specifications. The impedance of the terminations is set to $50\,\Omega$, and the slope parameters of all the resonators are set to 1, therefore, all the resonators are equal.

The chosen resonators are shunt ones. For them to have the same slope parameter b = 1 and the $f_0 = 5.8\,\text{GHz}$, the L and the C should all be w_0^{-1}. The values of the elements can be seen in table 3.3.

Regarding the inverters, they are calculated in table 3.4 using equations 3.14.

Table 3.3: Resonator element values

L_{reson}	27.44 pH
C_{reson}	27.44 pF

Table 3.4: Calculation of inverters

$Inverter_i$	$Formula_i$	$J_{i-1,i}$	C_i
1	$\sqrt{\frac{G_a b_1 w}{g_0 g_1 w_1'}}$	0.0329	0.9028 pF
2	$\frac{w}{w_1'}\sqrt{\frac{b_1 b_2}{g_1 g_2}}$	0.04986	1.368 pF
3	$\frac{w}{w_1'}\sqrt{\frac{b_2 b_3}{g_2 g_3}}$	0.03945	1.082 68 pF
4	$\frac{w}{w_1'}\sqrt{\frac{b_3 b_4}{g_3 g_4}}$	0.04986	1.368 pF
5	$\sqrt{\frac{G_b b_4 w}{g_4 g_5 w_1'}}$	0.0329	0.9028 pF

The values of the inverters are symmetric. This is because the selected slope parameters and impedance terminations are also symmetric, leading to a symmetric circuit. Nevertheless non symmetric configurations are also possible.

Figure 3.11 presents the ideal model of the circuit.

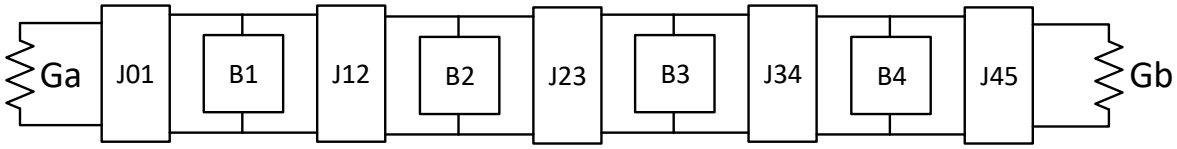

Figure 3.11: *Bandpass filter model using inverters and resonators*

The response of the filter using inverters and without using them (as in figure 3.8) is depicted in figure 3.12.

It is seen that their responses out of band are not exactly the same. This is caused by the non-idealities of the employed inverter model which does not behave exactly as expected when changing the frequency.

In this section a simplified model of a Chebyshev passband filter has been developed using inverters and resonators characterized by their resonance frequency, their slope parameter and the value of the inverter.

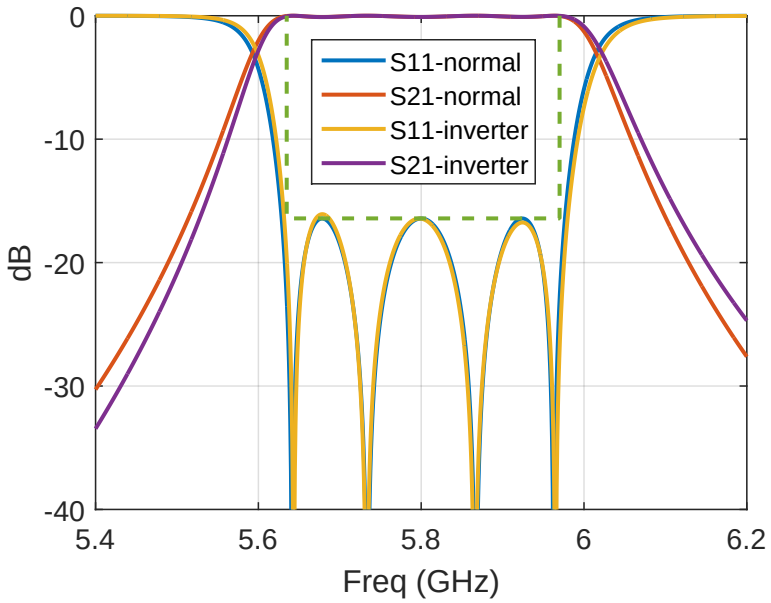

Figure 3.12: *Bandpass filter model using inverters and resonators*

3.1.4 Characterization using Q_e and k

It is difficult to determine the slope parameter of certain resonators or the J parameter of the inverters, for example in the case when there is only access to the resonator with an undetermined inverter.

This is because there are an infinite number of combinations of inverters and resonators (like in figure 3.13) that produce exactly the same frequency response.

When the slope parameter of the resonator is known, these equivalences can be used to change the resonators by others with a different slope parameter. If the inverters are

changed accordingly, the circuit produces the same response. When the slope parameter is not known, this equivalence makes it difficult to determine it.

There exist other parameters to model a filter which are easier to measure. They are the external quality factor (Q_e) and the coupling factor (k). The Q_e is inversely proportional to the coupling that exists between the resonator and the termination. It measures the power leaking outside the filter and therefore it is expressed as a component of the quality factor. On the other hand, the k represents the coupling existing between resonators.

The k's are a function of the slope parameter of the adjacent resonators and the inverter connecting both. The Q_e's are a function of the slope parameter of the ending resonators and the impedance of the terminations. These parameters do not change for the same filter, do not affect the resonators and are easier to measure. Therefore, they are more convenient to use in filter design with unknown resonators.

Equations 3.15 [20], can be used to determine the couplings and external Q factors of the example filter using the same specifications as in the previous sections. The values are stated in table 3.5.

$$\begin{aligned} (Q_e)_A &= \frac{b_1}{J_{01}^2/G_A} = \frac{g_0 g_1 w_1'}{w} \\ (Q_e)_B &= \frac{b_n}{J_{n,n+1}^2/G_B} = \frac{g_n g_{n+1} w_1'}{w} \\ k_{j,j+1}\mid_{j=1 \text{ to } n-1} &= \frac{J_{j,j+1}}{\sqrt{b_j b_{j+1}}} = \frac{w}{w_1' \sqrt{g_j g_{j+1}}} \end{aligned} \tag{3.15}$$

Table 3.5: Values of the k and Qe of the example filter

Qe_A	18.48
k_{12}	0.05
k_{23}	0.0395
k_{34}	0.05
Qe_B	18.48

It can be seen that these parameters are also symmetric. In this case it does not matter if the resonators are symmetric or not, these parameters should always be symmetric in a Chebyshev filter.

3.1.5 Quality factors of a resonator

Three different quality factors are defined for describing the behaviour (loss and coupling) of a resonator. The Q_0, referred sometimes as the unloaded Q or the selectivity factor, is a measurement of the losses that the resonator has.

$$Q_0 = \frac{2\pi \text{ Stored Energy}}{\text{Energy lost per cycle}} \tag{3.16}$$

In a circuit, this is equivalent to:

$$Q_0 = \frac{\text{Reactance of the circuit}}{\text{Resistance of the circuit}} \tag{3.17}$$

When connecting the resonator to a transmission line, like in figure 3.13, other two Q concepts arise.

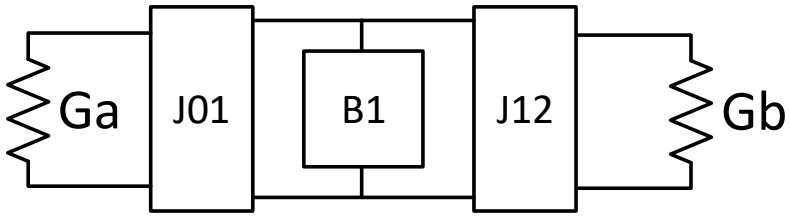

Figure 3.13: *Resonator fed at both sides by means of inverters*

The Q of the entire system is called the loaded quality factor (Q_l) and can be related to the Q_0 as:

$$Q_l = Q_0 \left(1 + \beta\right). \tag{3.18}$$

The external quality factor can be redefined as a function of β:

$$Q_e = \frac{Q_0}{\beta}. \tag{3.19}$$

β is called the coupling parameter. Combining:

$$\frac{1}{Q_l} = \frac{1}{Q_0} + \frac{1}{Q_e}. \tag{3.20}$$

In defining Q_0, the losses are due to the resonator (radiation and dissipation), whereas in Q_e, they are only due to the external load. The degree of coupling between a resonator and a transmission line can be therefore defined by the Q_e.

3.2 Measurement of k and Q_e parameters in resonators

It is necessary to change the Q_e and k parameters between resonators when synthesizing filters. These parameters are influenced by physical characteristics like the distances between the resonators or the feeding points.

In order to check which physical characteristics of the circuit are important and learn how to vary them in order to produce the necessary couplings, it is necessary to know methods to measure these couplings. In this section several methods are presented which would be used later in a practical case.

3.2.1 Measurement of k

Measurement of the couplings between resonators can be performed in several ways; two methods are presented in this section. Method 1 is less precise than method 2, but it is briefly introduced because it is later used in section 4.7 for obtaining equivalences between the overcoupled and normally synthesized filters.

Method 1

This method consists in synthesizing a symmetric filter with three resonators. A measurement of the ripple and the bandwidth gives the information about the Q_e (between the resonators at the endings and each of the terminations) and the k (between the ending resonators and the center resonator). Two k's and two Q_e's are obtained.

To prove the method 1, a filter with k = 0.06, $Q_e = 150$, $Q_{01} = 5000$ and $Q_{02} = 10000$ is considered and simulated.

With the points found in the filter response in figure 3.14, the ripple and the bandwidth can be estimated. With the ripple, the bandwidth and the order of the filter (in this case n = 3), the Q_e and the k are estimated in table 3.6 using equations 3.2 and 3.15 provided by Matthaei [20].

Table 3.6: Qe and k parameters of the filter example

L_a	13.56 dB
w	0.0982
Q_e	143.33
k	0.0603

It can be seen that this method can be used also to estimate the Q_e of the filter. Nevertheless, the measurement of this parameter is not as exact as necessary unless the Q_0's are very large. The measurement of the k is highly precise, obtaining more or less the same precision as with other methods.

Nevertheless this method has some drawbacks. There are certain situations in which the information about the filter bandwidth or ripple is difficult to extract, and therefore is not possible to obtain information about the couplings and quality factors.

That happens for example when the Q_0's of each of the resonators are low. Other situation in which these parameters are impossible to measure is when the combination of

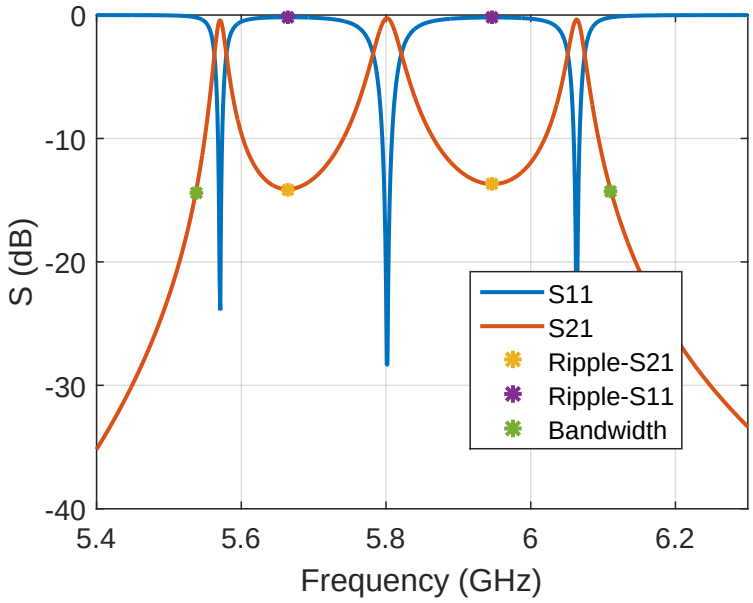

Figure 3.14: *Three resonator filter example response to measure the k and Q_e, including the points of interest for the ripple and the bandwidth*

Q_e and k is such that they fulfill the condition defined in equation 4.13. In this situation the Chebyshev formulas do not apply anymore and the filter loses two poles as explained in section 4.7.

Method 2

This method consist in using the formulas provided by Cohn and Simizu in [21] for the attenuation of a symmetrical pair of resonators. This method provides a series of formulas that have also been tested in asymmetrical pair of resonators providing high accuracy. This method is more direct than the previous one, not requiring to synthesize a filter. It can also provide information about the k when the other method fails. Both of them have a similar accuracy.

Equation 3.21 is an approximation for the attenuation, behaving better for small bandwidths. Equation 3.22 expresses the loss at midband.

$$L_A = 10\log_{10}\left\{\left[\frac{\left(1+\frac{Q_e}{Q_0}\right)^2}{2kQ_e}+\frac{kQ_e}{2}\right]^2+2\left[\frac{\left(1+\frac{Q_e}{Q_0}\right)^2}{k^2}-Q_e^2\right]u^2+\frac{4Q_e^2}{k^2}u^4\right\}\text{dB} \tag{3.21}$$

$$u=\frac{f-f_0}{f_0}$$

$$L_A = 20\log_{10}\left[\frac{\left(1+\frac{Q_e}{Q_0}\right)^2}{2kQ_e}+\frac{kQ_e}{2}\right]\text{dB} \tag{3.22}$$

This method can always be used to obtain the k of the resonators given the attenuation at midband. On the other hand, normally, the resonators used in the filters are overcoupled. That means that they fulfill the condition defined in equation 3.23.

$$k < \frac{1}{Q_e} + \frac{1}{Q_0} \tag{3.23}$$

In this situation a bump in the central frequency appears, leading to two maxima of the function as seen in figure 3.15.

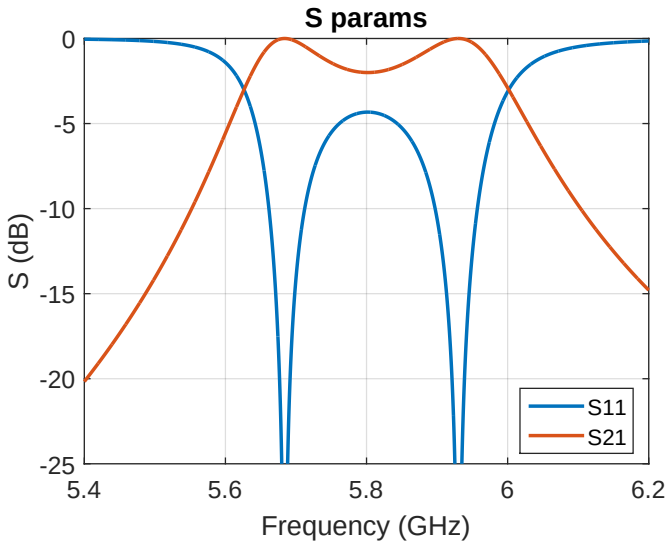

Figure 3.15: *Overcoupled pair of symmetrical resonators response*

In this case, equation 3.24 is obtained deriving the previous one and searching for the maxima.

$$\begin{aligned} k &= \sqrt{w_n^2 + \left(\frac{1}{Q_e} + \frac{1}{Q_u}\right)^2} \\ w_n &= \frac{f_b - f_a}{f_0} \end{aligned} \tag{3.24}$$

A more simplified form can be used when the Q_e and the Q_u are large enough using equation 3.25 [22].

$$k = \frac{f_a^2 - f_b^2}{f_a^2 + f_b^2} \tag{3.25}$$

Figure 3.16 shows the circuit that is used to test this method for a $Q_e = 1000$ and a k = 0.05. The response can be seen in figure 3.17.

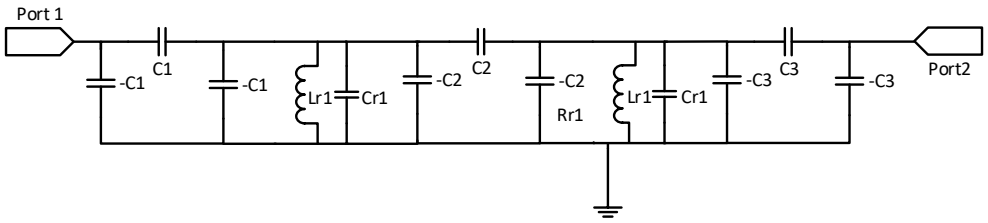

Figure 3.16: *Circuit used to measure the coupling between two resonators*

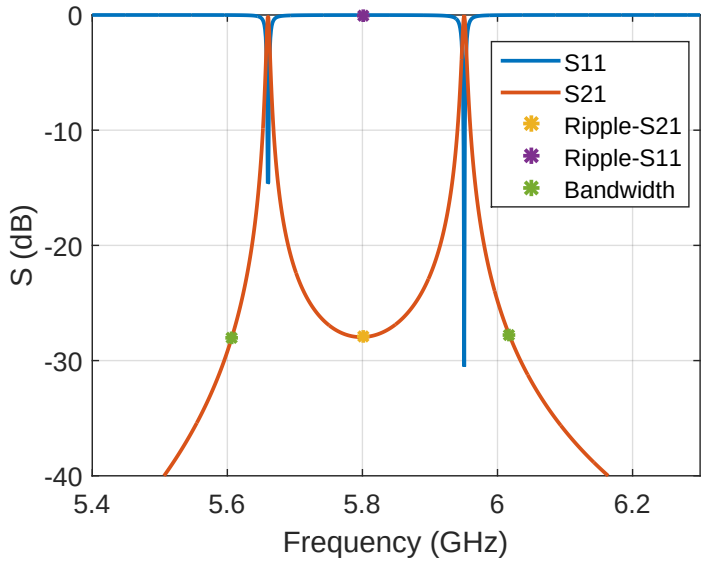

Figure 3.17: *Circuital response of a pair of resonators*

The measurements are shown in table 3.7 and the couplings using the different methods in table 3.8.

Table 3.7: Results of the coupled pair of resonators, including resonance frequencies and attenuation at midband

f_a	5.6602 GHz
f_b	5.9506 GHz
f_0	5.7982 GHz
L_{A0}	27.9636 dB

Table 3.8: Couplings using different equations

Using equation 3.22	0.0500076
Using equation 3.24	0.050094
Using equation 3.25	0.0499911

It has been tested that the bigger the Q_e, the more accurate it is the method.

Therefore, big values of this parameter will be set when measuring the coupling by simulation.

The first equation requires the exact knowledge of the resonance frequency of the resonators and provides an accurate measurement of the k. The second equation requires the previous knowledge of the resonance frequency and the Q_e and Q_0 of the resonators and provides as well a trustworthy approximation of the k. If there is no previous knowledge of the Q_e and Q_0 of the resonators, but they are known to have a big Q_u, and a big Q_e is forced in them, then the third formula can be used with insignificant error.

This third method works also with asymmetrical pairs of resonators accurately. However, maybe the resonators do not resonate at the same frequency. Therefore, the accuracy of this method is tested for resonators with slightly different resonance frequencies.

Figure 3.18 depicts the circuital response of a pair of resonators with $k = 0.06$, $Q_{e1} = 250$, $Q_{e2} = 600$, $Q_{01} = Q_{02} = \infty$, $f_{01} = 5.79\,\text{GHz}$ and $f_{02} = 5.81\,\text{GHz}$. Table 3.9 presents the results of the measurement.

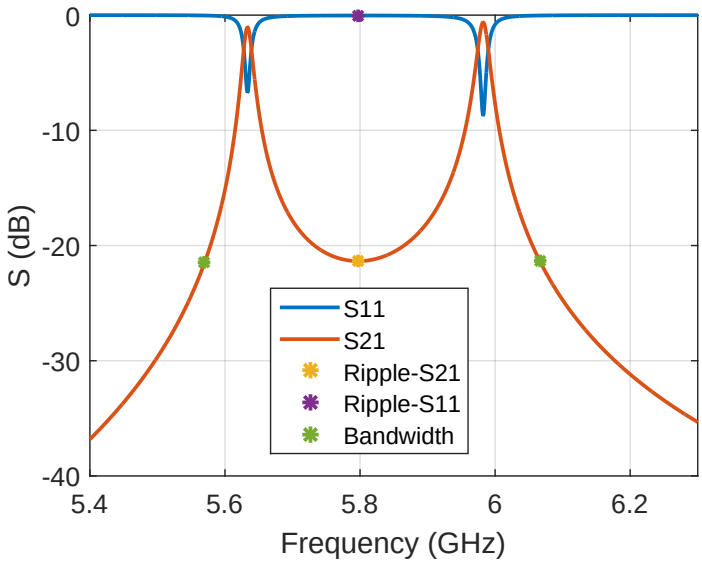

Figure 3.18: *Circuital response of a pair of resonators with slightly different resonance frequencies*

Table 3.9: Measurements of a pair of resonators with slightly different resonance frequencies

f_a	5.6334 GHz
f_b	5.9823 GHz
k	0.06002

It is seen that the result of k differs from the original by 0.03 % when the frequencies vary by 0.34 %.

Variations in the frequency of this order are to be expected. Nevertheless the variation of k is irrelevant when the frequency shift is as little as this and the method can still be applied with confidence.

3.2.2 Measurement of Q_e

The method presented in this section, called impedance method [23], is able to measure the Q_e, Q_0 and Q_l of a single filter using only one port using information of the input impedance.

To illustrate it, the circuit in figure 3.19 is simulated.

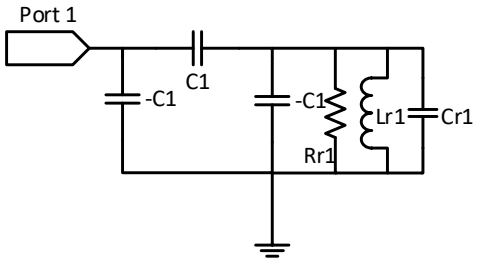

Figure 3.19: *Circuit used to test the impedance method*

A Q_u of 200 is selected for the resonator. The C1 is selected so that the Q_e is equal to 20. The slope parameter of the resonator is set to 5 and the resonance frequency $f_0 = 5.8\,\text{GHz}$. The impedance of the line Z_0 is set to $50\,\Omega$. The simulation gives the results seen in figure 3.20.

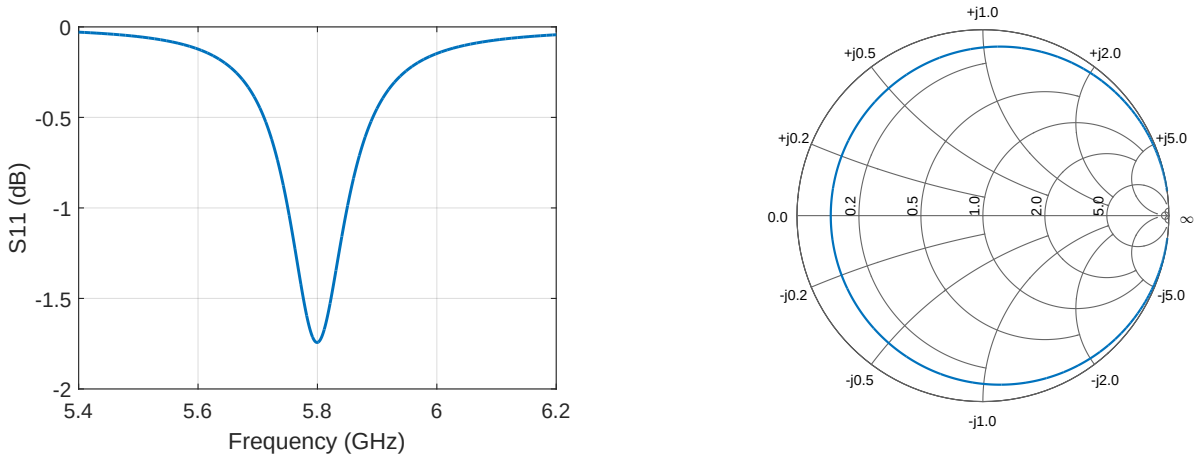

(a) (b)

Figure 3.20: *S11 response of one single resonator. (a) dB units. (b) Smith chart.*

The Q_0, Q_l and Q_e of the resonator can be computed when the circuit is known:

$$Q_0 = \frac{\text{Reactance}}{\text{Resistance}} = \frac{\frac{wC}{J^2}}{\frac{1}{RJ^2}} = wCR = \frac{R}{wL} \tag{3.26}$$

$$Q_l = \frac{\frac{wC}{J^2}}{Z_0 + \frac{1}{RJ^2}} = \frac{Q_0}{1 + Z_0 R J^2} = \frac{Q_0}{1+\beta} \tag{3.27}$$

$$\beta = Z_0 R J^2 \tag{3.28}$$

Having calculated the β, it is easy to calculate the Q_e as in equation 3.19.

$$Q_e = \frac{Q_0}{\beta} = \frac{Q_0}{Z_0 R J^2} \tag{3.29}$$

In this case, the coupling between resonators is represented by a J inverter. Assuming that the inverter of the circuit has a constant J = wC for all frequencies, the impedance seen at the input of the circuit is the following:

$$Z_{in} = \frac{1}{RJ^2} + jw\frac{C}{J^2} + \frac{1}{jwLJ^2} \tag{3.30}$$

The normalized impedance is then:

$$Z_{in}\mid_{norm} = \frac{1}{Z_0 R J^2}\left(1 + jwCR + \frac{R}{jwL}\right) \tag{3.31}$$

Knowing the equivalences for beta and Q_0 this equation can be expressed as:

$$Z_{in}\mid_{norm} = \frac{1}{\beta}\left(1 + jQ_0\left(\frac{w}{w_0} - \frac{w_0}{w}\right)\right) \tag{3.32}$$

When having relatively big Q_u the resonance is greatly pronounced and the frequencies are close to w_0. Therefore an approximation can be made introducing a new variable:

$$\delta = \frac{w - w_0}{w_0} \tag{3.33}$$

$$\begin{aligned} Z_{in}\mid_{norm} &= \frac{1}{\beta}\left(1 + j2Q_0\left(\delta - \delta_0\right)\right) \\ &= \frac{1}{\beta}\left(1 + j2Q_l\left(1+\beta\right)\left(\delta - \delta_0\right)\right) \\ &= \frac{1}{\beta}\left(1 + j2Q_e\beta\left(\delta - \delta_0\right)\right) \end{aligned} \tag{3.34}$$

Equations 3.34 relate the quality factors of the resonator with the impedance.

At the points where the impedance is in the form R = X means that the impedance is:

$$Z_{in}\mid_{norm} = \frac{1 \pm i}{\beta}\mid_{R=X} \tag{3.35}$$

Meaning that:

$$2Q_0\left(\delta - \delta_0\right) = \pm 1 \tag{3.36}$$

Taking the two frequency points in which this occurs, a expression for Q_0 is obtained:

$$Q_0 = \frac{f_0}{f_2 - f_1} = \frac{f_0}{BW_{21}} \tag{3.37}$$

Doing the same for the expressions with Q_l and Q_e results in the following expressions:

$$Z_{in}\,|_{norm} = \frac{1 \pm (1+\beta)\,i}{\beta}\,|_{R=X+1} \tag{3.38}$$

$$2Q_l\,(\delta - \delta_0) = \pm 1 \tag{3.39}$$

$$Q_l = \frac{f_0}{f_4 - f_3} = \frac{f_0}{BW_{43}} \tag{3.40}$$

$$Z_{in}\,|_{norm} = \frac{1 \pm \beta i}{\beta}\,|_{X=1} \tag{3.41}$$

$$2Q_e\,(\delta - \delta_0) = \pm 1 \tag{3.42}$$

$$Q_e = \frac{f_0}{f_6 - f_5} = \frac{f_0}{BW_{65}} \tag{3.43}$$

By finding these points in the Smith chart and finding the bandwidths, the Q's can be determined. In figure 3.21, the points of the Smith chart that fulfill the conditions stated above are plotted with dashed lines. It is easy to find their intersection with the S11. The actual values are stated in table 3.10

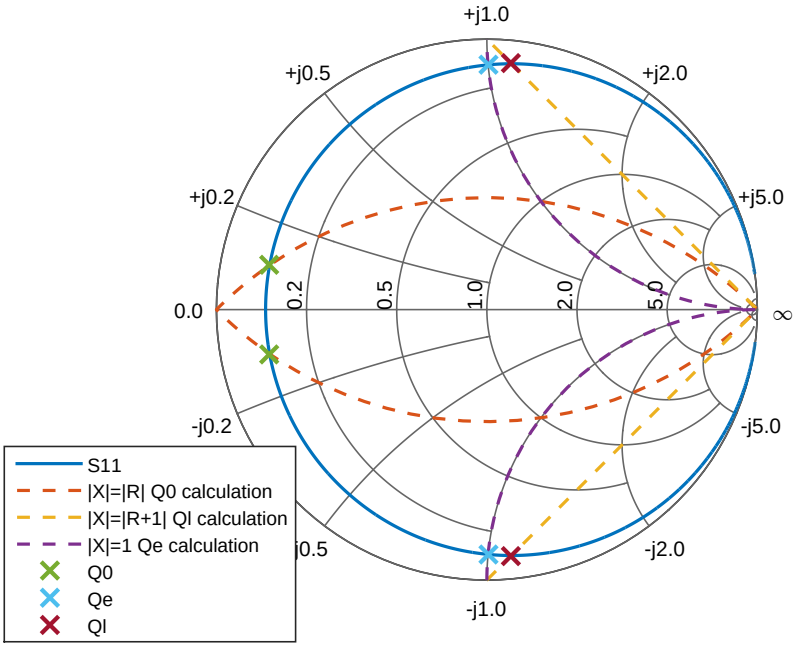

Figure 3.21: *Measurement of the Q's using the impedance method for the first example*

Table 3.10: Q and bandwidth values for the first example

	BW (MHz)	Q
Q_0	29	199.87
Q_l	289.8	20.0007
Q_e	319	18.1699

β is the inverse of the real part of the normalized impedance at resonance. It is also the relationship between the Q_0 and the Q_e. In this case $\beta = 9.9938$.

This method is more precise the more similar the Q_0 and the Q_e are, because then higher sensitivity is obtained. When these parameters are the same, the resonator is said to be critically coupled. An example is shown in figure 3.22 and table 3.11 in which the Q_0 has been set to 20, the same value as the Q_e.

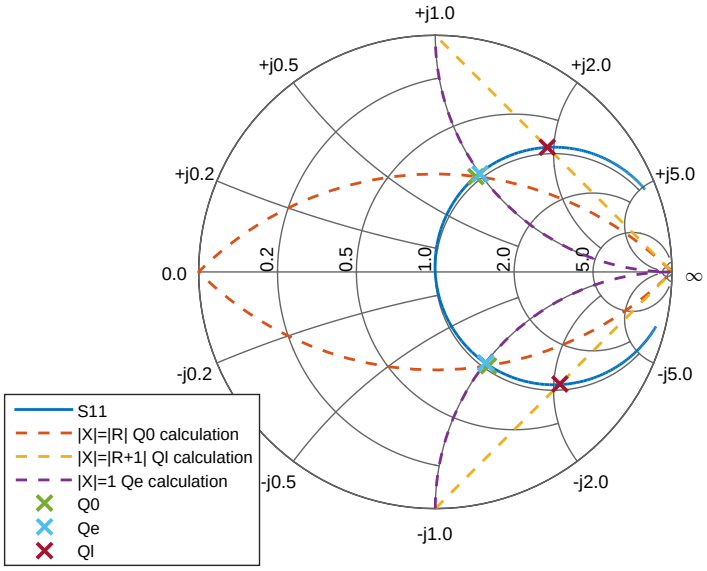

Figure 3.22: *Measurement of the Q's using the impedance method for the second example*

Table 3.11: Q and bandwidth values for the second example

	Bandwidth (MHz)	Q
Q_0	289.8	20.0138
Q_l	584.2	9.93
Q_e	291.6	19.8903

In this case, the Q_e has been determined more precisely.

The approximation made in equation 3.33 makes the Q's easy to calculate and sufficiently precise to synthesize normal filters. Nevertheless, it is not precisse enough when the Q_e is small. In section 4.7, filters with small Q_e's are synthesized, therefore another approach is needed.

Using equation 3.32, the β of the resonator can be calculated:

$$\beta = \frac{1}{Z_{in} \mid_{norm_{f=f_0}}} \tag{3.44}$$

Then, a new parameter called X_2 is extracted from the impedance:

$$X_2 = Q_0 \left(\frac{w}{w_0} - \frac{w_0}{w} \right) \tag{3.45}$$

Using this parameter, a fit of equation 3.45 can be performed, calculating the Q_0 that better fits the equation. The values of the Q_e and Q_l can be extracted now from equation 3.29 and 3.27.

This method is more precise for two reasons. First of all, the approximation performed in equation 3.33 is not carried out, therefore low Q_e's are calculated more accurately. And secondly, the method does not depend on the values of two points only, it uses the whole information of the impedance to calculate the value of the quality factors.

Chapter 4

Spherical dielectric resonator filters

4.1 Introduction

In this report, filters using alumina 18mm diameter spheres as resonators are synthesized. They have been simulated using the FEM (finite element method), specifically the FDS (frequency domain solver) of the CST software [24]. The parameters used in the simulations are compiled in appendix D.

Two parallel, large, conducting plates are put above and below the spheres in order to avoid radiation as in figure 4.1.

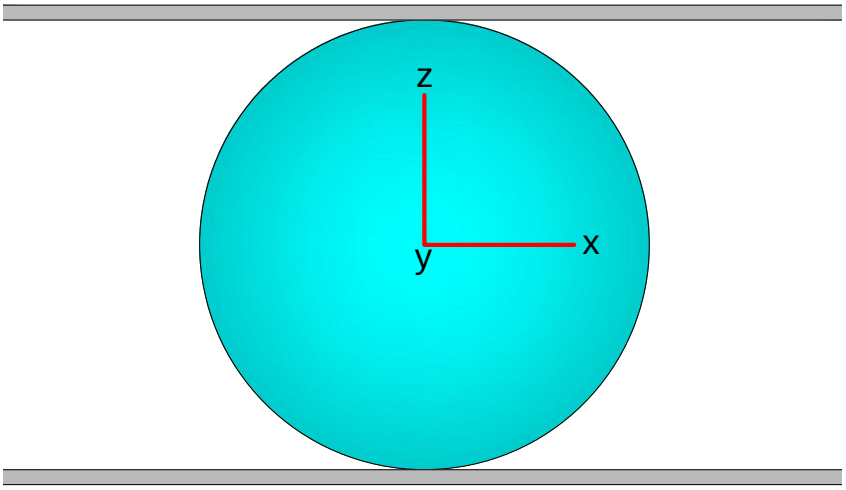

Figure 4.1: *Plates above and below the sphere to avoid radiation*

Coupling from the fundamental mode of the sphere to the TEM mode of the parallel plate structure is not possible because these modes are orthogonal [25], but coupling to superior modes can appear. The superior modes on a parallel plate have the cut off frequency given in equation 4.1 [26].

$$Fc_{TE1} = Fc_{TM1} = \frac{1}{2d\sqrt{\mu\epsilon}} \tag{4.1}$$

Since the medium is vacuum and the distance between the plates is the same as the sphere diameter, the cutoff can be calculated to be:

$$Fc_{TE1} = Fc_{TM1} = \frac{c_0}{2d} = 8.3\,\text{GHz} \tag{4.2}$$

Special care must be taken above these frequencies. The resonant modes of a dielectric sphere are explained in [27].

The electric and magnetic fields of the fundamental mode are represented in figure 4.2.

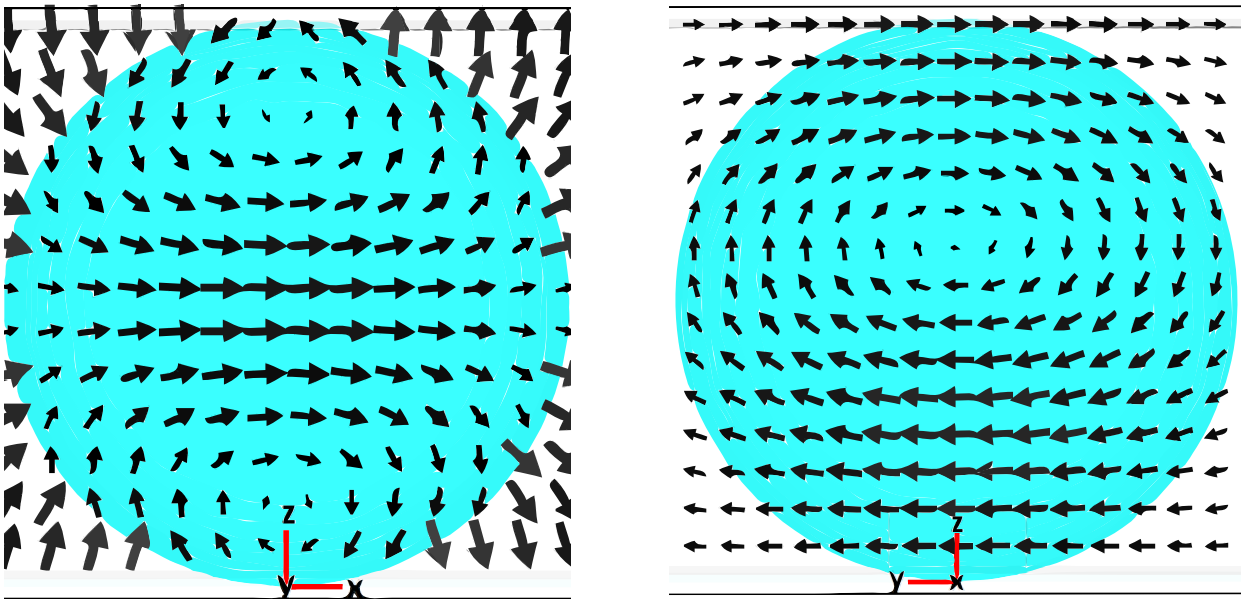

(a) (b)

Figure 4.2: *Cut of the fields of the fundamental mode of a dielectric sphere between two metal plates fed with a microstrip line. (a) E field. (b) H field.*

This mode is an hybrid mode that can be named HE_{Z111} as seen in [28]. The Z is because the propagation is considered in the z axis direction. The ones are because there are 1 half wavelengths in each direction.

This mode resonates at aproximately 5.8 GHz using these spheres, as seen in figure 4.5. An analysis of the resonance frequency of the spheres when changing the radius and the permittivity has been performed. The resonance frequency of the sphere also changes with the substrate properties, but this variation is negligible. A series of simulations changing the radius and the permittivity were made as seen in figure 4.3.

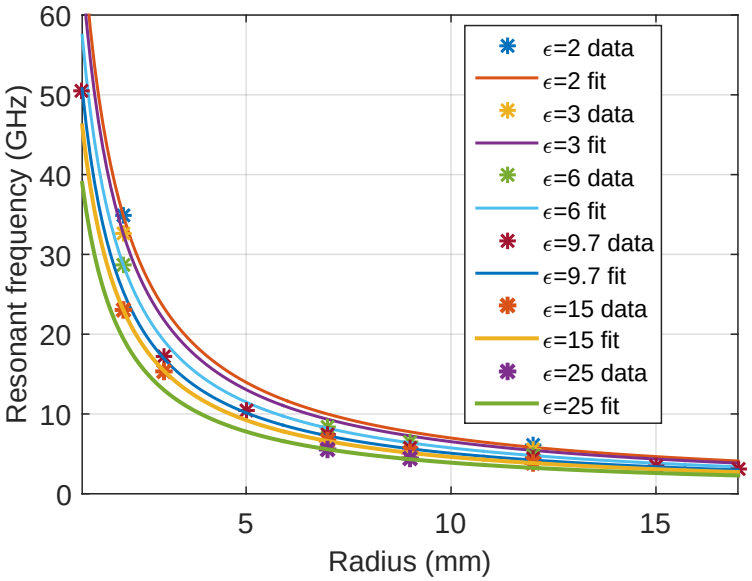

Figure 4.3: *Relationship between the radius and the frequency for different permittivities*

The fit corresponds to a rational function in a way that the product of the radius and the frequency remains constant for each of the permittivities. A relationship between the permittivities and these constants was found in the form of equation 4.3.

$$F(GHz) = \frac{a}{r(mm)\sqrt[b]{\epsilon_r}} \tag{4.3}$$

The fit can be seen in figure 4.4 and the final relationship in equation 4.4.

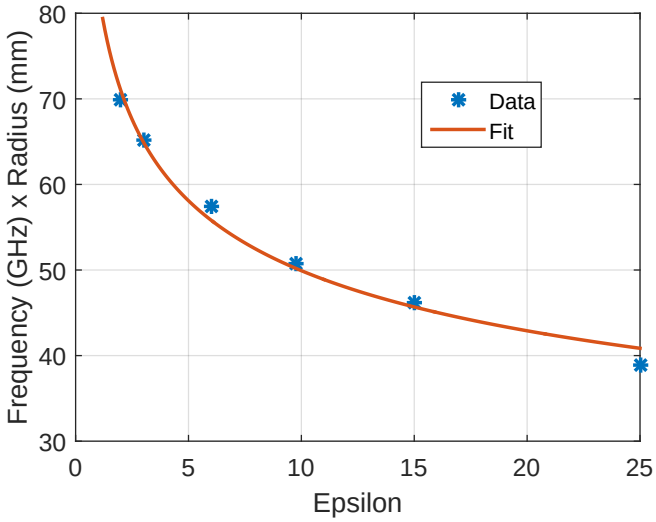

Figure 4.4: *Relationship between the radius and the frequency for different permittivities*

$$F(GHz) = \frac{83}{r(mm)\sqrt[4.6]{\epsilon_r}} \tag{4.4}$$

In this case, the radius of the spheres is 9mm and the permittivity is approximately 9.5, therefore the resonance frequency according to equation 4.4 is about 5.65 GHz. As said before, this equation is just an approximation, since the resonance frequency depends also on other variables.

Other higher-order modes are present at 7.3 or 7.6 GHz as seen in figure 4.5 which represents the frequency response of the sphere when fed with two microstrip lines. Therefore, care must be taken when designing filters because some passbands could appear at these frequencies or superior ones.

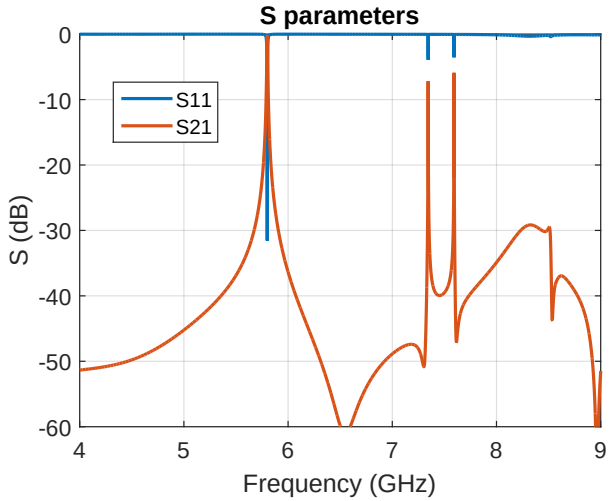

Figure 4.5: *Frequency response of one single sphere* ($\epsilon_r \approx 9.5, r = 9\,\text{mm}$)

To excite the fundamental resonant mode, the sphere should be fed in the x direction using microstrip lines as seen in figure 4.6.

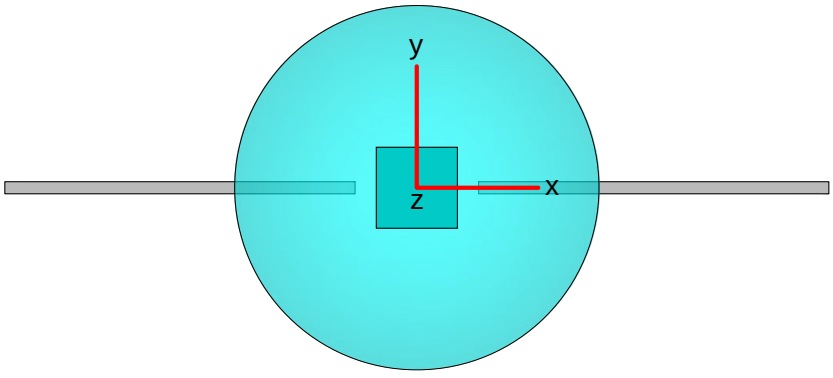

Figure 4.6: *Feeding of the sphere with a microstrip transmission line*

Therefore, the lower metal plane should be a circuit board with dielectric. Also, to place the sphere in the plane with precision, a hole is made in the dielectric. This hole can be a square of side L like in figure 4.7 or circular with diameter L.

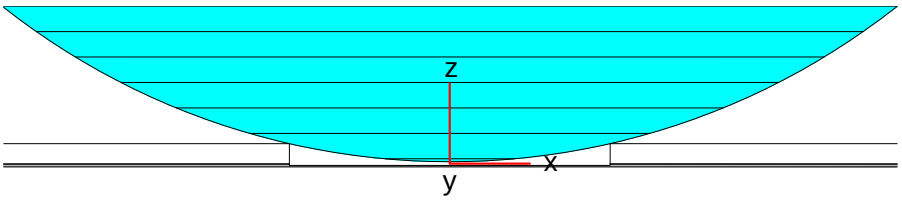

Figure 4.7: *Hole in the dielectric to place the sphere*

The achievable couplings between the line and the sphere (represented by the Q_e's) are limited by physical constrains. The achievable Q_e's are not small enough to obtain useful filters, therefore another coupling method has to be implemented. As explained in [26], the use of a resonant structure that maximizes the electric field near the sphere should produce a much better coupling.

A microstrip $\lambda/4$ resonator like in figure 4.8 has been selected for several reasons. This resonator has less loss than a $\lambda/2$ resonator and occupies less space on the board. The feeding point of the resonator can also be changed to vary the input impedance and therefore the Q_e. Also, the microstrip resonator can be positioned with the maximum of the electric field near the sphere, maximizing the coupling.

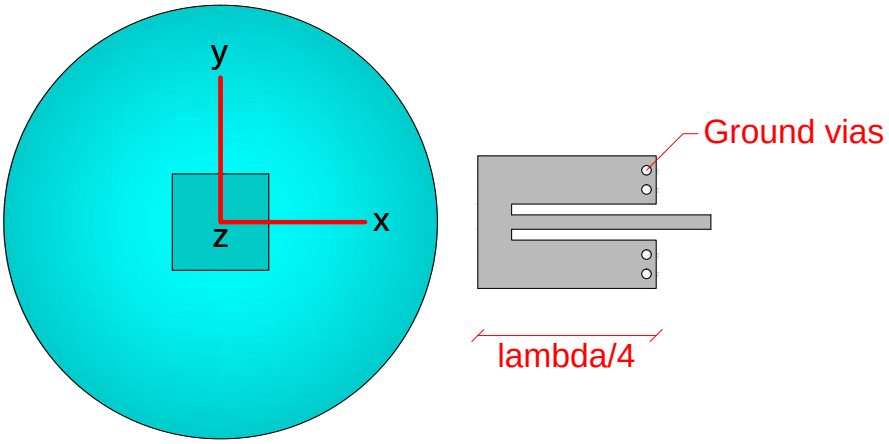

Figure 4.8: *Feeding of the sphere with a microstrip resonator*

This $\lambda/4$ resonator needs a connection to ground. This connection is carried out with four conducting vias.

Filters of more than three poles can be achieved by cascading several spheres. Therefore a 6 pole filter can be made by cascading 4 spheres like in figure 4.9. The

microstrip resonators are used both to couple to the spheres and as resonators of the filters.

The Q_e's of the filter can be controlled varying the feeding point of the microstrip resonators. The k's are divided into two groups: the k_1's between the microstrip resonators and the ending spheres and the k_2's between the spheres. Both of them are controlled varying the distances between the elements as seen in 4.10.

To synthesize a filter, the relationship between these distances and the Q_e and k should be known. In the next sections the determination of these parameters is addressed.

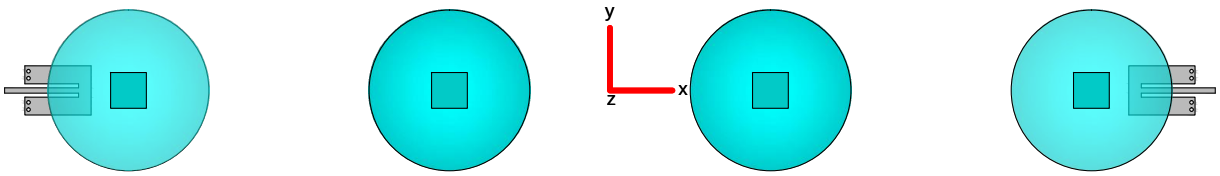

Figure 4.9: *Six pole filter structure*

Some secondary problems arise during the determination of these parameters. The presence of spheres near the microstrip resonators and near other spheres contribute to a small change in the resonance frequency of both spheres and microstrip resonators which should be quantified in order to be compensated. When synthesizing a filter using the network method, each of the resonators should have the same resonance frequency. This problem is addressed in the next sections.

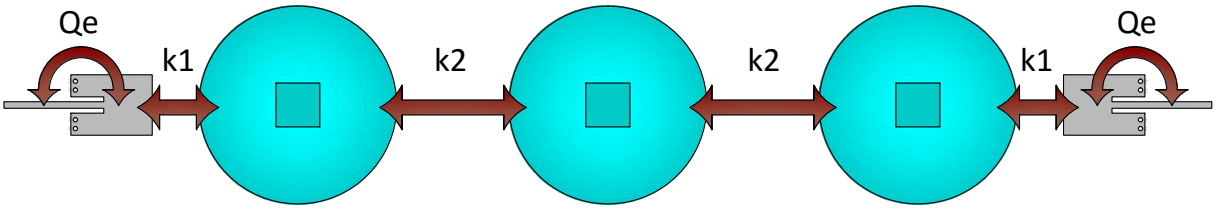

Figure 4.10: *Parameters of a filter with spheres*

4.2 Measurement of important filter parameters

In this section it is explained how the important parameters for synthesizing filters are determined.

4.2.1 Resonance frequency of the sphere

The resonance frequency of a single sphere is easily determined by means of a circuit like in figure 4.6.

The sphere is fed with two lines and a simulation is run. The maximum of the transmission curve coincides with the resonance frequency of the sphere.

4.2.2 Resonance frequency of the microstrip resonator

The resonance frequency of the microstrip resonator can be set varying its length.

It is important for the filter synthesis that all the resonators resonate at the same frequency. The resonance frequency of these resonators varies when they are near a sphere because the dielectric of the sphere varies the electrical length of the resonator making it to appear longer. Also, it varies when the feeding point is changed. To correct this effect, it is necessary to determine this variation.

First of all the length of the resonator is set to resonate at the resonance frequency of a single sphere varying its length.

Secondly, the resonator is simulated at different conditions, varying the distance to the sphere and the feeding point. The sphere cannot be put in its whole because it would present unwanted resonances that could disturb the simulations. Therefore just a small piece of the sphere is simulated as in figure 4.11, just to be a representative piece of dielectric, but not big enough to resonate at a nearby frequency.

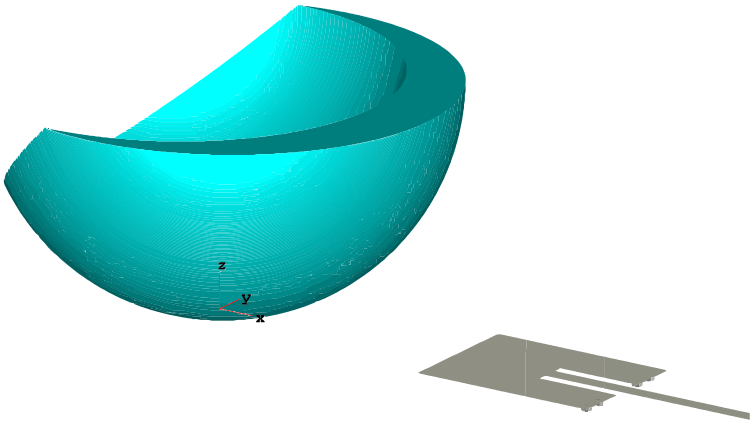

Figure 4.11: *Simulation of the microstrip resonator's resonance frequency with a piece of the sphere*

A set of one port simulations is made varying the gap_1 and the l_square_2 parameters as seen in figure 4.13 and the resonance frequency is measured for each case. A plot of this is represented in figure 4.12.

To correct the resonance frequency to a new one f_obj, the length of the resonator should be varied accordingly as it is inversely proportional to the resonance frequency.

$$L\_resonator\_new = L\_resonator\_old \cdot \frac{f\_reson}{f\_obj} \tag{4.5}$$

The length of the resonator is a magnitude complex to measure, because the exact position of the short circuit with the vias is not precisely known as the vias introduce

parasitic effects that change the effective length of the resonator. The length of the resonator is taken as:

$$L\_resonator = L\_stub - 3 \cdot r\_vias \tag{4.6}$$

Therefore the new l_stub would be:

$$L\_stub\_new = (L\_stub\_old - 3 \cdot r\_vias) \cdot \frac{f\_reson}{f\_obj} + 3 \cdot r\_vias \tag{4.7}$$

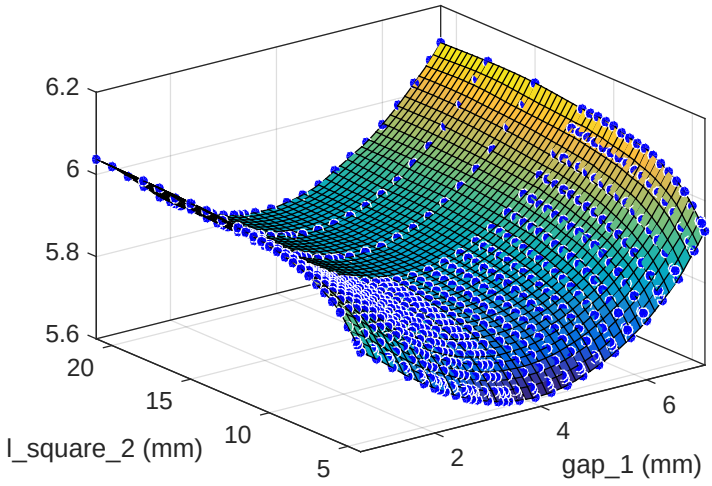

Figure 4.12: *Resonance frequency of the microstrip resonator as a function of the distance to the sphere (l_square_2/2) and the feeding point (gap_1)*

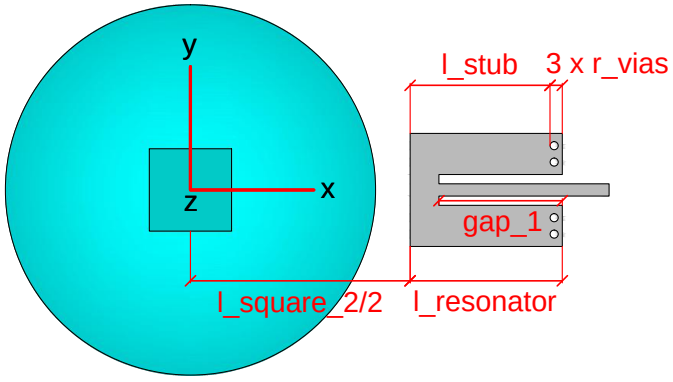

Figure 4.13: *Detail of the varied l_square_2/2 and gap_1*

4.2.3 Coupling between spheres

The method to measure the k for symmetric resonators explained in section 3.2.1 is used to determine the coupling (k_2) between spheres. This method needs the Q_0 and Q_e of the

spheres to be large enough. Therefore the circuit in figure 4.14 is simulated without losses (obtaining a high Q_0) and the spheres are fed using open-ended microstrip lines (which produce large Q_e's) to warranty the accuracy of the measurements.

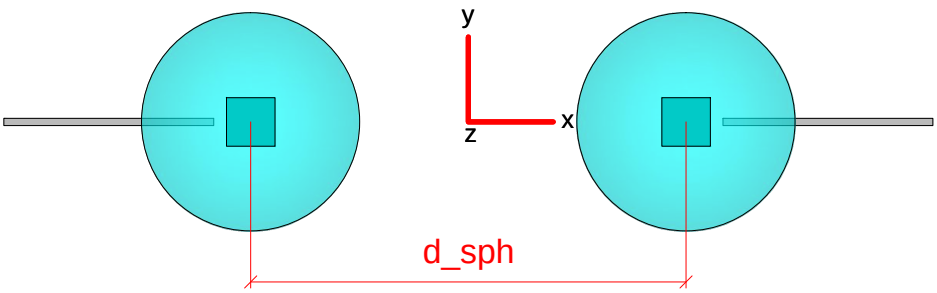

Figure 4.14: *Circuit used to measure the coupling between spheres and detail of the varied d_sph.*

Two spheres are fed with two lines and their separation distance is changed varying the parameter *d_sph* as seen in figure 4.14. The k and the resonance frequency of each sphere are measured obtaining responses like in figure 4.15. With this, two graphs are obtained, represented in figures 4.16 and 4.17.

Also an exponential fit of the curve is carried out to compute the k and resonance frequencies more efficiently.

The resonance frequency of the spheres varies but not much, so this effect is ignored.

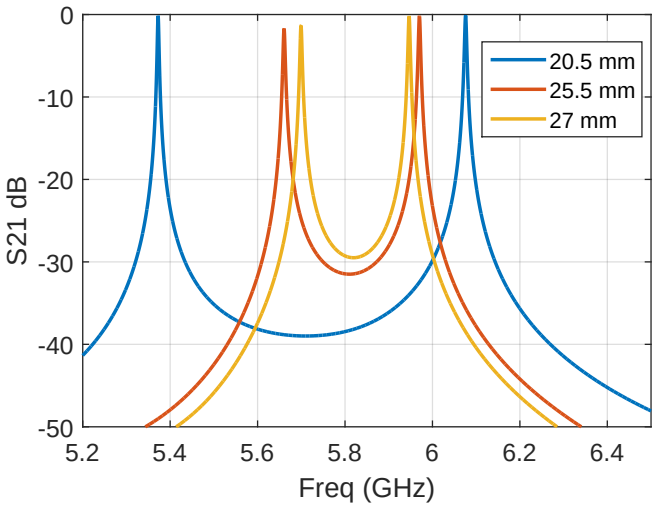

Figure 4.15: *S21 parameter of two spheres fed by microstrip lines varying the distance between their centers d_sph*

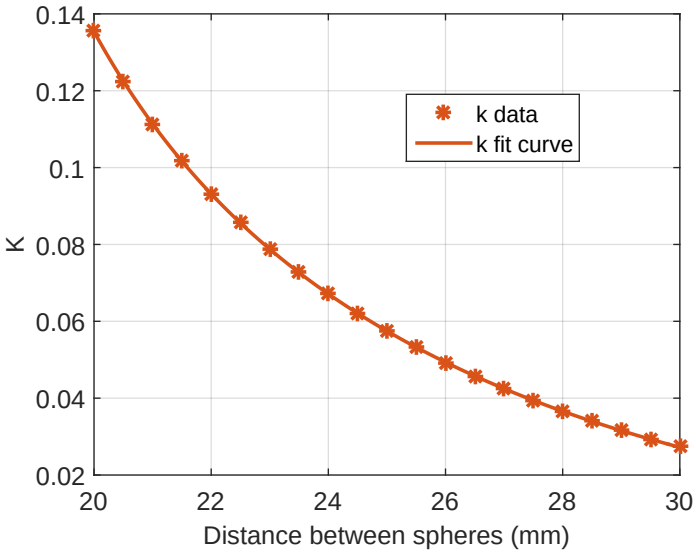

Figure 4.16: *k_2 parameter between two spheres as a function of the distance between their centers*

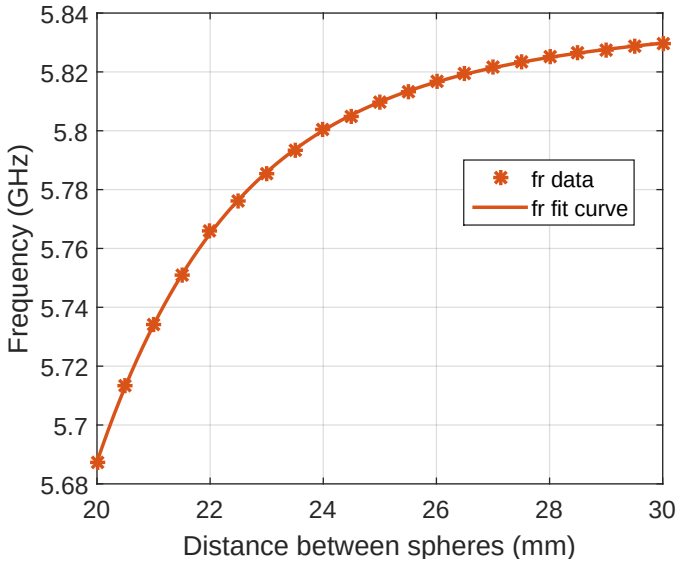

Figure 4.17: *Resonance frequency of two spheres as a function of the distance between their centers*

4.2.4 External quality factor of the microstrip resonator

The determination of the Q_e of the microstrip resonator is carried out using the method described in section 3.2.2.

The circuit in figure 4.11 is the one used to simulate the Q_e varying the parameter *gap_1* as seen in figure 4.19. Graphs like the ones in figures 4.18a and 4.18b are obtained.

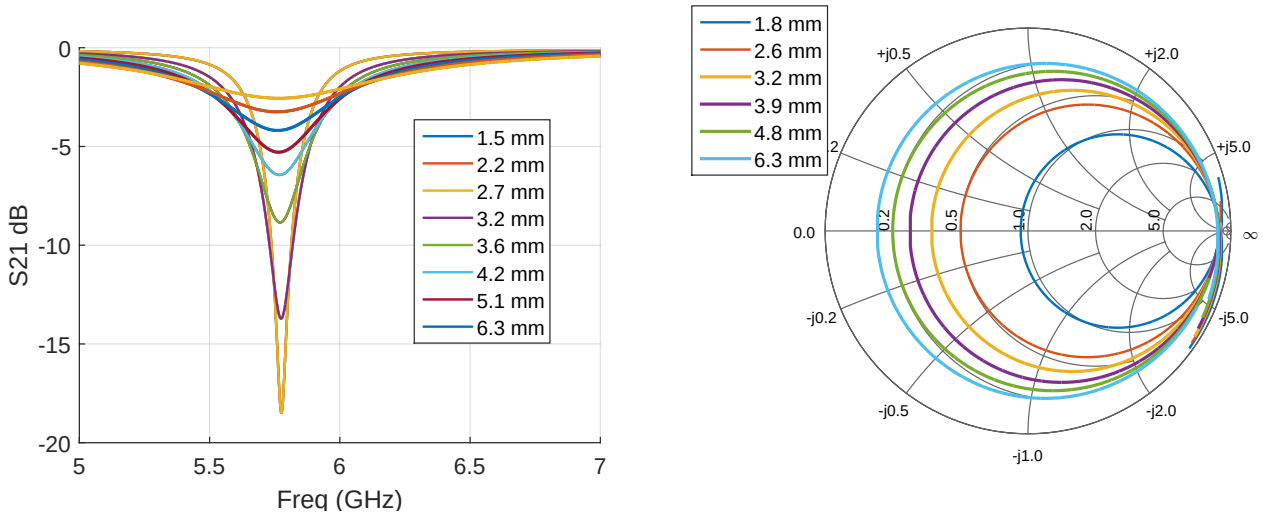

(a) (b)

Figure 4.18: *S11 parameter of the microstrip resonator fed by a microstrip line varying the parameter gap_1. (a) dB units. (b) Smith chart.*

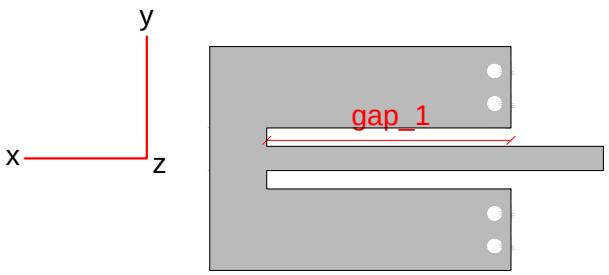

Figure 4.19: *Detail of the varied distance gap_1*

A sliced sphere has been added in order to check its influence in the Q_e when the parameter *l_square_2* is changed. Also losses have been added to the resonator, since a one port measurement of the Q_e is not possible without losses.

The important parameter to change the Q_e is *gap_1*. Q_e can be altered varying this parameter. Also the resonance frequency of the resonator changes when this parameter is varied. Therefore a recurrent algorithm is used in order to obtain both the desired *gap_1* and the desired resonance frequency of the resonator.

A study of the sensitivity of the Q_e to the parameter *l_square_2* is performed with the developed algorithm. Variations of the *l_square_2* parameter, keeping constant the *gap_1* parameter, are made for different *gap_1* values.

Figure 4.20 shows that the dependence is of no significance when the *gap_1* is large enough. That means that it only causes significant variations when the feeding point of the

resonator is near the short circuit. All the filters with usable ripples have a feeding point that is not near the short circuit, therefore, the Q_e has been considered to be independent of the *l_square_2* parameter.

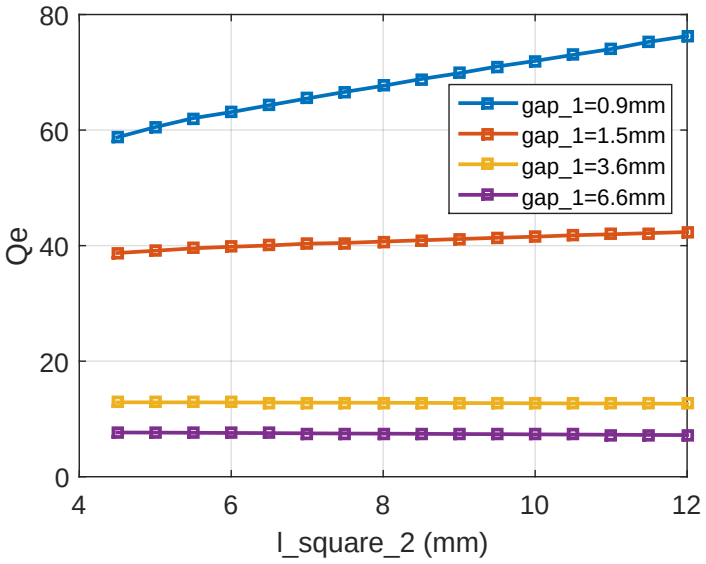

Figure 4.20: *Q_e of the microstrip resonator as a function of gap_1 for different l_square_2*

A study of the sensitivity to the f_obj has also been carried out. The Q_e is expected to change with the target resonance frequency of the resonator. This is because the feeding point should be placed at the same electrical point, not at the same physical point. Therefore, the *gap_1* should not be kept constant, but it should vary to match the intended electrical length.

Figure 4.21 shows an illustration of these effects, both corrected and uncorrected. In the uncorrected case, the *gap_1* parameter is kept constant when varying the length of the resonator, and in the corrected case, the electrical length of *gap_1* is kept constant. It can be seen that even though the frequency variation effect is not significant, it can be corrected.

At this point there are two effects present: *l_square_2* and f_obj. The first one is negligible and the second one can be corrected. Nevertheless, there exist also a third effect. As it was stated in this methods description: the more similar the Q_0 and the Q_e are, the more precise the measurement of the Q_e is.

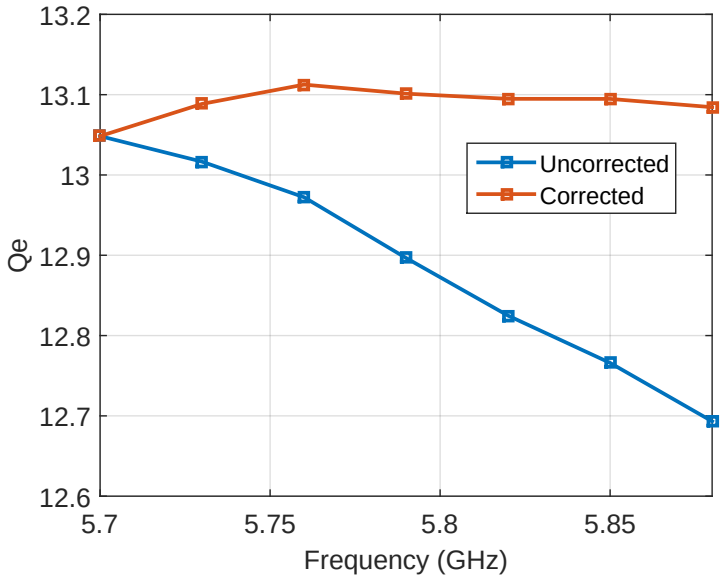

Figure 4.21: Q_e *of the microstrip resonator as a function of gap_1 for different f_obj*

A metal conductivity is selected so that the Q_e and the Q_0 are similar at a typical *gap_1* (which is close to 2 mm for the filters that are being simulated). The conductivity in that case is $5.8 \cdot 10^5\,\mathrm{S\,m^{-1}}$, about 1 % of copper conductivity. The resonator is simulated at an arbitrary distance from the sphere (it does not matter since it has a small influence) and changing the *gap_1* parameter results in a graph as shown in figure 4.22.

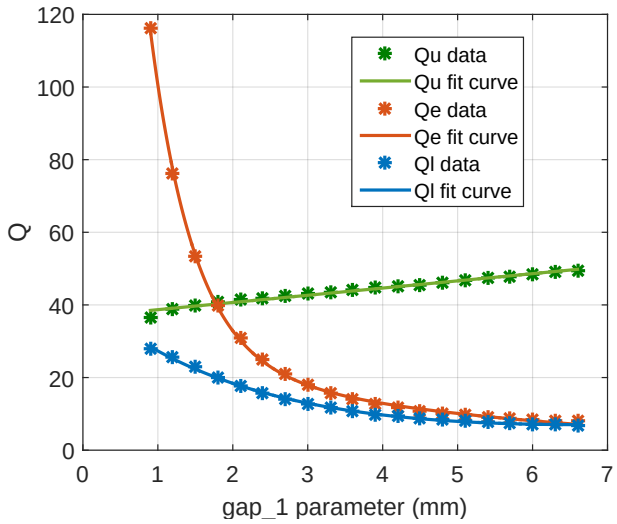

Figure 4.22: Q_e, Q_u *and* Q_l *for the resonator for different gap_1*

The Q_l is a combination of the other two quality factors. The Q_u is observed to be very stable, changing its value very little with the variation in the feeding point. The Q_e on the contrary depends exponentialy on this parameter. Values of Q_e lower than 7 are very difficult to obtain.

Figure 4.22 has been generated for a certain f_obj, which is the resonance frequency

of a single sphere. The *gap_1* for other f_obj can be calculated using equation 4.8.

$$gap\_1\_new = gap\_1\_old \cdot \frac{f\_obj}{f\_obj\_new} \tag{4.8}$$

4.2.5 Coupling between the microstrip resonator and the sphere

The determination of the coupling parameter k_1 between the microstrip resonator and the sphere is also carried out using the method described in section 3.2.1 using the circuit seen in figure 4.23. The Q_u and the Q_e of the resonators are selected to be high. Therefore the sphere and the microstrip are considered lossless. The sphere is fed with a line, which produces a high Q_e and the microstrip resonator is fed close to the short circuit, producing also high Q_e's. This is important in order to improve the accuracy of the method, as explained in the precedent sections.

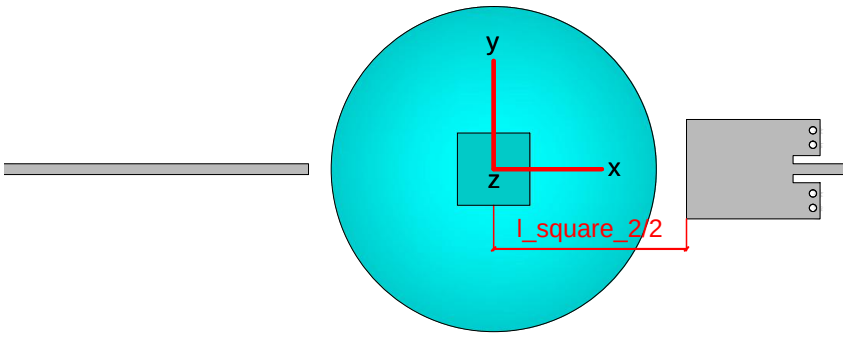

Figure 4.23: *Circuit used to measure the k_1 and detail of the distance l_square_2/2.*

The distance between the resonator and the sphere is changed varying the parameter *l_square_2* as seen in figure 4.23. Also the length of the resonator has to be varied accordingly to keep the resonance frequency constant and equal to the resonance frequency of the sphere.

Several simulations are carried out resulting in the graph in figure 4.24.

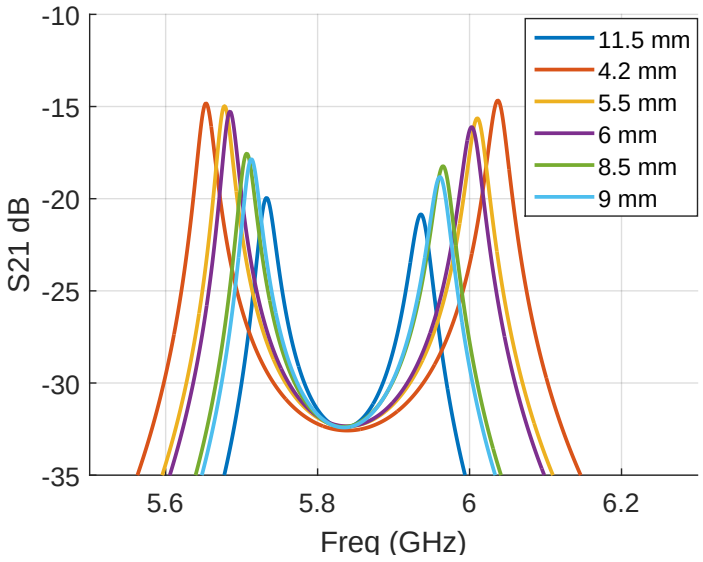

Figure 4.24: *Simulation of the resonator and the sphere varying their distance l_square_2/2*

A graph with the k_1 is shown in figure 4.25 where an exponential fit of the curve is made. The coupling achieved in this case is lower than in the case of k_2 seen in figure 4.16.

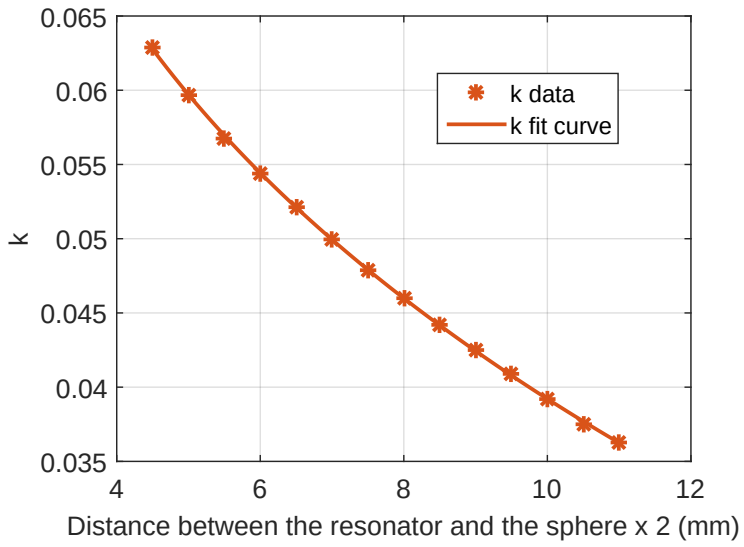

Figure 4.25: k_1 *as a function of l_square_2*

4.3 Achievable filters

Knowing the physical limitations of the filters and the equivalences between the filter parameters and the physical dimensions, a graph with all the achievable filters can be

made. These graphs represent the achievable bandwidths and ripples for different filter orders. A graph for order 4 filters can be seen in figure 4.26.

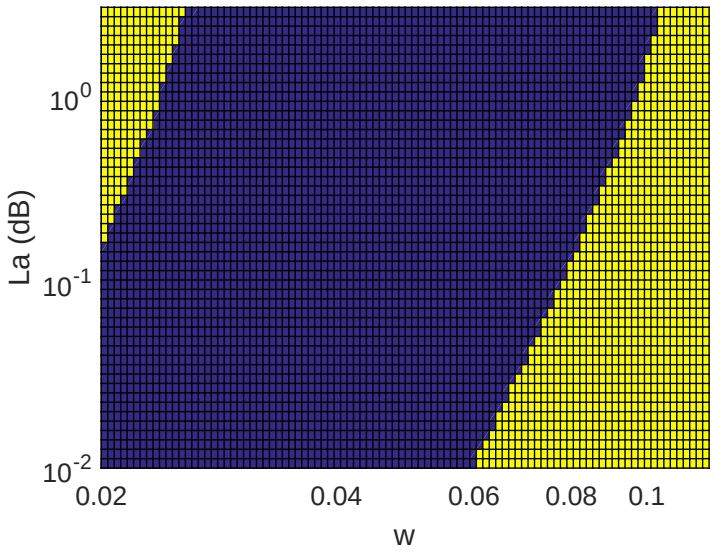

Figure 4.26: *Achievable filters of order 4. The blue zones represent achievable filters, the yellow zones are not physically possible.*

The blue zones represent the achievable filters and the yellow zones represent filters which require physical parameters out of range. The left yellow zone that appears in the graph corresponds to three effects: *d_sph* bigger than simulated, *l_square_2* bigger than simulated and *gap_1* smaller than simulated. The two first effects are not a problem, because these distances can be enlarged as much as desired, therefore there exist no limitation. The third effect appears only as a limitation when the required ripples are two big; so big that they are not considered as useful filters. Therefore the left yellow zone is not considered as a limitation in the filter synthesis.

On the other hand, the right yellow zone is delimited by two constraints: *l_square_2* smaller than simulated (which means high k_1) and *d_sph* smaller than simulated (meaning high k_2). These parameters have been simulated to their limits: it is not possible to make them smaller, therefore this is a real physical limitation of these kind of filters.

A double logarithmic graph with this limit is shown in figure 4.27. It details the minimum achievable ripple for each filter's bandwidth for several filter orders.

The bigger the order is, the more filters can be achieved. Nevertheless, little improvement in the achievable ripple can be expected from an increment in the order while the size of the filter gets significantly large.

Normally there also exist space constrains in filter design. The length of this filter varies with the order, with the bandwidth and with the ripple. Figure 4.28 shows a graph of the different lengths for 4 order filters. The filters get longer as the bandwidth is decreased and/or the ripple is increased.

Figure 4.28 representing the length of the filters, figure 4.27 representing the minimum achievable ripple and figure 3.2 representing the out of band attenuation help to determine

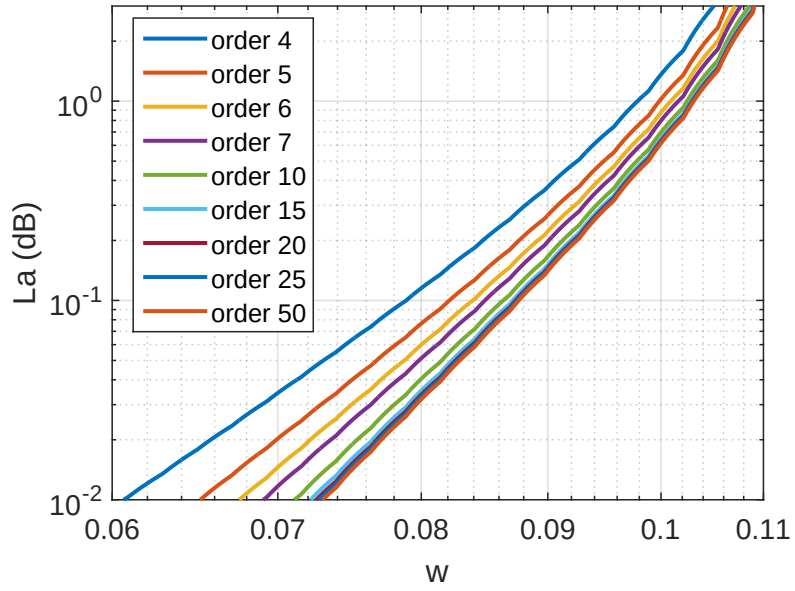

Figure 4.27: *Minimum achievable filter ripple for different filter orders*

if certain filter specifications can be physically reached.

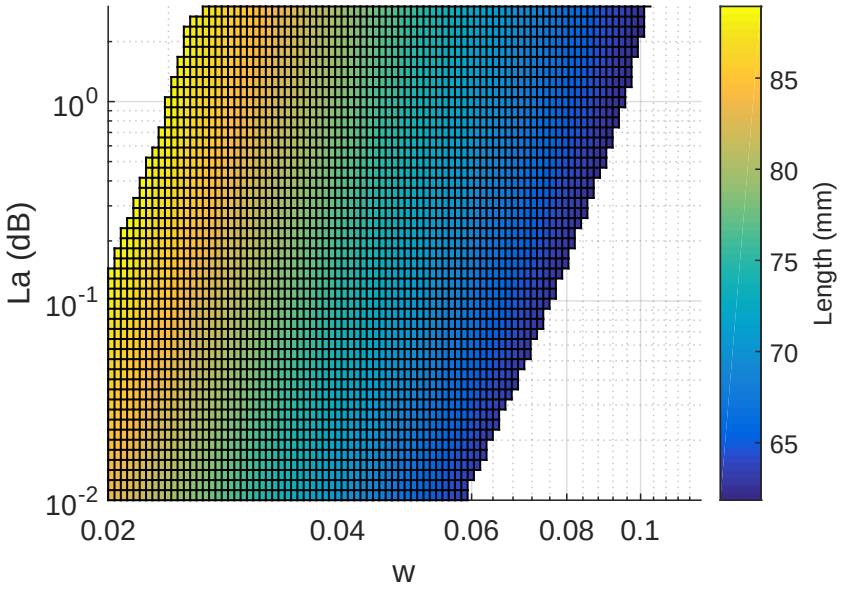

Figure 4.28: *Order 4 filters length*

More graphs can be seen in appendix E.

4.4 Filter examples

With all the information obtained in the precedent sections, filters of different ripples and bandwidths can be simulated to test the accuracy. Two filter example responses and layouts are depicted in figures 4.29 and 4.30.

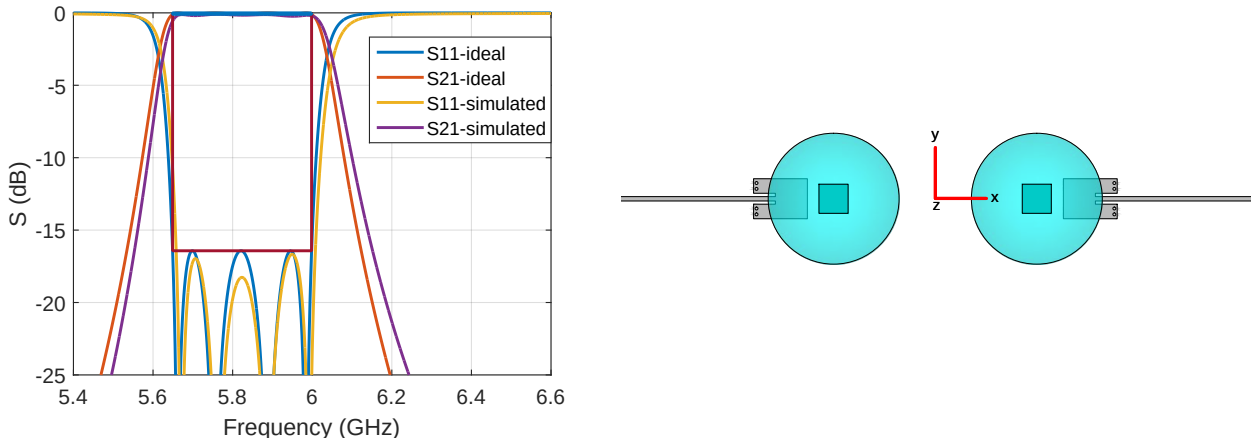

(a) (b)

Figure 4.29: *Filter of order 4, 0.1 dB ripple and 6 % bandwidth. (a) Response. (b) Layout*

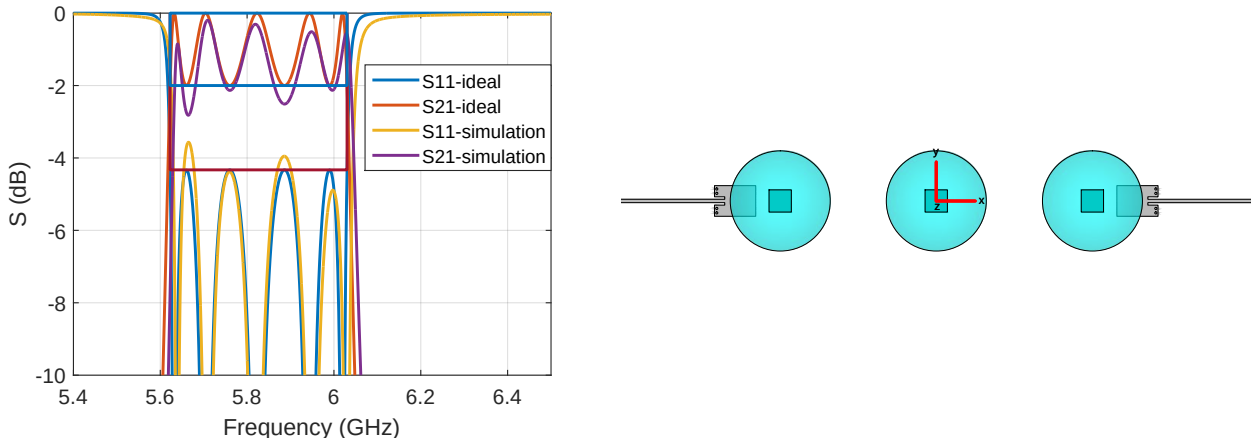

(a) (b)

Figure 4.30: *Filter of order 5, 2 dB ripple and 7 % bandwidth. (a) Response. (b) Layout*

In these figures, the blue and red lines represent the ideal Chebyshev filter obtained using the equations. The yellow and purple lines represent the simulated filter with the spheres. The specification masks are also depicted, the S11 mask in red and the S21 mask in blue.

Very good agreement between the simulated and expected results is seen. More simulated filters can be found in appendix A.

As seen before, the spheres have higher-order resonance modes. These modes can produce passbands in the filter at higher frequencies. In consequence, the decay of the

out-of-band transmission curve of the filter is not as pronounced as the ideal one. In figure 4.31, these passbands can be appreciated.

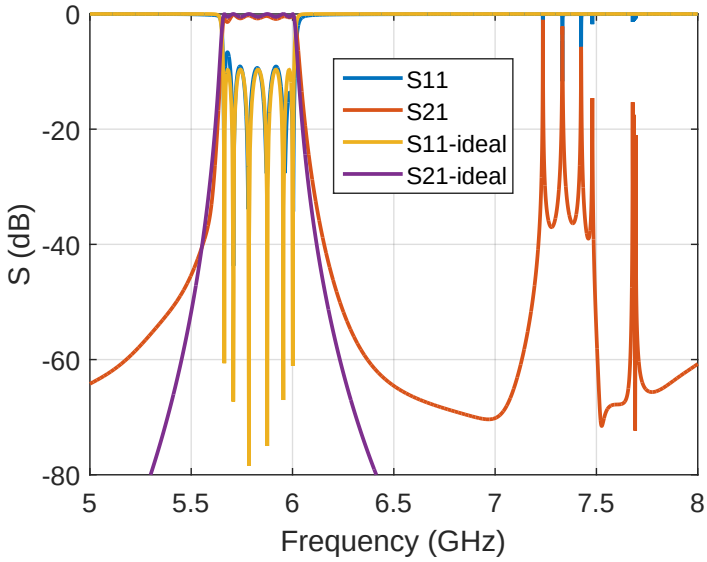

Figure 4.31: *Filter of order 6, 0.5 dB ripple and 6 % bandwidth response including superior passbands and ideal response*

4.5 Automation of the process

The filter creation process is automated and is described in appendix G. The values of the parameters are inserted into a txt file. The program builds all the necessary CST files and starts simulating all of them in order, making sweeps of the important parameters. First, the resonance frequency of a single sphere is determined, secondly, the k_2 between two spheres, then, the resonance frequency of the microstrip resonator for different distances and feeding points is simulated, then, the k_1 between the sphere and the resonator is calculated, and lastly, the Q_e of the resonator is measured for different feeding points.

When all the parameters are extracted from the simulations, the image of the possible filters for different orders can be extracted. Then, some filter examples are simulated and compared to the ideal ones obtained using the Chebyshev equations to check the accuracy of the simulations. Finally a report of the filter is generated automatically with all information.

This automatic process can also be used to evaluate the performance of the filters for other resonator topologies or dimensions, other dielectric constants, other sphere diameters (and therefore other frequency bands) or other substrate thicknesses.

4.6 Power loss

Until now, only lossless filters have been simulated. All the power loss is due to radiation of the filter, not to material loss. In this section, material loss is studied.

It is desirable to estimate the loss of a filter. According to [29], the midband insertion loss of a filter can be estimated with equation 4.9.

$$L_0 = 4.343 \frac{w_1'}{w} \sum_{i=1}^{n} \frac{g_i}{Qu_i} \text{dB} \tag{4.9}$$

Where w1' is the bandwidth of the low pass equivalent circuit (in our case 1), w is the relative bandwidth of the simulated filter, and g_i and Q_{ui} are the g coefficient and quality factor of resonator i.

The Q_u of the resonators is determined with the impedance method. One port lossy simulations are performed to each resonator and the Q_u's are obtained.

The losses of the line should be taken into account for a more accurate result. To do so, a simulation of one single line is performed and the complex propagation constant is extracted. With this information for each frequency of interest, the S parameters of the lines can be determined for any arbitrary length.

The Q_u's are seen in table 4.1.

Table 4.1: Q_u values of the resonators

Q_u sphere	≈6000
Q_u microstrip resonator	≈115

The Q_u of the microstrip resonator depends very little on the *gap_1* parameter, as seen in image 4.22 (in that case it depends more because the conductivity of the metal has been highly decreased). Nevertheless, a sweep of this parameter is performed in figure 4.32. The value expressed in table 4.1 is taken as an approximate Q_u.

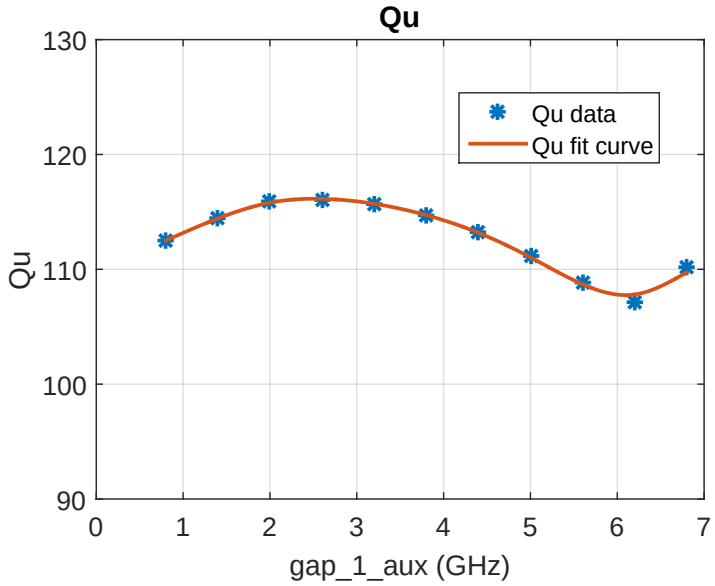

Figure 4.32: Q_u *of the microstrip resonator varying its feeding point*

It is seen that the losses are mainly caused by the microstrip resonator, therefore

equation 4.9 can be simplified:

$$L_0 = \frac{4.343}{w \cdot Q_{u-micro}} \cdot (g_1 + g_n)\,\mathrm{dB} \tag{4.10}$$

With this formula, the loss of each filter is estimated. The loss of the transmission lines should also be taken into account in the simulations.

In figure 4.33 the attenuation for different order 4 filters is calculated in dB units. It is seen that the power loss increases when decreasing the bandwidth and/or increasing the ripple of the filter. More graphs for different orders are given in appendix F. In figures 4.34 and 4.35 two filters have been simulated with attenuation. Also the expected ideal results are included. More simulated lossy filters can be found in appendix B.

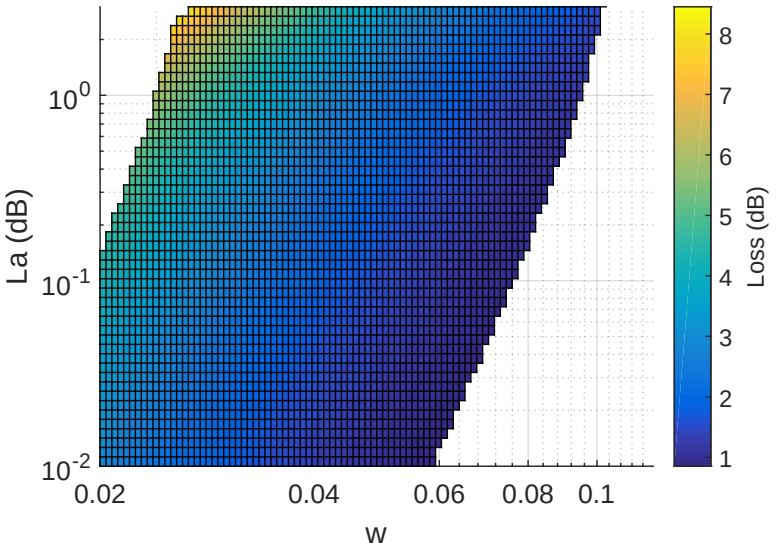

Figure 4.33: *Power loss of a 4 order filter*

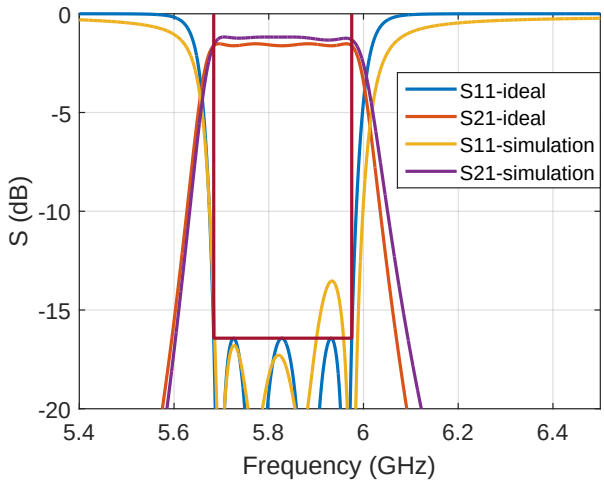

Figure 4.34: *Lossy filter of order 4, 0.01 dB ripple and 5 % bandwidth response*

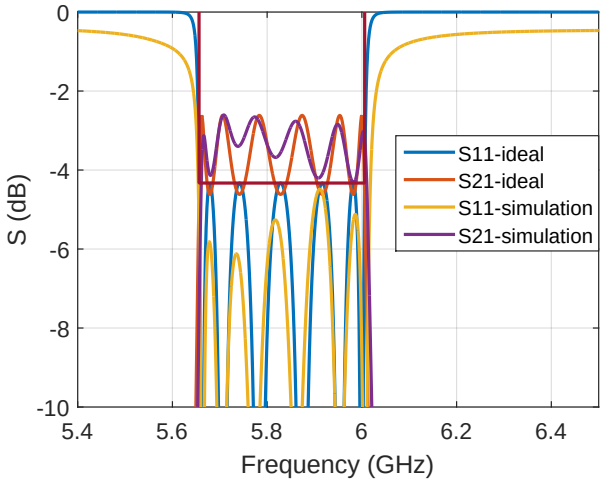

Figure 4.35: *Lossy filter of order 6, 2 dB ripple and 6 % bandwidth response*

4.7 Overcoupling of the spheres

The ending microstrip resonators are an excellent way to couple to the sphere. Nevertheless, they are the main source of loss in the filter. One of the main reasons of doing filters with dielectrics is that they introduce a low amount of loss. Regarding this matter, the introduction of these microstrip resonators is counterproductive.

This section explains that there exist combinations of Q_e and k that allow an extremely strong coupling from the microstrip resonator to the sphere and that causes them not to be part of the filter.

4.7.1 Equivalent circuits

Equations 4.11 and 4.12 show how to obtain the ripple and the bandwidth of a filter knowing the couplings and external quality factors for order 2 and order 3 filters.

$$L_a = 17.37\text{acoth}\left\{\exp\left(4 \cdot \text{acoth}(kQ_e)\right)\right\}\,\text{dB} \tag{4.11}$$

$$L_a = 17.37\text{acoth}\left\{\exp\left(6 \cdot \text{asinh}\sqrt{\frac{3}{8Q_e^2k^2 - 4}}\right)\right\}\,\text{dB} \tag{4.12}$$

With these equations and equation 3.2, the information about the bandwidth for each order is extracted.

The condicions defined in equations 4.13 and 4.14, lead to $La \leq 0\,\text{dB}$. It has been tested experimentally that these conditions lead to filters of reduced order as seen in figure 4.36. In this figure three order 2 filter responses are shown maintaining the $Q_e = 50$ and varying the k with three values: 0.05, 0.02 and 0.01. The second and the third filter are overcoupled since they fulfill the condition stated in equation 4.13.

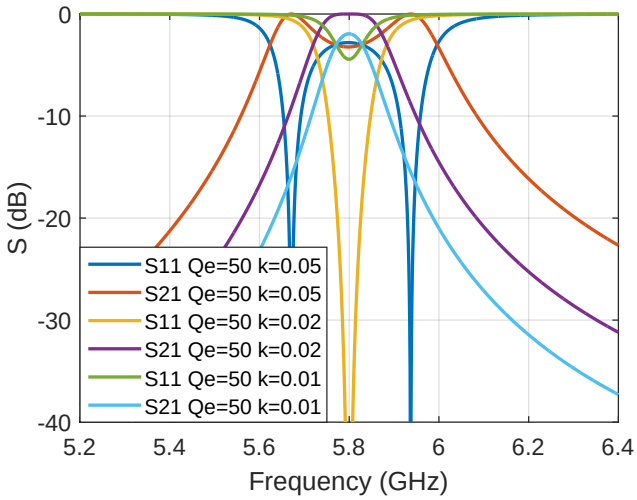

Figure 4.36: *S parameters response of three order 2 filters varying the k*

$$kQ_e \leq 1 \tag{4.13}$$

$$kQ_e \leq \frac{\sqrt{2}}{2} \tag{4.14}$$

The limits for higher orders can be computed calculating the limit of equations 3.2 when the ripple approaches to 0 dB.

Three lumped element filters were simulated, one of order 2 and two of order 4 to check the equivalence. The values of the order 2 filter were computed using the equations to obtain a ripple of 0.5 dB and a bandwidth of 6 %. The values of the order 4 filters were selected experimentally to fit the order 2 module response as faithfully as possible. The values can be consulted in table 4.2 and the response of each filter in figures 4.37a and 4.37b.

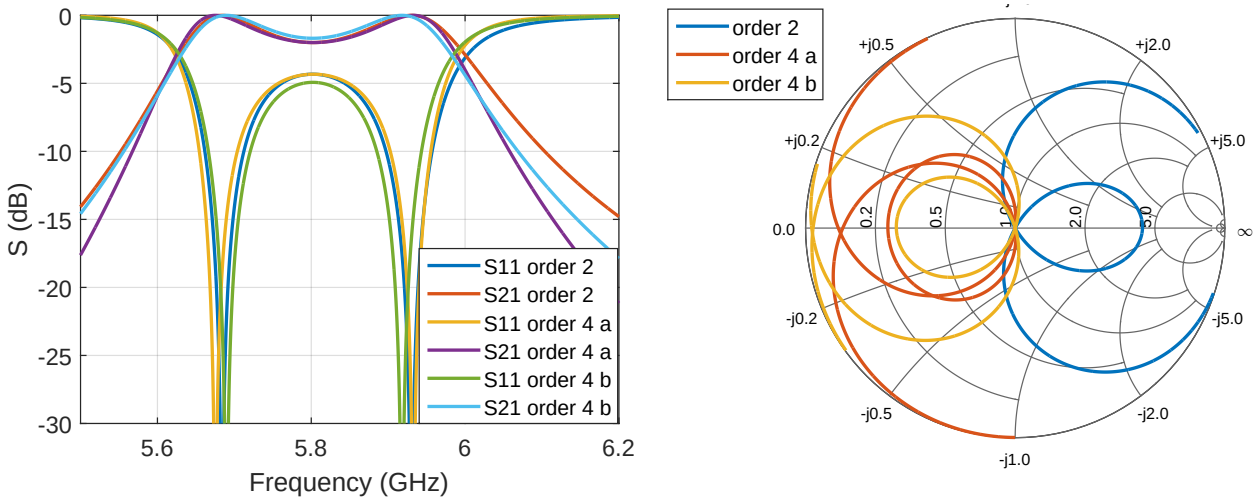

(a) (b)

Figure 4.37: *S parameter response of equivalente filters with different number of resonators. (a) dB units. (b) Smith chart.*

Table 4.2: Equivalence between filters of different orders with and without overcoupling of the ending resonators

	Order 2	**Order 4 a**	**Order 4 b**
Q_e	41.47	7.03	3
k_1	0.0488	0.0549	0.0867
k_2	-	0.0429	0.0429

It is seen in figure 4.37a that the magnitude response of the filters of order 4 a and b are similar to the one of order 2. On the other hand, the phase is quite different as seen in 4.37b. The order 4 b filter phase is more similar, but has a 180° shift in comparison with the order 2 filter. It can also be appreciated that the bigger the k_1 of the order 4 filter is and the smaller the Q_e is, the better the responses fit.

Equation 4.15 has been extracted experimentally for the calculation of the Q_e and k when the Q_e is low enough and the equivalence has been sketched in figure 4.38.

$$k_{\,\mathrm{n+2}}\sqrt{Q_{e,\,\mathrm{n}}Q_{e,\,\mathrm{n+2}}} = 1 \text{ for } Q_{e,\,\mathrm{n+2}} \to 0 \tag{4.15}$$

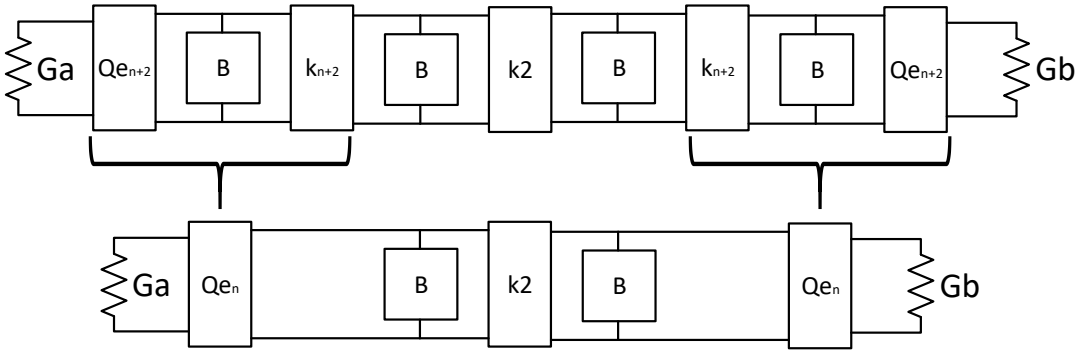

Figure 4.38: *Equivalence between an order 2 filter with overcoupling (above) and normally synthesized (below) using equation 4.15*

This formula is precise when the Q_e of the overcoupled filter is low enough. When the Q_e increases, it produces a filter with the expected ripple but with more bandwidth. Therefore a correction can be made in the bandwidth of the non-overcoupled filter to decrease it. By doing it several times in an iterative process, the overcoupled filter can have the expected bandwidth.

This has been tested using an order 2 filter, with 0.5 dB ripple and 6 % bandwidth. Using equations 3.15, 3.2 and 4.15, the values of the Q_e and k can be extracted for the non-overcoupled and the overcoupled filters. When choosing a Q_e of 8 for the overcoupled filter, the values can be consulted in table 4.3. It is seen that the correction in the bandwidth of the initial filter is 0.76 to obtain the desired bandwidth in the overcoupled filter. With this value, the bandwidth of the order 2 filter is corrected and the order 4 values are calculated again.

Table 4.3: Equivalence between filters of different orders with and without overcoupling while correcting the bandwidth

	Order 2	**Order 4 formula**	**Order 2 corrected**	**Order 4 formula corrected**
Q_e	23.3824	8	30.80	8
k_1	0.0602	0.07312	0.0457	0.0637
k_2	-	0.0602	-	0.0457

Figure 4.39 shows the response of the ideal order 2 filter and the order 4 corrected filter. It is seen that they have now similar bandwidth and ripple. The overcoupled filter nevertheless has a better out of band attenuation, because it has in reality 4 resonators.

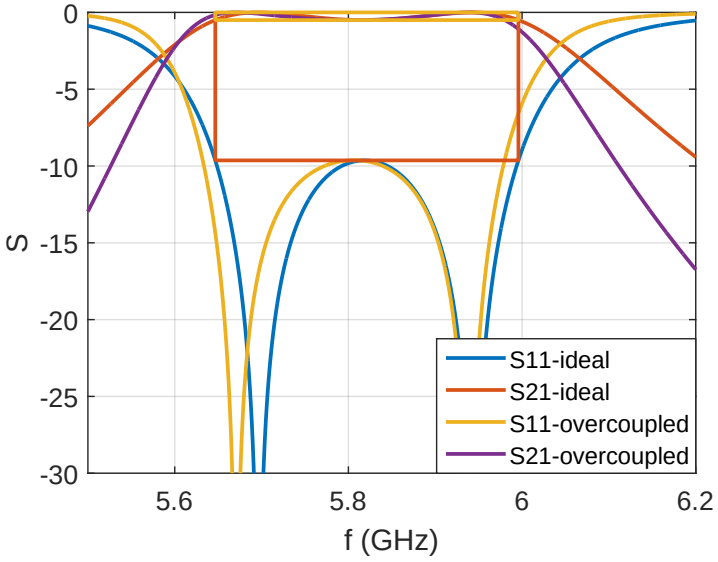

Figure 4.39: *S parameters response of an order 2 filter and its order 4 overcoupled equivalent filter*

Equation 4.15 shows that there is an infinite number of combinations of $Q_{e\text{ order n+2}}$ and $k_{\text{order n+2}}$ that produce the same equivalent $Q_{e\text{ order n}}$. Nevertheless low values of $Q_{e\text{ order n+2}}$ are desirable to obtain a good approximation with equation 4.15. Also the conditions expressed in equations 4.13 and 4.14 or the equivalent condition corresponding to the filter order must be fulfilled to obtain overcoupling. Finally, the values of $Q_{e\text{ order n+2}}$ and $k_{\text{order n+2}}$ should be physically achievable with the spheres. Therefore, the process to synthesize this filters starts trying with the lowest achievable Q_e for the spheres and check if all the other conditions are fulfilled; if all of them are fulfilled, the correction is applied and the filter is synthesized, if not, a bigger Q_e is tried until the filter is realizable or until the Q_e's do not produce overcoupling.

To illustrate the differences between the ideal Chebyshev filter, the normal and the overcoupled one using spheres, an order 6 filter with 0.5 dB ripple and 5 % bandwidth is simulated. The differences in a lossless scenario are shown in figure 4.40. In figure 4.41, the layouts of the normal and the overcoupled filters are represented. It is seen that in the overcoupled filter, the microstrip resonator is very near the sphere (obtaining a big k_1) and the *gap_1* parameter is as large as possible (leading to a small Q_e).

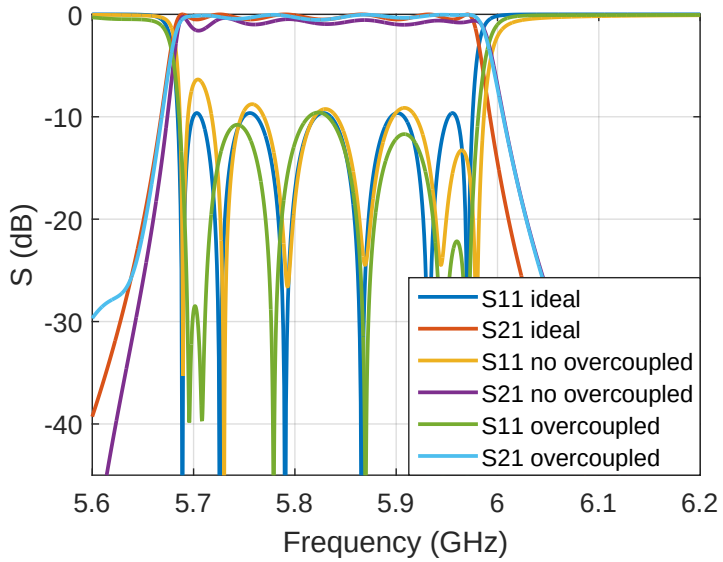

Figure 4.40: *S parameters response of an order 6 filter with 0.5 dB ripple and 5 % bandwidth, including the ideal response, the simulated without overcoupling and the simulated with overcoupling*

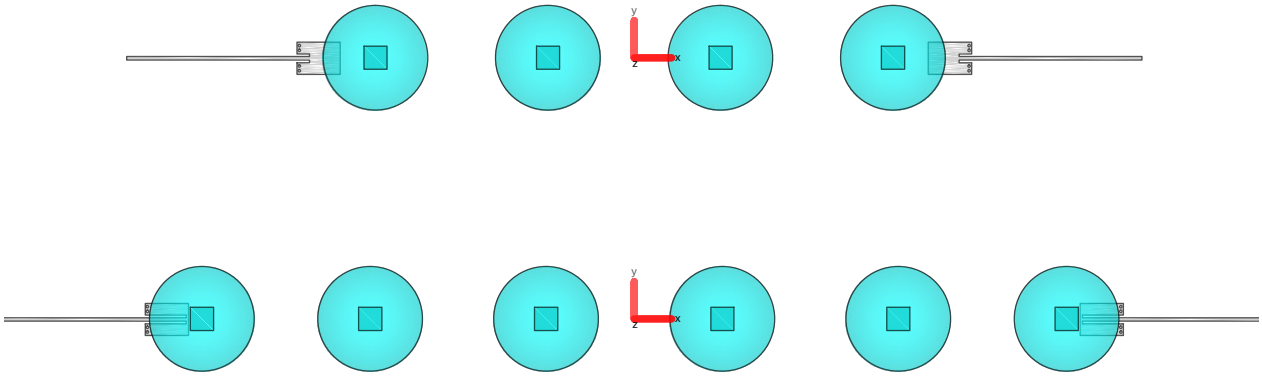

Figure 4.41: *Layouts of order 6 filters with 0.5 dB ripple and 5 % bandwidth. Above no overcoupled layout, below overcoupled layout*

It is seen that the responses of the filters are similar in this lossless case. Nevertheless, both filters can be simulated with loss. In figure 4.42a it is seen that the S11 parameter of the filters are similar. Nevertheless, the S21 parameter changes a lot.

In figure 4.42b, a detail of the S21 parameter of the ideal, the overcoupled and the normal filter lossy responses is appreciated. It is seen that while the filter without overcoupling has a 2.1 dB loss in the band pass, the overcoupled filter achieves a loss of less than 1 dB.

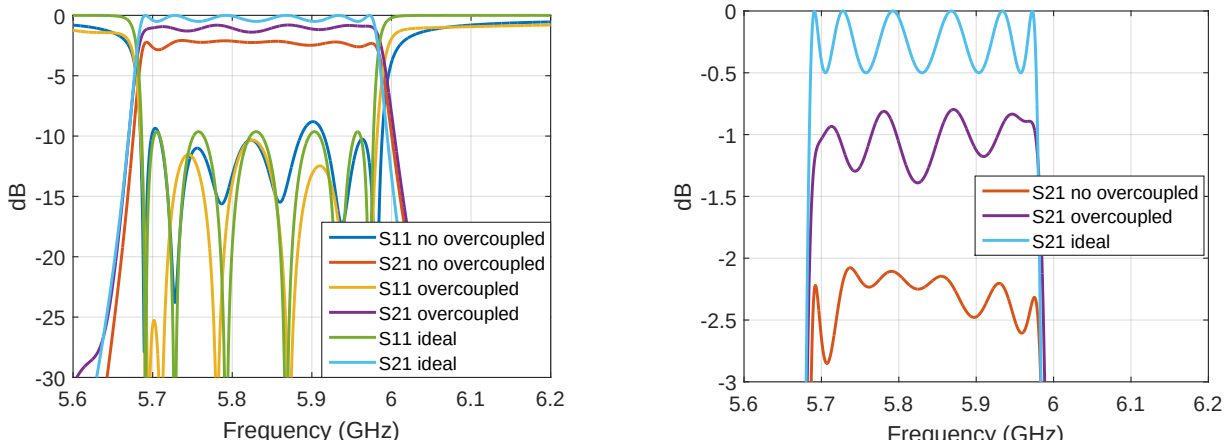

(a) (b)

Figure 4.42: *S parameters of an order 6 filter with 0.5 dB ripple and 5 % bandwidth, including the ideal response, the simulated without overcoupling and the simulated with overcoupling with losses. (a) S parameters. (b) S21 detail.*

It is therefore extremely advantageous to use the overcoupled filters in scenarios where avoiding loss is important.

More figures of filters with overcoupling are found in appendix C.

4.8 Anisotropy of the spheres

The spheres are supposed to be isotropic. Nevertheless, inconsistencies between simulations and measurements indicate that they are not; that they have a small uniaxial anisotropy. This effect is shown in the measurements section 5.1.2.

The effect is explained in [25]. Basically, the spheres show an anisotropy axis (also called c-axis) with a dielectric constant epsilon$\parallel$. In the direction perpendicular to this axis, the dielectric constant is epsilon$\perp$. The c-axis is depicted in figure 4.43.

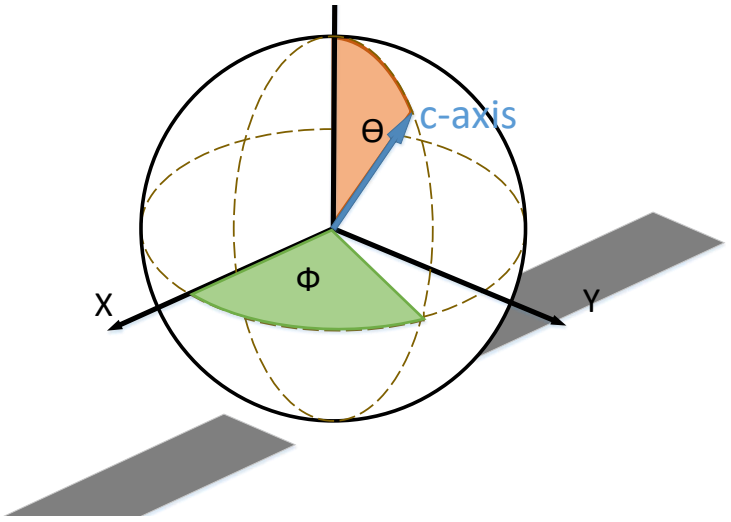

Figure 4.43: *Sphere with the c-axis positioned in a random position [25]*

When the symmetry of the filters is broken, the mode perpendicular to the one of interest is also excited in the sphere. The two modes of the sphere couple between each other, and with the ones in the adjacent spheres. This causes the filter to have zeros of transmission in the passband. A solution to this would be to find the anisotropy axis of the spheres and place them in the board in a way that the symmetry of the circuit is not broken. There are two possibilities for this, one is to place the axis in the direction perpendicular to the filter and parallel to the board (with $\theta = 90°$ and $\phi = 90°$, like in figure 5.5b), and the other one is to place the anisotropy axis perpendicular to the board (with $\theta = 0°$).

The first possibility is considered to be the best because the electric fields in the sphere are primarily contained in the plane perpendicular to the board. This matter causes them to have an equivalent permittivity equal to epsilon⊥, therefore the spheres can be simulated as isotropic with a permittivity equal to epsilon⊥, simplifying the simulation.

4.8.1 Determination of the dielectric constants

The anisotropy axis of a sphere can be found using the methods described in [25]. Once this is known, the epsilon⊥ and epsilon∥ can be determined using a procedure of measurements and simulations [25].

First the c-axis is positioned perpendicular to the filter and parallel to the board (like in figure 5.5b) and a measurement is taken. It should only show one peak, which would be the same as the resonance frequency of an isotropic sphere with a dielectric constant of epsilon⊥. It is also the maximum resonance frequency that the dielectric resonator sphere can show. A set of simulations using an isotropic sphere varying its permittivity are made, until simulations coincide with measurement, obtaining the epsilon⊥.

Once this permittivity is determined, a measurement with the c-axis oriented parallel to the board and to the filter (like in figure 5.7b) is taken. Only one peak appears, and this resonance frequency is the minimum one that the resonator can show. A set of simulations using an anisotropic sphere with its c-axis oriented in the same direction as in the measurements is performed. The epsilon⊥ is set to the calculated one, and the epsilon∥ is varied until the simulation coincides with the measurement.

The permittivities are determined in the measurements section 5.1.2.

Chapter 5

Prototypes and measurements

Several prototypes have been fabricated and measured to precisely determine the parameters of the spheres and to check the validity of the simulations.

Three prototypes have been fabricated. In the first one, the attenuation of the lines and the permittivity of the spheres are measured. In the second one, some filters are built to check the loss and in the last one, some overcoupled filters are fabricated to check the improvement in the loss.

5.1 First prototype. Lines, connectors and filters without resonators

This first prototype is fabricated to measure the permittivity of the spheres and to get an idea of the losses that the microstrip lines introduce in the model.

Figure 5.1 shows the four circuits that were built with coaxial ports on the backside of the board. The holes for the spheres are circular instead of quadrangular, as the behavior is identical and are easier to fabricate.

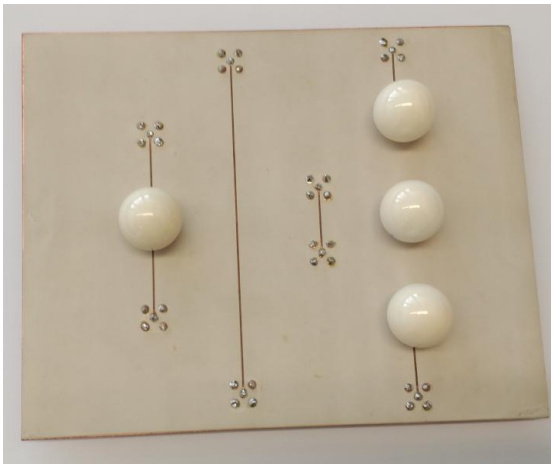

Figure 5.1: *Photo of the first prototype. Two transmission lines of 20 mm and 100 mm length each. Two circuits with one and three spheres. Board Rogers RO 3003. Microstrip lines: impedance 50Ω, width 0.595 mm. Permittivity of the dielectric of the board 3. Thickness: board 0.254 mm, copper 0.0175 mm.*

The first one (starting from left to right) is used to measure the resonance frequency of the sphere, so the permittivity can be determined.

The second and third circuits are microstrip transmission lines of 100 mm and 20 mm used to estimate the loss of the microstrip lines and coaxial feeds.

The last one is used to check how the spheres behave when they are coupled. It is in fact a 3 pole filter, but due to the coupling, performed by means of two lines, the achieved Q_e are too high and the filter has too much ripple to be useful.

5.1.1 Lines and connectors

In figure 5.2 the S21 parameters of each of the lines are presented. The big ripples that appear are because of reflexions at the ends of each line.

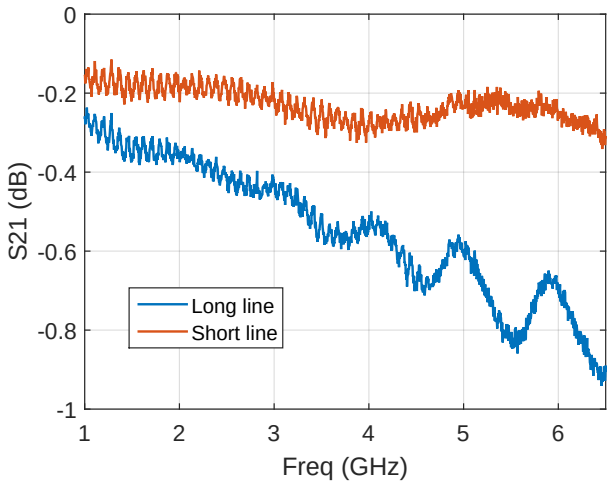

Figure 5.2: *Measurement of the two lines*

It is easy to extract from here information about the attenuation of the connectors and the attenuation of the lines. In figures 5.3a and 5.3b the result of the calculations and a fitting are presented. The fitting in figure 5.3a is performed in the minimums of the attenuation, because these points have perfect matching: no reflection occurs, representing the real attenuation.

In table 5.1 the attenuations of the connectors and the lines at the frequency of interest ≈ 5.8 GHz are presented.

Table 5.1: Attenuation of the connectors and the lines at 5.8 GHz

Connectors	0.075 dB
Line	5.2 dB m^{-1}

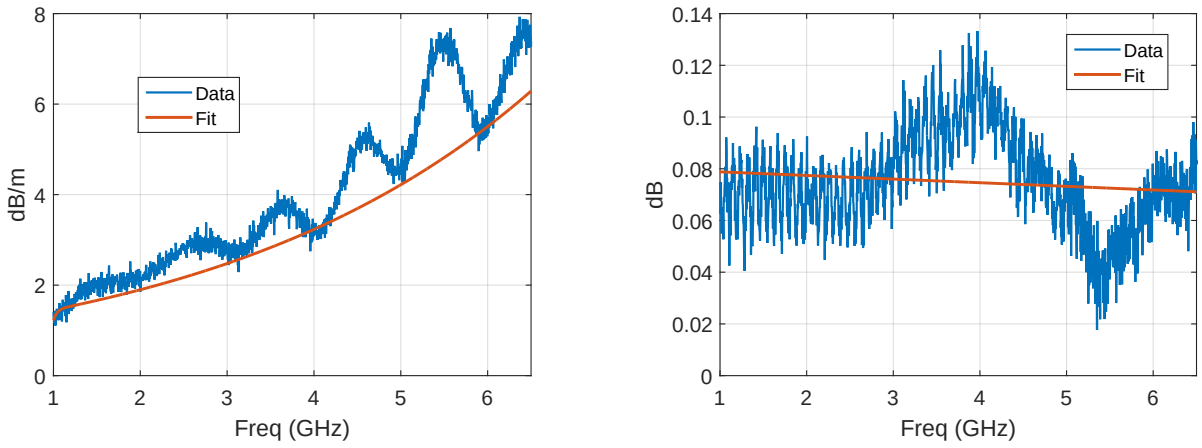

(a) (b)

Figure 5.3: *Calculation of the attenuation. (a) Line attenuation. (b) Connector attenuation.*

5.1.2 Circuit with one sphere

With this circuit, it can be seen that the spheres are slightly anisotropic.

In figure 5.4a two peaks appear for each sphere, meaning that the circuit is not symmetric anymore and the orthogonal mode is also excited. When taking this measurements, the spheres where positioned like in figure 5.4b, at a position of 45°.

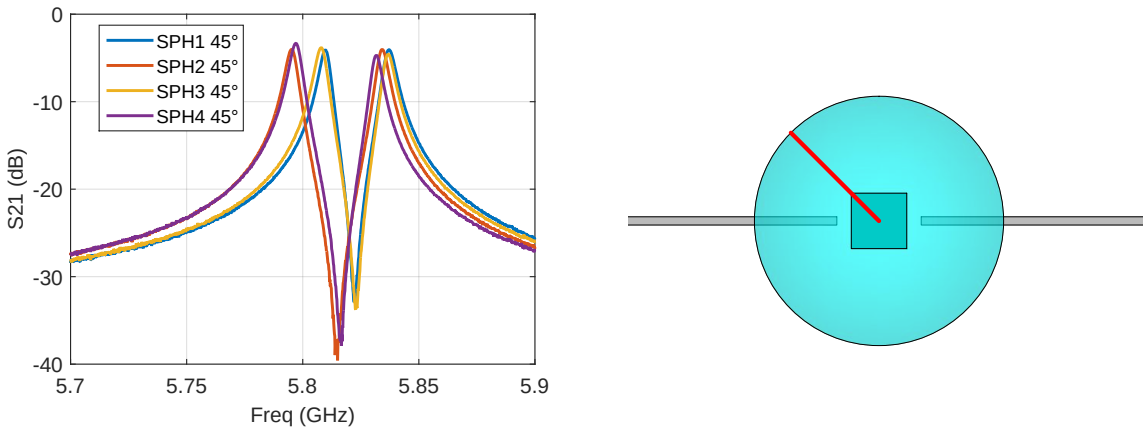

(a) (b)

Figure 5.4: *Measurement of the sphere oriented to 45°. (a) Four measurements of four almost identical spheres. (b) Circuit used to perform the measurement.*

As explained in the previous sections, if the axis is localized and positioned perpendicular to the filter symmetry plane and parallel to the board as in figure 5.5b, the symmetry is conserved again and the equivalent permittivity of the sphere would be $\epsilon_\perp$. The measurements are seen in figure 5.5a.

Only one peak appears now for each of the spheres. It can be appreciated that the frequency variation is small, meaning that the spheres have similar permittivity. The permittivity is calculated for each of the spheres in table 5.2.

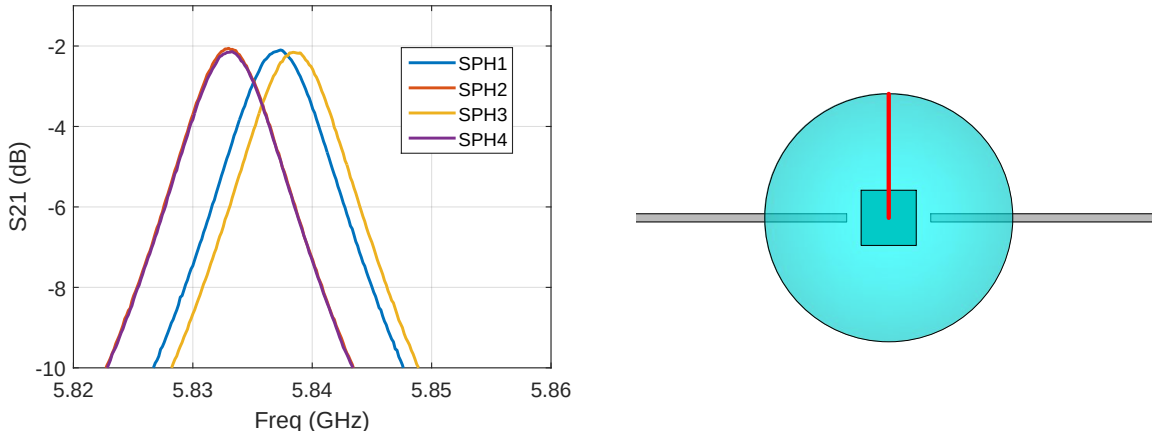

(a) (b)

Figure 5.5: *Measurement of the sphere oriented perpendicular to the filter symmetry plane. (a) Four measurements of four almost identical spheres. (b) Circuit used to perform the measurement.*

Table 5.2: Calculation of the $\epsilon_\perp$ of the sphere

Sphere	**Frequency (GHz)**	**Permittivity**
Sphere 1	5.833	9.5395
Sphere 2	5.8332	9.5381
Sphere 3	5.8374	9.5097
Sphere 4	5.8386	9.5015

Therefore the $\epsilon_\perp$ of the spheres at this point is considered to be around 9.52.

To check the grade of anisotropy of the spheres, a set of simulations maintaining the $\epsilon_\perp$ equal to 9.52 but changing the $\epsilon_\parallel$ are performed. According to [25], if the sphere axis is positioned parallel to the axis of the filter as in figure 5.7b, then the symmetry is maintained and therefore only one peak appears. The resonance frequency depends strongly on the $\epsilon_\parallel$. By doing so the graph of figure 5.6 is obtained.

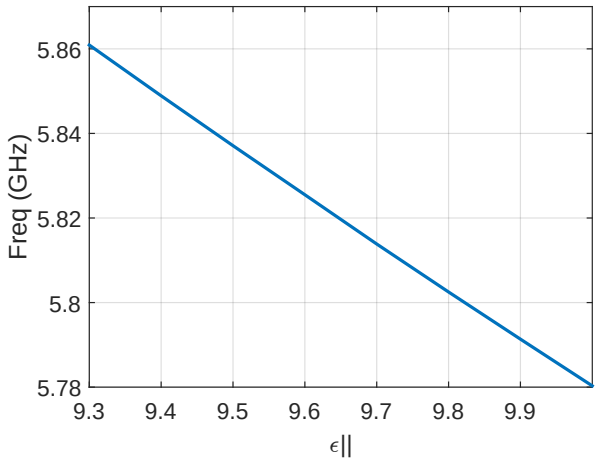

Figure 5.6: *Relationship between the $\epsilon_\parallel$ and the resonance frequency of a sphere.* $\epsilon_\perp = 9.52$

Three measurements with the c-axis parallel to the filter as in figure 5.7b give as result figure 5.7a.

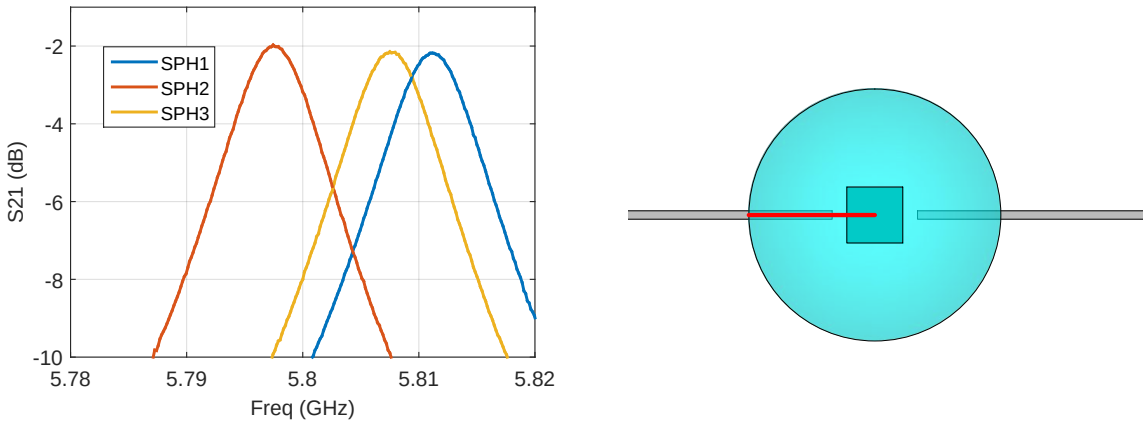

(a) (b)

Figure 5.7: *Measurement of the sphere oriented parallel to the filter symmetry plane. (a) Four measurements of four almost identical spheres. (b) Circuit used to perform the measurement.*

Using these figures, the $\epsilon_{\parallel}$ is extracted using table 5.3.

Table 5.3: Calculation of the $\epsilon_{\parallel}$ of the sphere

Sphere	**Frequency (GHz)**	**Permittivity**
Sphere 1	5.797	9.8501
Sphere 2	5.8076	9.7581
Sphere 3	5.8111	9.7277

Taking this into consideration, an $\epsilon_{\parallel}$ of 9.78 is assigned.

5.1.3 Circuit with three spheres

This second circuit has been measured with the spheres positioned to keep the symmetry with the c-axis perpendicular to the filter as in figure 5.5b.

Several measurements are performed and a $\epsilon_{\perp}$ of 9.5 is considered because it fits better with the simulations as seen in figure 5.8.

Simulations and measurements match very well. The value of relative permittivity equal to 9.5 fits better, therefore this is the selected value to perform all the simulations.

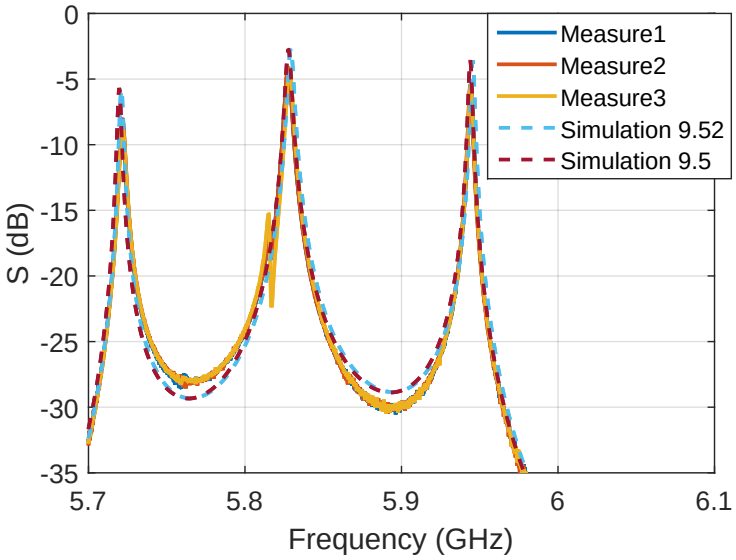

Figure 5.8: *Measure of the circuit with three spheres in different positions.*

5.2 Second prototype. Filters with resonators.

A second prototype has been fabricated to check the accuracy of the simulations and their similarity with the measurements. In this case, three filters including the microstrip resonators have been built as figure 5.9 shows. The contribution of the microstrip lines and the connectors has been taken into account from the filters response both in the simulations and the measurements using the information extracted in section 5.1.1. Table 5.4 shows the characteristics of the three filters seen in the image.

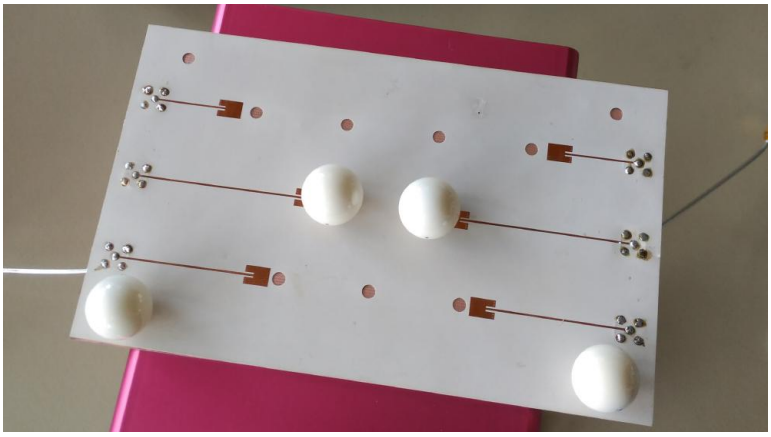

Figure 5.9: *Photo of the second prototype with the filters in table 5.4.*

Table 5.4: Characteristics of the filters of the second prototype

Filter	**Order**	**Ripple**	**Bandwidth**
1	4	0.1 dB	5 %
2	5	0.5 dB	8 %
3	6	0.5 dB	6 %

Four holes are performed in the four corners of the board to place spheres and help to support the upper metal plate and keep the parallelism. The filters are measured and compared with the simulations.

5.2.1 Order 4 filter

In figures 5.10a and 5.10b, the simulations and measurements of the order 4 filter are presented. Several measurements are performed changing the spheres of relative position and trying to orient their anisotropy axis as well as possible. The S21 parameter of the simulation is quite similar to the measurements. Nevertheless, the S11 parameter misses two poles and gets worse in the upper half passband.

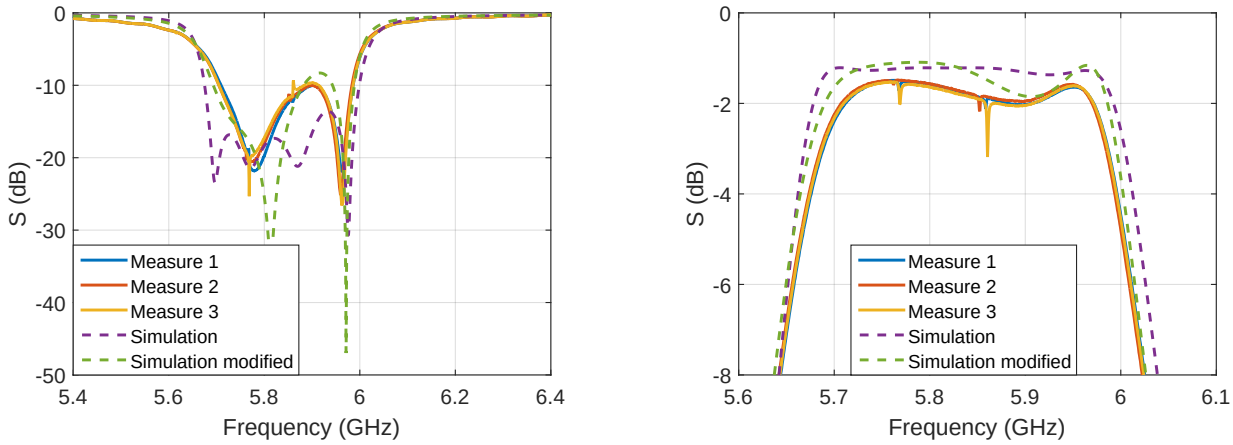

Figure 5.10: *Filter response order 4, ripple 0.1 dB, bandwidth 5 %. Measures and simulations. (a) S11 parameter. (b) S21 parameter.*

To check the origin of these differences, several simulations are performed changing slightly some of the parameters. In prototype 1, less differences are observed between the simulations and measurements. Therefore, it is to expect that the differences in this prototype are caused by the introduction of the microstrip resonators, not present in the previous prototype. Thus, the length of the resonator and the feeding point are changed to check the built model.

The parameter *gap_1* (that determines the feeding point and is related with the Q_e) is changed by +0.26 mm and the parameter *l_stub* (that determines the resonance frequency of the microstrip resonator) is changed by +0.04 mm. This modified simulation is also presented in figures 5.10a and 5.10b. It is seen now that the simulations agree better with the measurements, therefore the differences are caused by imprecisions building the microstrip resonator. Similar imprecisions are expected for the other filters.

5.2.2 Order 5 filter

In this filter the simulations agree quite well with the measurements. This is due to the increased number of spheres causing the imprecisions in the microstrip resonators to be

less relevant.

Nevertheless, similar corrections as in the previous filter are performed in the simulations to check the causes of the differences between the simulations and measurements. This is seen in figures 5.11a and 5.11b. In this case the parameter *gap_1* is changed by -0.13 mm and the parameter *l_stub* is changed by +0.04 mm.

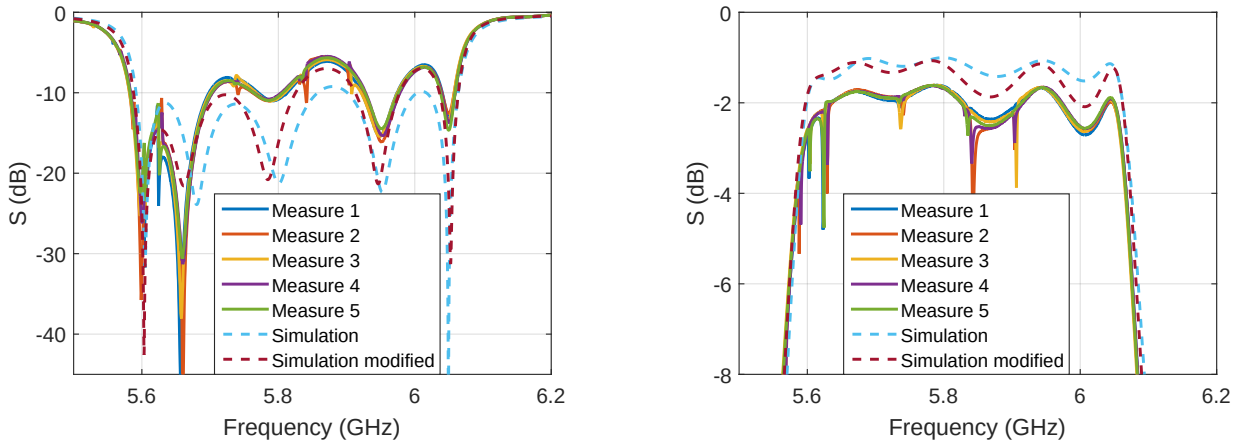

(a) (b)

Figure 5.11: *Filter response order 5, ripple 0.5 dB, bandwidth 8 %. Measures and simulations. (a) S11 parameter. (b) S21 parameter.*

Figures 5.12a and 5.12b, show measurements of this filter with the c-axis of the resonators pointing to 45° as in figure 5.4b. The alterations in the response of the filter are obvious, distinguishing the peaks that appear in the S21 response. In fact, the peaks that appear in the measurements in figure 5.11b are due to a non perfect alignment of the spheres.

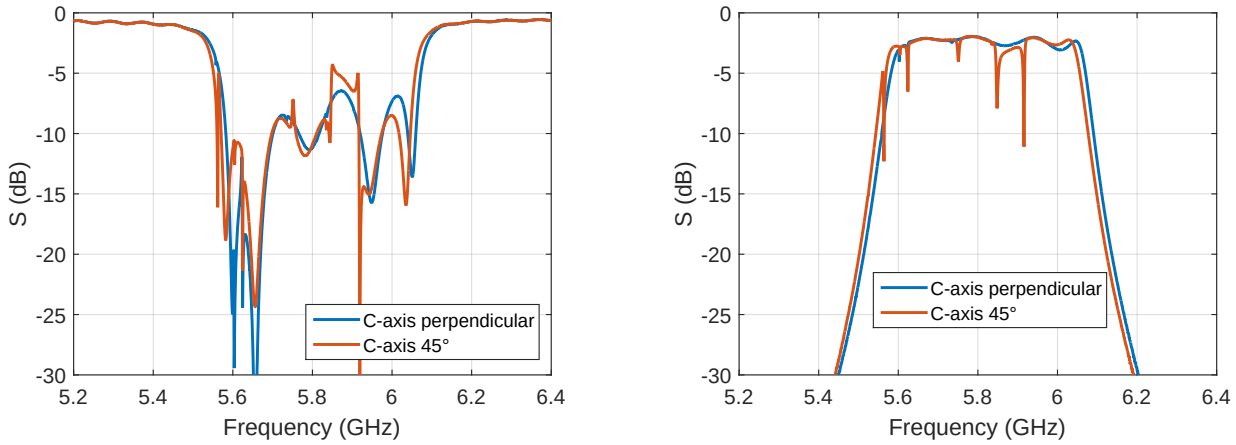

(a) (b)

Figure 5.12: *Filter response order 5, ripple 0.5 dB, bandwidth 8 %. Measures and simulations of the S11 parameter with the c-axis pointing to 45° and perpendicular. (a) S11 parameter. (b) S21 parameter.*

5.2.3 Order 6 filter

This filter results to be more complicated due to errors in the fabrication process. One of the vias, as seen in figure 5.14 is not connected to the ground. Therefore, the electrical length of the resonator is increased leading to big differences between the simulations and the measurements.

A modified simulation, seen in figures 5.13a, 5.13b and 5.13c without this hole is performed.

The modified simulation fits very well to the measurements, therefore the vias is the main cause for the differences between original simulation and measurements.

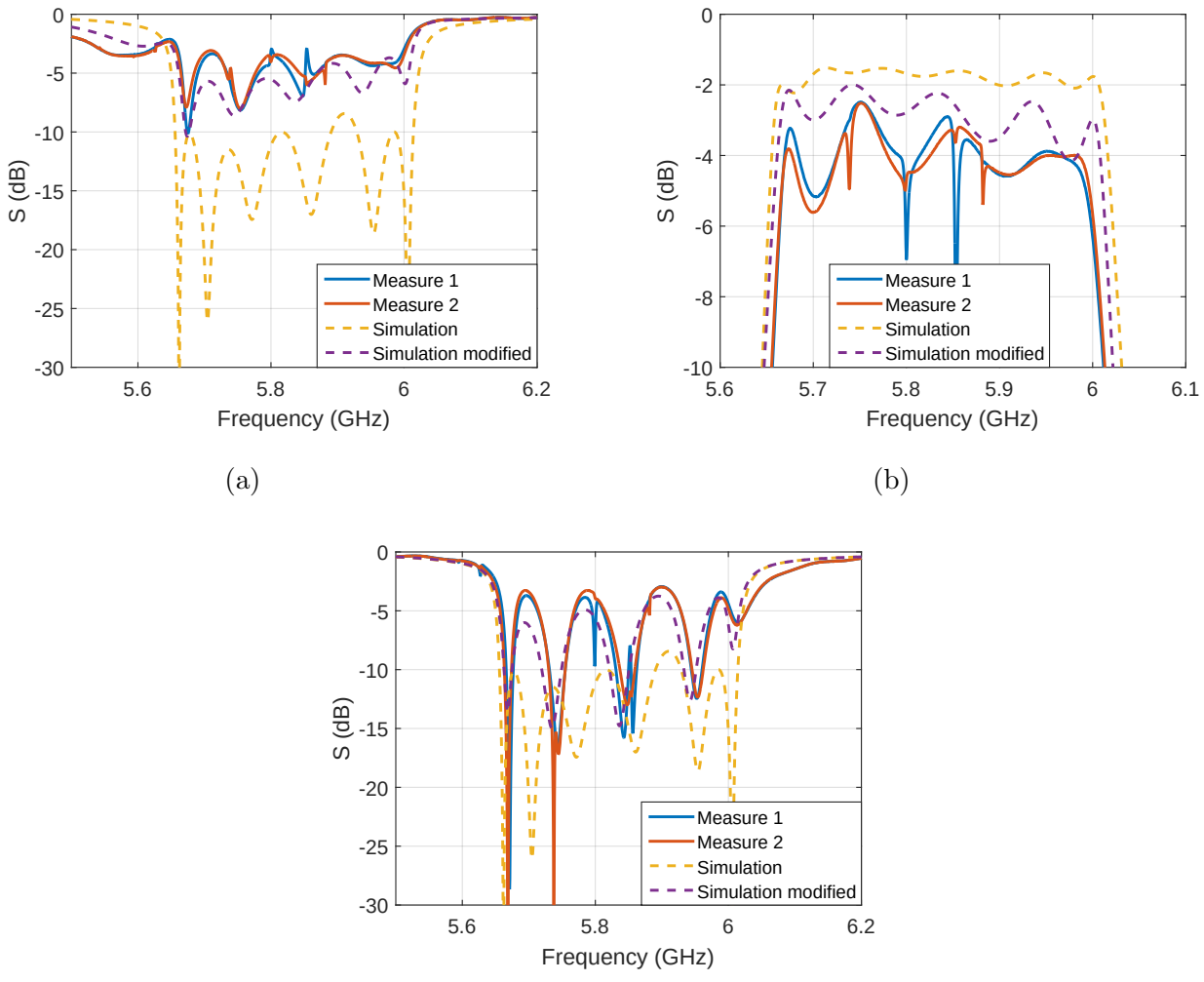

(a)

(b)

(c)

Figure 5.13: *Filter response order 5, ripple 0.5 dB, bandwidth 8 %. Measures and simulations. (a) S11 parameter. (b) S21 parameter. (c) S22 parameter.*

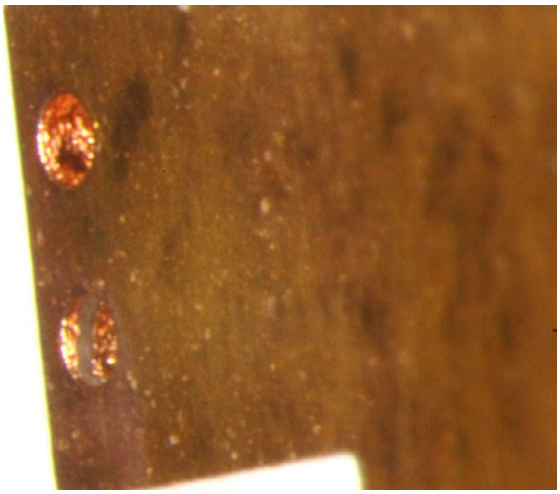

Figure 5.14: *Photo of the unconnected via. The lower via has a non-connected ring in its middle, not performing the ground connection. Radius of the hole 0.2 mm. Thickness of the board 0.254 mm.*

5.3 Third prototype. Filters with overcoupling.

A final prototype has been fabricated to check the overcoupled filters. Four filters have been simulated as seen in figure 5.15. Table 5.5 shows that filters one and two are equivalent narrowband filters, but one of them is overcoupled and the other one is normally synthesized. The same occurs with the wideband filters three and four. The contribution of the microstrip lines and the connectors has also been taken into account from this prototype.

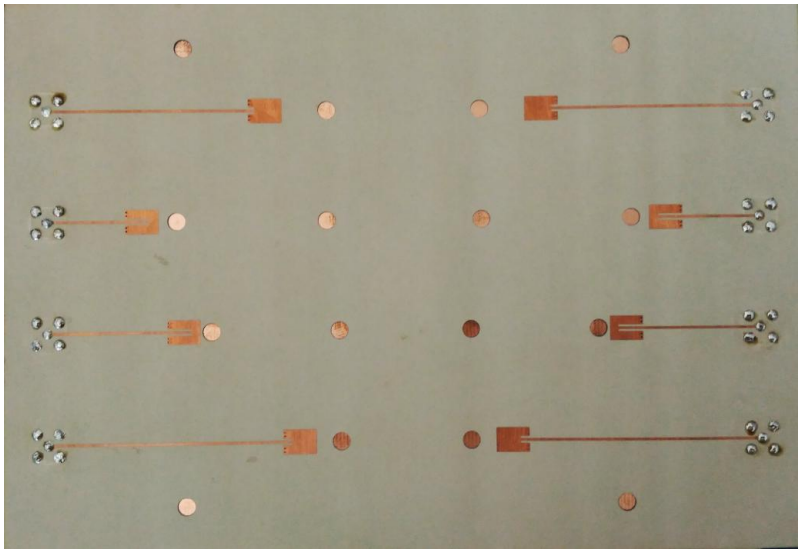

Figure 5.15: *Photo of the third prototype with the filters in table 5.5*

Table 5.5: Characteristics of the filters of the third prototype

Filter	Order	Ripple	Bandwidth	Type
1	4	0.1 dB	2 %	Normal
2	4	0.1 dB	2 %	Overcoupled
3	4	0.5 dB	5 %	Overcoupled
4	4	0.5 dB	5 %	Normal

5.3.1 Narrowband filters. Filters 1 and 2

Filter one is not correctly fabricated as seen in figures 5.16a and 5.16b. One of the resonances is situated at less than 5.7 GHz and therefore the S11 level is increased. This is because the microstrip resonator is not resonating at the same frequency as the spheres. The second prototype shows that these filters are very sensitive to the inaccuracies in the microstrip resonator. The most probable reason of these differences is that the microstrip resonators are longer than specified, resonating at a lower frequency.

Due to this imperfections it is not possible to compare this filter with the overcoupled one.

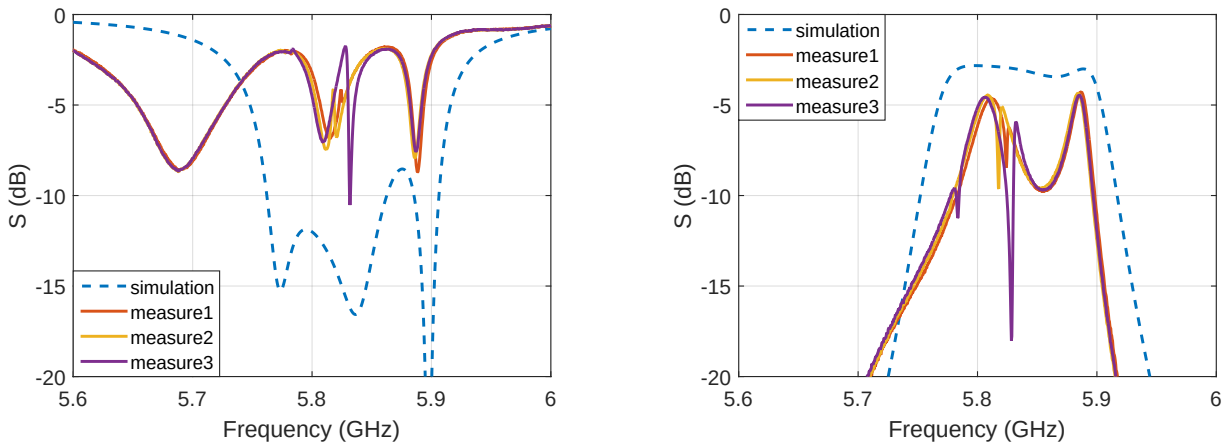

(a) (b)

Figure 5.16: *Filter 1: order 4, ripple 0.1 dB, bandwidth 2 % and normally synthesized. (a) S11 parameter. (b) S21 parameter.*

Figures 5.17a and 5.17b show the overcoupled filter two. The simulation, in dashed lines fits very accurately the measurements. It is seen that some peaks appear in measurements one and two. The overcoupled filters are apparently more sensitive to the anisotropy of the spheres. This can be due to two effects, first the spheres are now the ending resonators, having more influence in the filter, and second, the resonators are nearer the spheres, exciting more of the orthogonal mode due to the anisotropy.

A third measurement, performed holding some metal sheets near the ending spheres in order to load the orthogonal mode, shows that these peaks can be easily erased. These metallic sheets do not increase the filter loss by much as seen in figure 5.17b and in the next filter insertion loss (figure 5.19b).

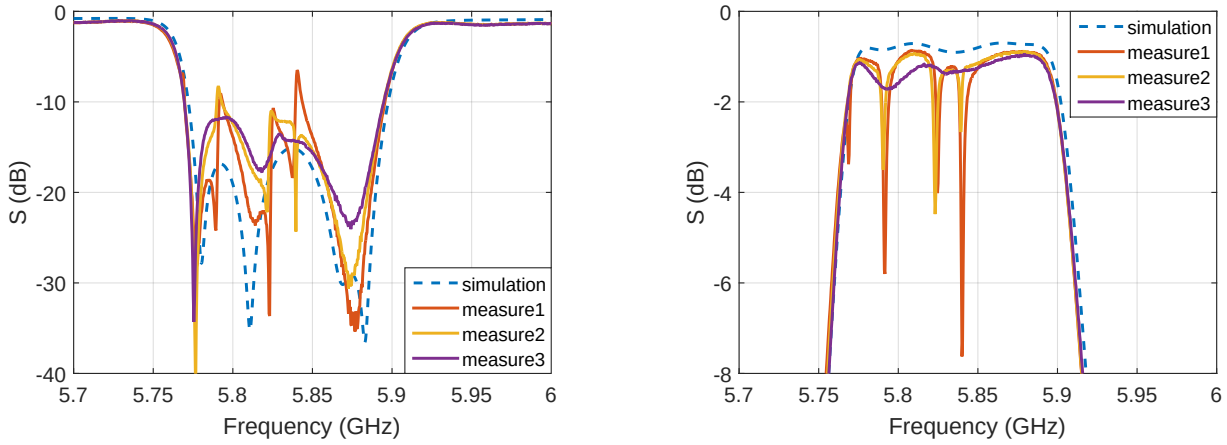

(a) (b)

Figure 5.17: *Filter 2: order 4, ripple 0.1 dB, bandwidth 2 % and overcoupled. (a) S11 parameter. (b) S21 parameter*

5.3.2 Wideband filters. Filters 3 and 4

Figures 5.18a and 5.18b, show the S parameters of filter four. This normally synthesized filter fits better with the simulation than filter one but it has the same problem with the microstrip resonators, being longer than specified, and therefore, not resonating at the same frequency as the spheres. Nevertheless, the problem is less notable, being the length of the microstrip resonator more similar to the specified one.

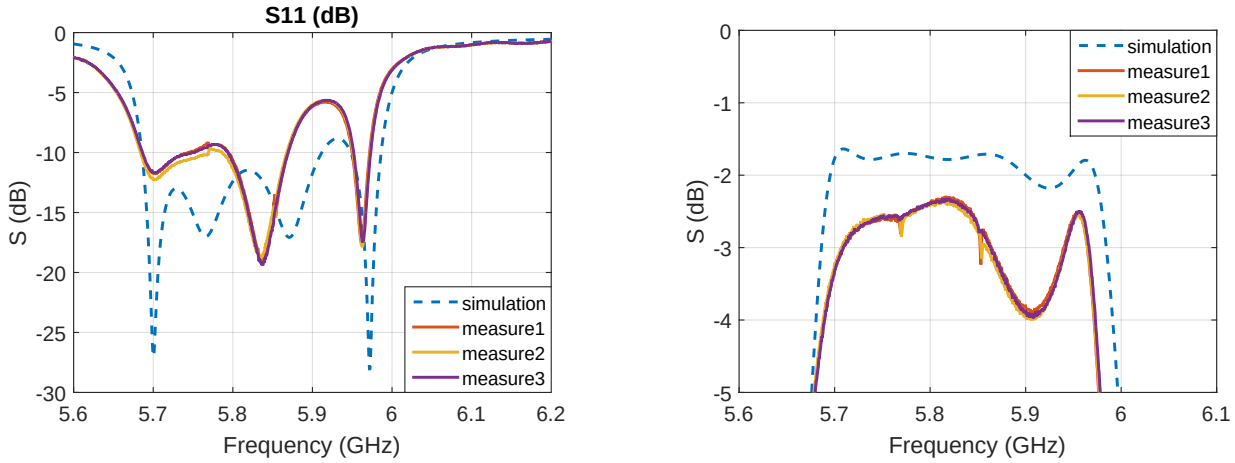

(a) (b)

Figure 5.18: *Filter 4: order 4, ripple 0.5 dB, bandwidth 5 % and normally synthesized. (a) S11 parameter. (b) S21 parameter.*

Figures 5.19a and 5.19b, show the S parameters response of the overcoupled filter three. The three first measurements of this filter have the same problem as filter two with the anisotropy of the spheres, so a fourth measurement was performed solving the problem in the same way.

This measurement fits very accurately with the simulation. All the resonances are sharply marked, due to the lower power loss in comparison with the normally synthesized filter.

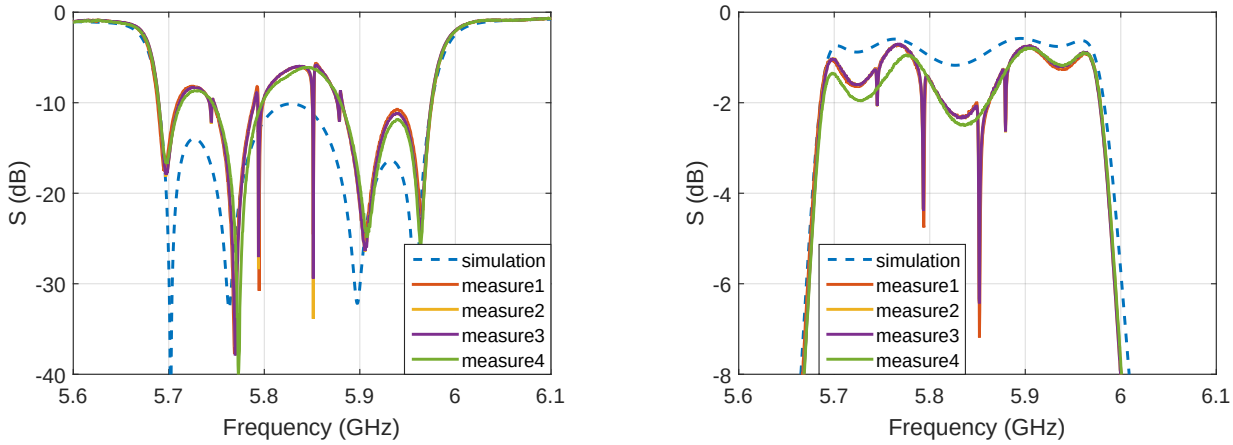

Figure 5.19: *Filter 3: order 4, ripple 0.5 dB, bandwidth 5 % and overcoupled. (a) S11 parameter. (b) S21 parameter.*

The improvement in the power loss in the overcoupled filter with respect to the normally synthesized one is of more than 1.5 dB. Figure 5.20 shows in the same graph a comparison between the measurements of filters three and four.

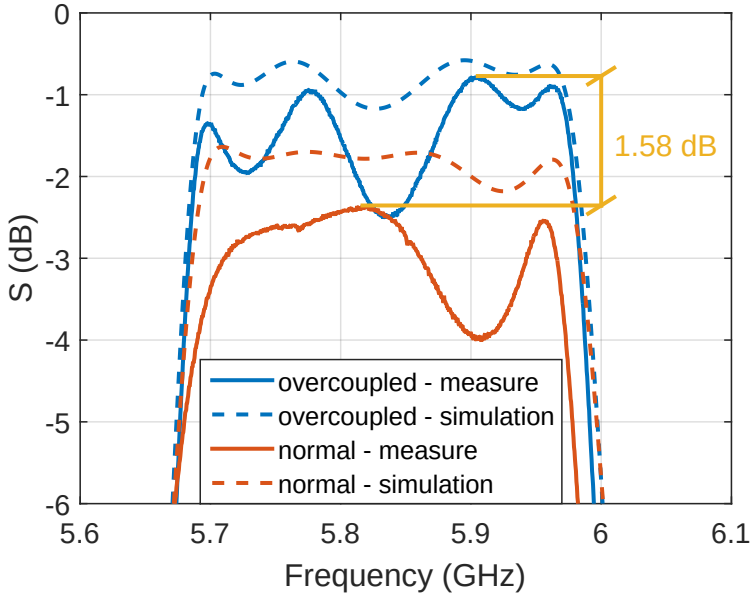

Figure 5.20: *Comparison of the S21 parameter of filters three and four*

Chapter 6

Conclusions

This report presents spherical dielectric resonator-based filters, which are an excellent alternative to construct filters at high frequencies. Their advantages are low loss, compact size and lack of conductors.

To synthesize these filters in a fast way, equations and graphs are necessary. If these do not exist, then a lot of time would be spent in trial and error and in optimization. In this report, these equations are calculated for alumina 9 mm radius spheres with a relative permittivity of 9.5.

Some filters are simulated, testing that the equations are accurate enough. Several prototypes are built in order to check the validity of the simulations. It is seen that both the equations and the simulations are correct, leading to really competent prototypes. In fact, no optimization was performed in any of the filters, so the results are direct application of the graphs.

Besides, a method to minimize the loss of the filters by overcoupling some of the resonators is presented. These filters are also built and compared with the normal ones, reaching improvements of more than 1.5 dB. This method is very important, because it improves one of the main characteristics of these resonators which is low loss.

The methods described in this report allow to create filters with dielectric sphere resonators in a fast way. Giving the specifications of the filter, an engineer can obtain its physical parameters. The created prototypes need no further optimization. The resultant filters have the advantages of being on-chip and having compact size and low loss.

The advantage of the described methods to obtain the equations and graphs is that they are automatic and are scalable to other frequencies, resonators and topologies.

Further steps would be to optimize the microstrip resonator in order to try to reduce more the losses. It is also interesing to obtain resonators with lower achievable Q_e's and higher k's to improve significantly the performance of the overcoupled filters. Calculating the slope parameter of the resonators deepens the knowledge of the dielectric spheres. It would be very advantageous to obtain a formula to estimate the power loss of the overcoupled filters. Finally, these methods can also be applied to higher frequencies in which the low-loss characteristic is accentuated due to the lack of conductors. 3D printing techniques can also be explored [30] to generate alumina resonators of the desired shape.

Appendix A

Lossless filter examples

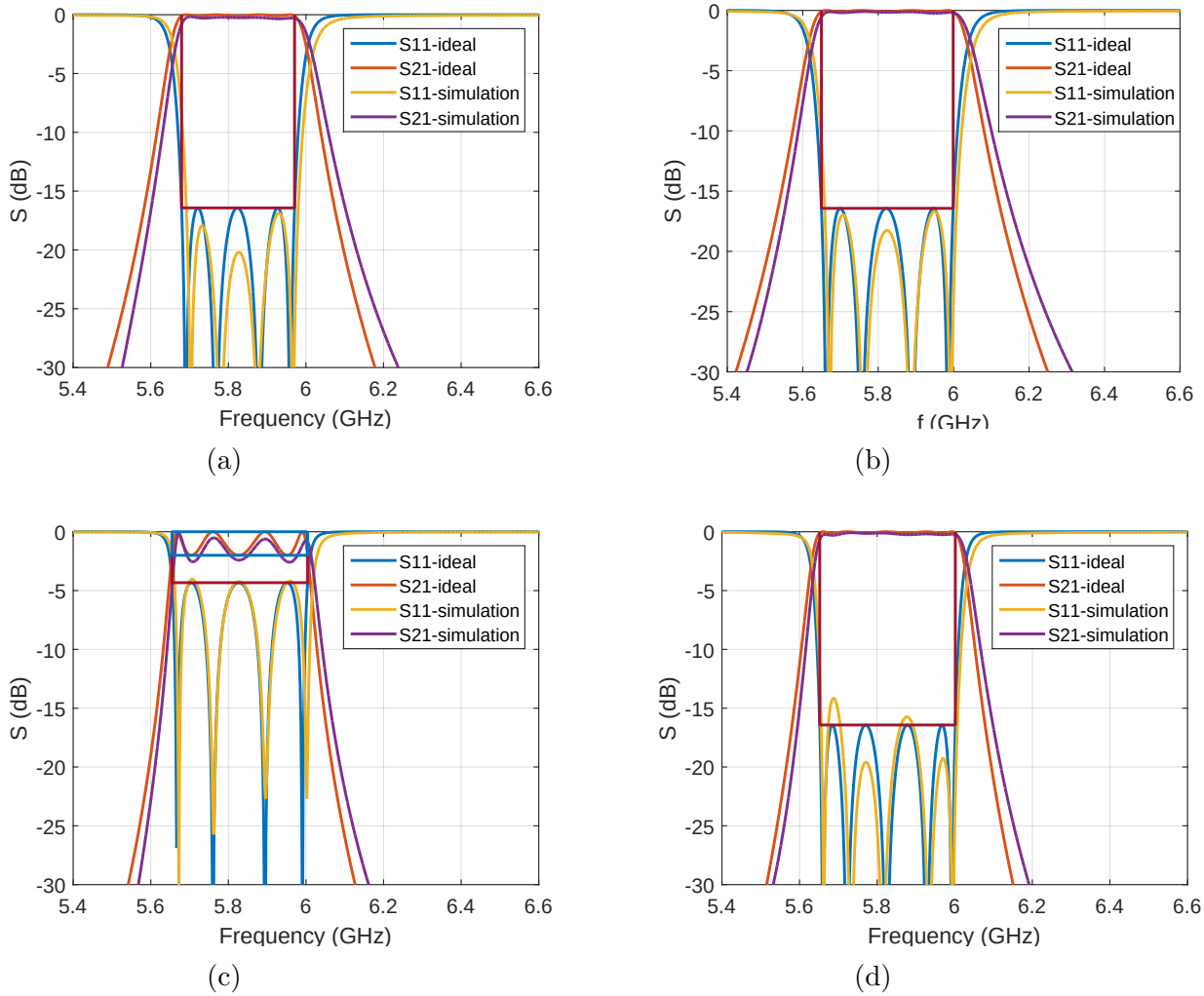

Figure A.1: *Filters responses. (a) Order 4, ripple 0.1 dB, bandwidth 5 %. (b) Order 4, ripple 0.1 dB, bandwidth 6 %. (c) Order 4, ripple 2 dB, bandwidth 6 %. (d) Order 5, ripple 0.1 dB, bandwidth 6 %.*

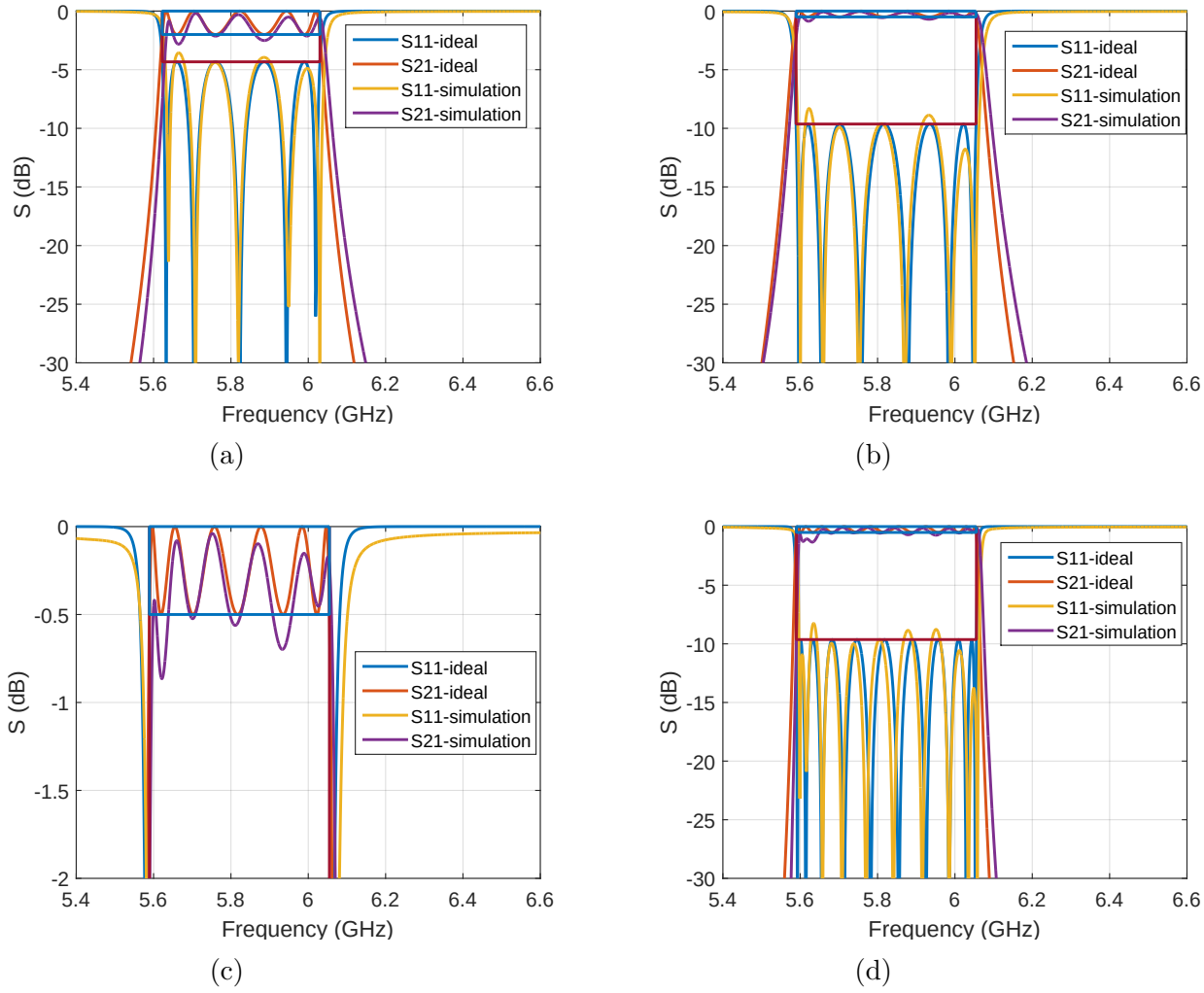

Figure A.2: *Filters responses. (a) Order 5, ripple 2 dB, bandwidth 7 %. (b) Order 6, ripple 0.5 dB, bandwidth 8 %. (c) Order 6, ripple 0.5 dB, bandwidth 8 % detail S21 parameter. (d) Order 10, ripple 0.5 dB, bandwidth 8 %.*

Appendix B

Filter examples with losses

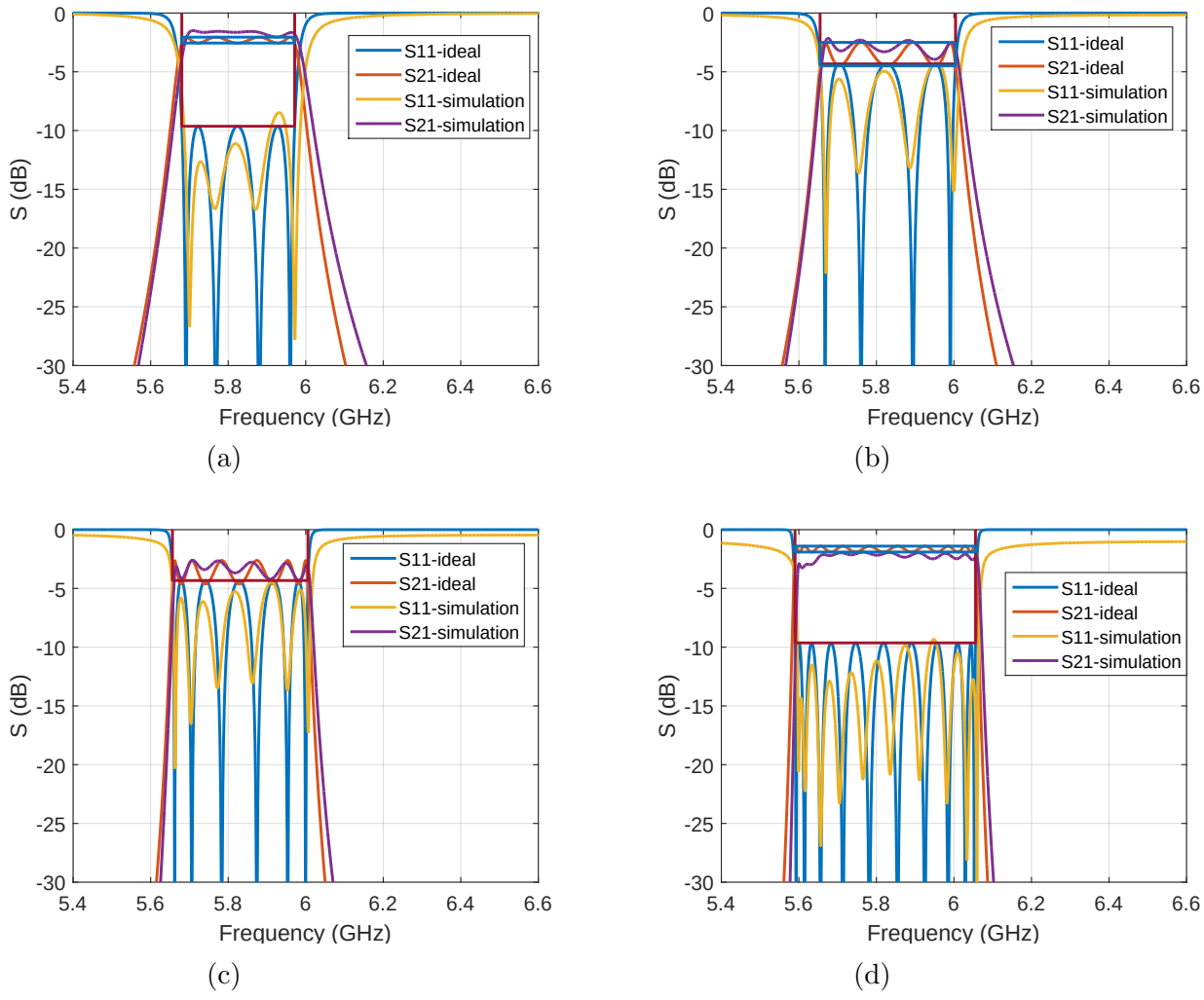

Figure B.1: *Filters responses with loss. (a) Order 4, ripple 2 dB, bandwidth 5 %. (b) Order 4, ripple 2 dB, bandwidth 6 %. (c) Order 6, ripple 2 dB, bandwidth 6 %. (d) Order 10, ripple 0.5 dB, bandwidth 8 %.*

Appendix C

Filter examples with overcoupling and losses

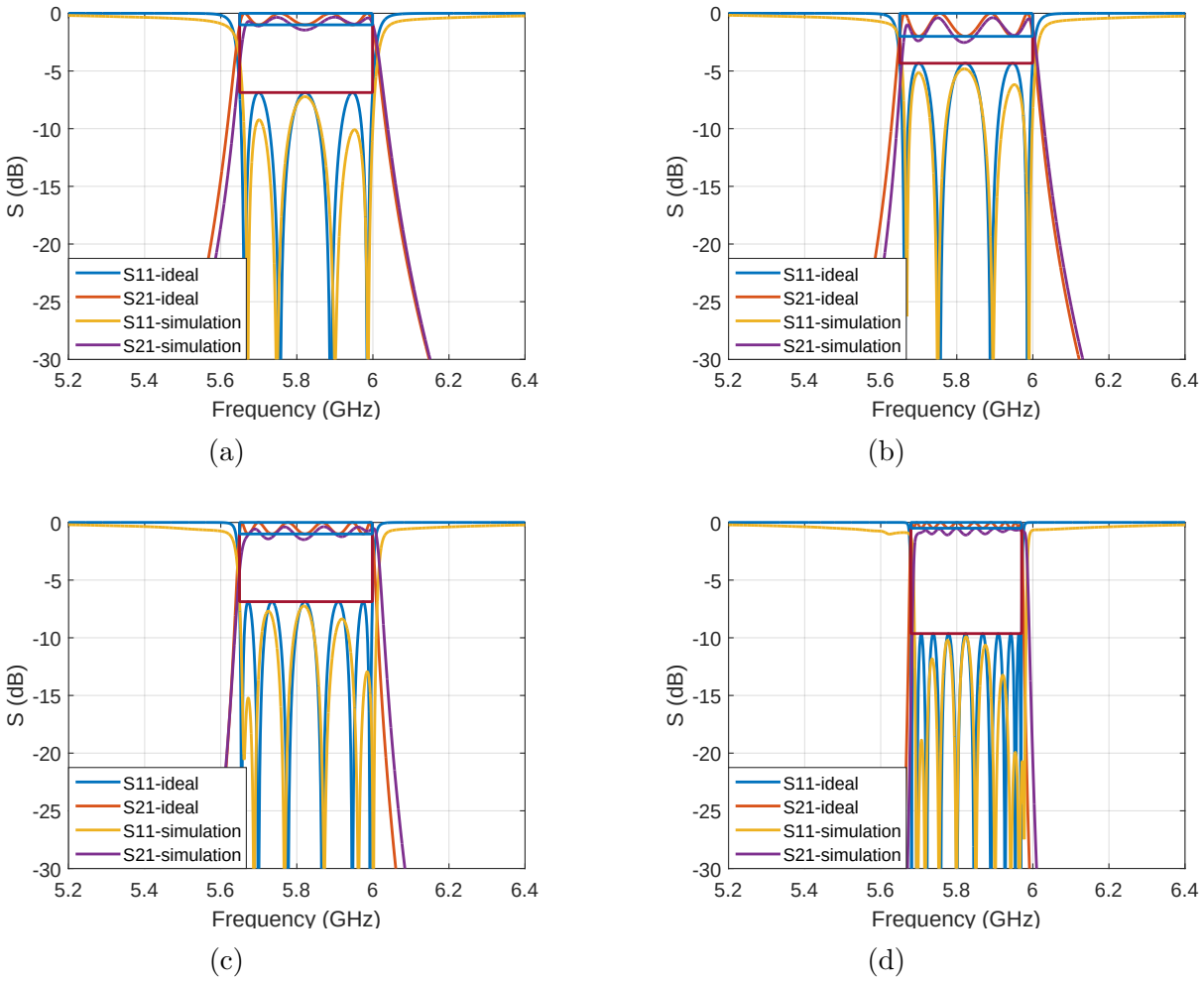

Figure C.1: *Filters responses with loss and overcoupling. (a) Order 4, ripple 1 dB, bandwidth 6 %. (b) Order 4, ripple 2 dB, bandwidth 6 %. (c) Order 6, ripple 1 dB, bandwidth 6 %. (d) Order 10, ripple 0.5 dB, bandwidth 5 %.*

Appendix D

Relevant parameters

Here the most relevant parameters when simulating the filters are presented.

Table D.1: Material parameters

tandSubs	Delta tangent of the substrate	0.001
tandSph	Delta tangent of the sphere	0.0002
epsilonSubstrate	Epsilon of the substrate	3
epsilonSph	Epsilon of the sphere	9.5
metalConduc	Conductivity of the metal	$5.8 \cdot 10^7\,\mathrm{S\,m^{-1}}$

Table D.2: Sphere hole parameters

l_square	4 mm
thick_subs	0.254 mm
thick_cu	0.0175 mm
prof_1	$R\_sph - \sqrt{R\_sph^2 - l\_square^2/4}$ mm

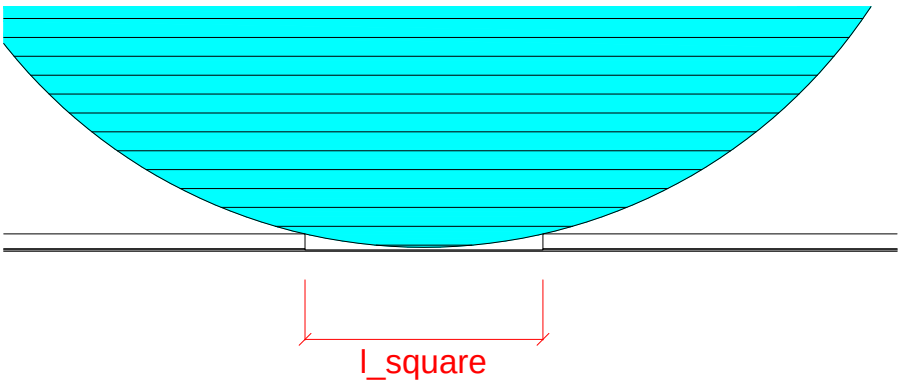

Figure D.1: *Placement of the sphere in the circuit and dimensions*

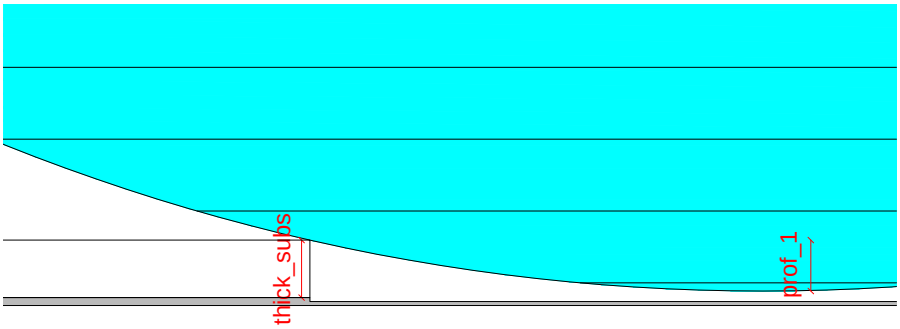

Figure D.2: *Placement of the sphere in the circuit and dimensions. Detail 1*

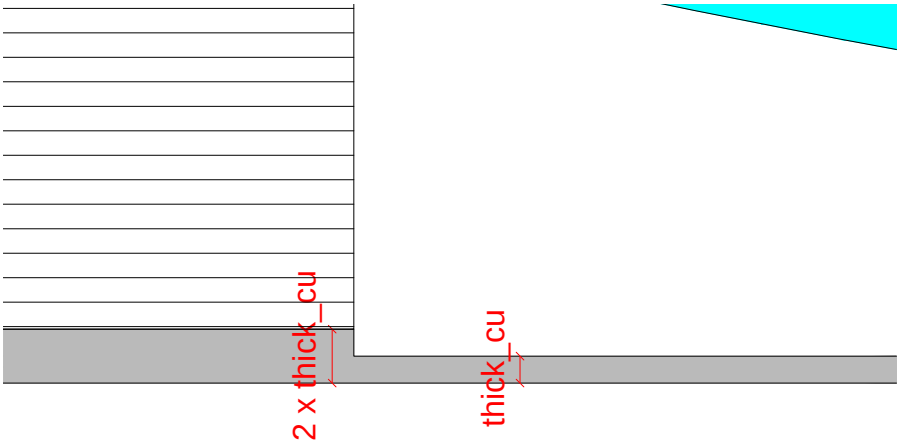

Figure D.3: *Placement of the sphere in the circuit and dimensions. Detail 2*

Table D.3: Microstrip parameters

l_square_2	variable [4.5 - 11]mm
w_stub	2 mm
l_stub	variable
w_50	0.595 mm
gap_2	1.5 mm
gap_1	variable [0.6 - 6.6]mm
gap_1_aux	l_stub - gap_1 mm
r_vias	0.2 mm

Table D.4: Other parameters

r_sph	Radius of the sphere	9 mm
D_sph	Distance between the centers of two spheres	variable
W_board	Length of the board	variable
L_board	Width of the board	90 mm

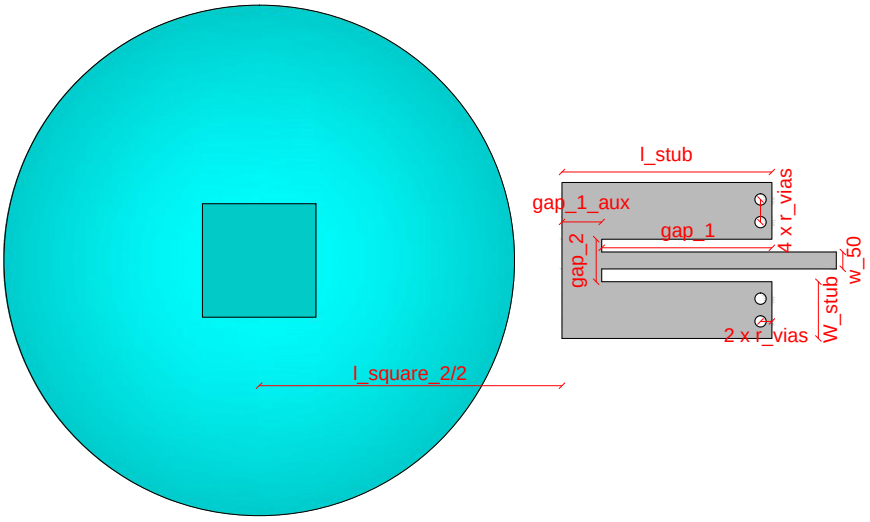

Figure D.4: *Placement of the resonator in the circuit and dimensions*

Appendix E

Possible filters and lengths

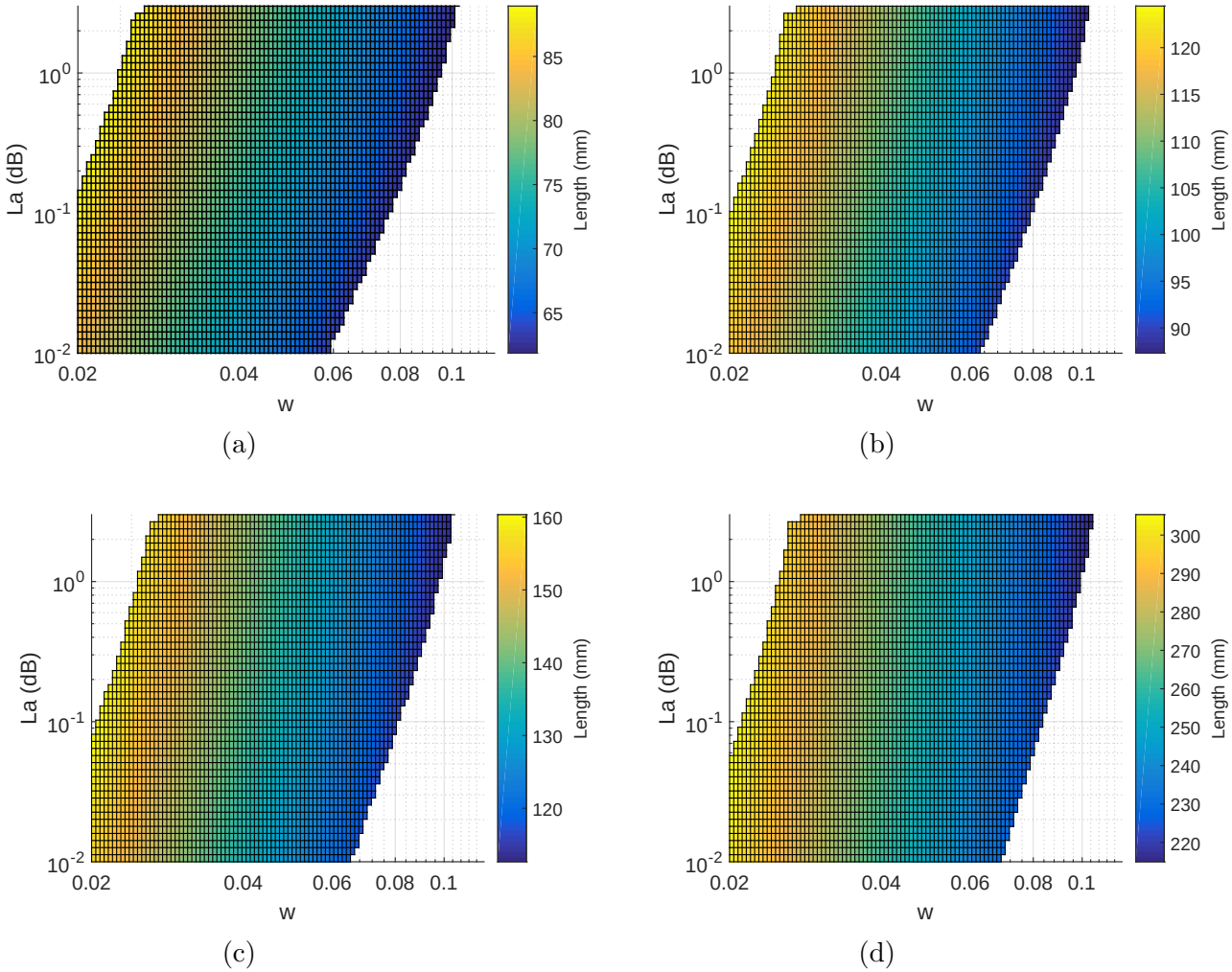

Figure E.1: *Possible filters and lengths. (a) Order 4. (b) Order 5. (c) Order 6. (d) Order 10.*

Appendix F

Possible filters and losses

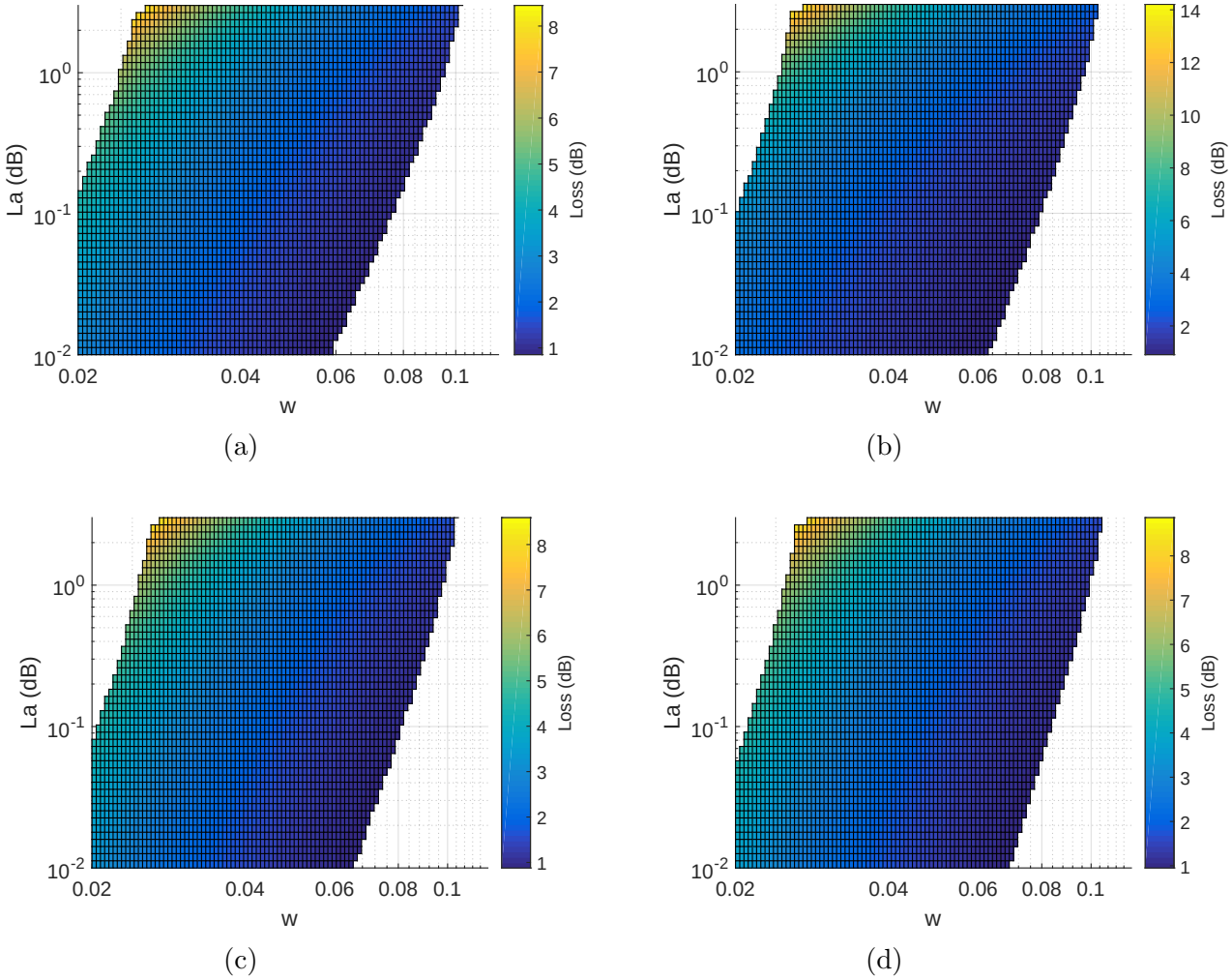

Figure F.1: *Possible filters and loss. (a) Order 4. (b) Order 5. (c) Order 6. (d) Order 10.*

Appendix G

Flowchart of the program

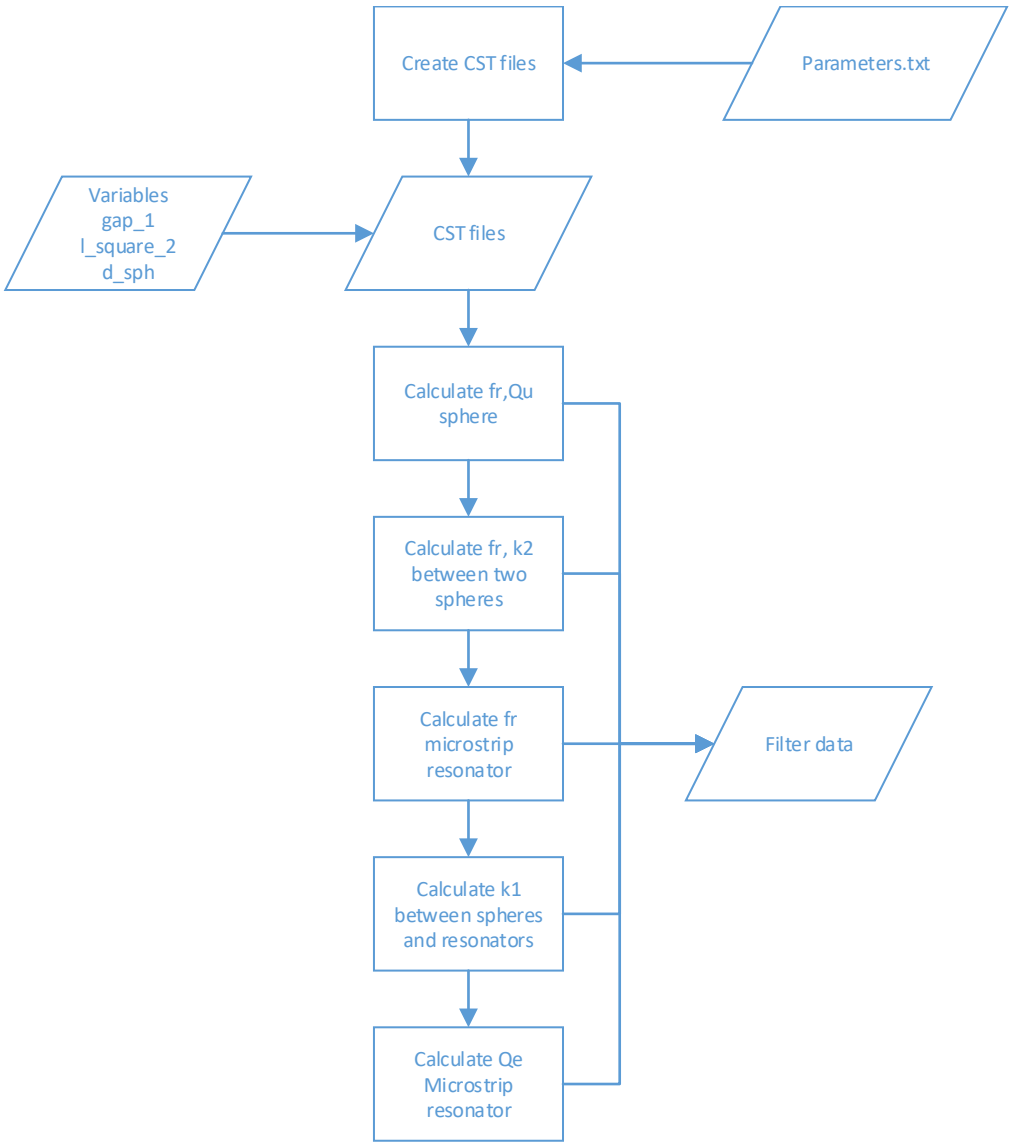

Figure G.1: *Flowchart of the program*

Bibliography

[1] L. Rayleigh, "XVIII. on the passage of electric waves through tubes, or the vibrations of dielectric cylinders," *The London, Edinburgh, and Dublin Philosophical Magazine and Journal of Science*, vol. 43, no. 261, pp. 125–132, 1897.

[2] R. Richtmyer, "Dielectric resonators," *Journal of Applied Physics*, vol. 10, no. 6, pp. 391–398, 1939.

[3] S. A. Long, M. W. McAllister, and L. C. Shen, "The resonant cylindrical dielectric cavity antenna," *IEEE Trans. Antennas Propag.*, vol. 31, pp. 406–412, 1983.

[4] M. McAllister, S. Long, and G. Conway, "Rectangular dielectric resonator antenna," *Electronics Letters*, vol. 19, p. 218, 1983.

[5] M. McAllister and S. Long, "Resonant hemispherical dielectric antenna," *Electronics Letters*, vol. 20, pp. 657–659, 1984.

[6] A. Petosa and A. Ittipiboon, "Dielectric resonator antennas: A historical review and the current state of the art," *IEEE Antennas Propag. Mag.*, vol. 52, no. 5, pp. 91–116, 2010.

[7] W. R. Day, "Dielectric resonators as microstrip circuit elements," in *Microwave Symposium, G-MTT 1970 International*, pp. 24–28, IEEE, 1970.

[8] P. Guillon, M. Chong, and Y. Garault, "Dielectric resonators band pass filter with high attenuation rate.," in *Microwave Symposium Digest, 1984 IEEE MTT-S International*, pp. 240–242, IEEE, 1984.

[9] M. Ain, Z. Ahmad, M. Othman, I. Zubir, S. Hutagalung, A. Sulaiman, and A. Othman, "Dielectric resonator bandpass filter for X-band application," in *TENCON 2010-2010 IEEE Region 10 Conference*, pp. 2048–2052, IEEE, 2010.

[10] A. K. Jyani, S. Awasthi, and A. Biswas, "Design of dielectric resonator antenna and filter for X-band application," in *Applied Electromagnetics Conference (AEMC), 2013 IEEE*, pp. 1–2, IEEE, 2013.

[11] R. Zhang and R. R. Mansour, "Dual-band dielectric-resonator filters," *IEEE Trans. Microw. Theory Techn.*, vol. 57, no. 7, pp. 1760–1766, 2009.

[12] F. Huang and R. Mansour, "Tunable compact dielectric resonator filters," in *European Microwave Conference, 2009. EuMC 2009.*, pp. 559–562, IEEE, 2009.

[13] R. Saliminejad and M. R. Ghafouri Fard, "A novel and accurate method for designing dielectric resonator filter," *Progress In Electromagnetics Research B*, vol. 8, pp. 293–306, 2008.

[14] E. M. Y. Sandhu, E. S. Afridi, and E. Y. S. Junejo, "Designing of high Q dielectric resonator filter by 3-D finite element method (FEM),"

[15] R. Borowiec, "Dielectric resonator filters," in *Microwaves, Radar, and Wireless Communication (MIKON), 2014 20th International Conference on*, pp. 1–4, June 2014.

[16] R. R. Mansour, "High-Q tunable dielectric resonator filters," *IEEE Microw. Mag.*, vol. 10, no. 6, pp. 84–98, 2009.

[17] K. W. Leung, "Development of dielectric resonator antenna (DRA)," *State Key Laboratory of Millimeter Waves and Department of Electronic Engineering, City University of Hong Kong*, 2012.

[18] P. I. Richards, "Resistor-transmission-line circuits," *Proceedings of the IRE*, vol. 36, pp. 217–220, Feb 1948.

[19] H. Ozaki and J. Ishii, "Synthesis of a class of strip-line filters," *IRE Transactions on Circuit Theory*, vol. 5, pp. 104–109, Jun 1958.

[20] G. L. Matthaei, L. Young, and E. M. T. Jones, *Microwave filters, impedance-matching networks, and coupling structures*. Artech house, 1980.

[21] S. Cohn, L. Robinson, and J. Shimizu, *Strip Transmission Lines and Components*. Stanford Research Institute, 1968.

[22] V. V. Tyurnev, "Coupling coefficients of resonators in microwave filter theory," *Progress In Electromagnetics Research B*, vol. 21, pp. 47–67, 2010.

[23] E. L. Ginzton, *Microwave measurements*. McGraw-Hill, 1957.

[24] CST, "CST - computer simulation technology." https://www.cst.com, 2016.

[25] D. L. Cuenca, R. Dudi, and J. Hesselbarth, "Measurement of complex permittivity of anisotropic dielectric spheres," in *2016 German Microwave Conference (GeMiC)*, pp. 461–464, 2016.

[26] D. M. Pozar, *Microwave engineering*. John Wiley & Sons, 2009.

[27] D. L. Cuenca and J. Hesselbarth, "Self-aligned microstrip-fed spherical dielectric resonator antenna," in *2015 9th European Conference on Antennas and Propagation (EuCAP)*, pp. 1–5, 2015.

[28] Y. Kobayashi and S. Tanaka, "Resonant modes of a dielectric rod resonator short-circuited at both ends by parallel conducting plates," *IEEE Trans. Microw. Theory Techn.*, vol. 28, pp. 1077–1085, Oct 1980.

[29] S. B. Cohn, "Dissipation loss in multiple-coupled-resonator filters," 1959.

[30] "Hotend works, high quality rapid prototypes." http://www.hotendworks.com. Online; accessed 29 August 2016.